

THESIS FOR THE DEGREE OF LICENTIATE OF ENGINEERING

Plasmons in Nanostructured Graphene

Tobias Wenger

Applied Quantum Physics Laboratory
Department of Microtechnology and Nanoscience (MC2)
Chalmers University of Technology
Göteborg, Sweden 2015

Plasmons in Nanostructured Graphene
Tobias Wenger

Copyright © Tobias Wenger, 2015

Applied Quantum Physics Laboratory
Department of Microtechnology and Nanoscience (MC2)
Chalmers University of Technology
SE-412 96 Göteborg, Sweden
Telephone: +46 (0)31-772 1000

ISSN 1652-0769
Technical Report MC2-312

Cover: Brillouin-zone plot of the tight-binding energy dispersion of graphene where the valence band is shown in blue and the conduction band is shown in orange.

Printed by Chalmers Reproservice
Göteborg, Sweden 2015

Plasmons in Nanostructured Graphene
Thesis for the degree of Licentiate of engineering

TOBIAS WENGER

Applied Quantum Physics Laboratory
Department of Microtechnology and Nanoscience (MC2)
Chalmers University of Technology

Abstract

Plasmons, collective electron density oscillations, provide physicists with intriguing challenges and possibilities. The inherent many-body properties of the plasmons together with their ability to localize light into small volumes make the plasmons interesting from both a purely theoretical viewpoint and an applications point of view. Graphene, with its rather special electronic properties, provides the field of plasmonics with a new material that exhibits large localization of the electric field together with low losses.

In this thesis we cover the basic theory underlying modern theoretical plasmonics research. We do so in the context of linear response functions and the Random Phase Approximation that are standard tools in the field. We apply the theory to plasmons in different contexts, trying to highlight differences and similarities between graphene plasmons, plasmons in 2DEG's and conventional interface plasmons.

We present light scattering results from a nanostructured graphene surface, tailored specifically to allow plasmon excitation. We investigate the reflection, transmission and absorption of such surfaces and also analyze the plasmon resonances that arise.

Keywords: Plasmons, plasmonics, graphene, surface plasmon-polaritons, linear response theory, random phase approximation, surface electro-dynamics.

Acknowledgments

I would first and foremost like to thank my supervisors Mikael Fogelström and Jari Kinaret for their supervision and support during the past couple of years, leading to this thesis. I would also like to thank all of the people, past and present, at the Applied Quantum Physics Laboratory at MC2 where this work has been performed. I thank them for their moral support, questions and interesting discussions over coffee. I would like to especially thank Giovanni Viola for valuable discussions regarding the work presented in this thesis.

Finally, I wish to thank Sofia for her continuous support. Thank you for always being there.

Tobias Wenger
Göteborg, May 2015

Dedicated to all my teachers.

Contents

1	Introduction	1
1.1	Graphene	1
1.2	Plasmonics	3
1.3	Graphene plasmonics	6
1.4	Overview of the thesis	9
2	Theory	11
2.1	Maxwell equations	11
2.2	Fresnel scattering at an interface	13
2.2.1	Dielectric interface	14
2.2.2	Dielectric interface with current sheet	15
2.3	Graphene	16
2.4	Linear response theory	19
2.4.1	Formal development	19
2.4.2	External electric field: conductivity and dielectric function	25
2.5	Random phase approximation	27
2.6	Plasmons and related quantities	28
2.6.1	Surface plasmon polaritons in metal-dielectric interfaces	29
2.6.2	Surface plasmon polaritons in two-dimensional sheets	30
2.6.3	Wave localization	31
2.7	Two-dimensional electron gases	32

3	Scattering Results	39
3.1	Light scattering results of a nanostructured graphene surface	39
3.1.1	Suspended graphene	41
3.1.2	Graphene on dielectric substrate with $\epsilon_r = 4$	42
3.1.3	Graphene on dielectric substrate with $\epsilon_r = 10$	43
3.2	Investigation of scattering resonances	44
3.2.1	Scattering coefficients along the plasmon dispersion	45
3.2.2	Resonance widths	45
4	Summary and Outlook	49
Appendix A Derivation of the RPA dielectric function using the method of self-consistent fields		53
A.1	Electrodynamics	53
A.2	Self consistent field method	54
Appendix B Green's function for quantities confined to surfaces		59
B.1	Bulk Green's function for the Poisson equation	59
B.2	Surface Green's functions for the Poisson equation	59
Appendix C Calculation of the polarizability $\Pi(q, \omega)$ for a 2DEG with parabolic dispersion at zero temperature		61
C.1	Preliminaries	61
C.1.1	Formulas and Identities	61
C.2	Calculation	64
C.3	Results and analysis	72
Appendix D Calculation of the polarizability, $\Pi(q, \omega)$ for graphene at zero temperature		75
D.1	Preliminaries	75
D.2	Calculation	76

D.2.1	$\Pi^-(q, \omega)$	77
D.2.2	$\Pi^+(q, \omega)$	82
D.3	Summary of results	94
D.4	Long wavelength expansion of the polarizability	95

Chapter 1

Introduction

In this chapter we discuss the history and current status of graphene research and plasmonics as separate fields of research. We then proceed to merge the two fields and discuss the rather young field of graphene plasmonics. We will focus on theoretical developments but we will also consider experimental demonstrations of graphene plasmons.

1.1 Graphene

Graphene is a single atomic layer of carbon atoms arranged in an hexagonal honeycomb lattice. The two-dimensional nature of the graphene surface together with its lattice symmetry gives graphene many special properties. Graphene is for example one of the strongest materials ever [1], a single layer graphene of size one by one meter could in fact suspend something as big as a cat, assuming that the graphene is completely free from defects. Graphene is also a very good conductor, it has a larger electrical conductivity than silver [2] and a larger thermal conductivity than diamond [3].

Graphene, in the context of single layer graphite, was first theoretically considered by Wallace in 1947 using a tight-binding formulation to study the band structure, see Ref. [4]. Mono-layer graphene was long seen as an impossibility and thus focus was on producing and investigating thin graphite films. There are several papers discussing the special transport properties of thin film graphite, see for instance Ref. [5] and Ref. [6].

In 2004, Novoselov and co-workers managed to isolate a single layer of

graphene and transfer it onto an SiO₂ (silicon dioxide) wafer [2]. This made it possible to use a microscope and detect a contrast between areas of monolayer graphene and areas that had no graphene or multilayers patches. In this paper the graphene was produced using mechanical exfoliation and it was shown to be possible to externally gate the sample to change its properties. Much effort is now being devoted to scaling up the production of high quality graphene, for which mechanical exfoliation is not well suited, and to further theoretical investigation of the properties of graphene. Much of the effort is motivated by the objective to create new technological devices that harness the previously mentioned properties of graphene, e.g. the large electrical and thermal conductivity. Since graphene is also extremely light-weight and very strong it is also interesting for applications in for example aviation and space flight. The European Commission has devoted a substantial financial contribution to start a so called Graphene Flagship that aims to bring graphene from the academic world to the technological industry. Some of the targeted areas that are of relevance to this thesis are optoelectronics, high frequency electronics, energy applications, flexible electronics and sensor applications.

The full band diagram of graphene can be obtained using tight-binding calculations and it contains two inequivalent points in the Brillouin-zone where the two energy bands touch. These points are called Dirac points and they separate the valence band from the conduction band. It is possible to linearize the band diagram around these two points and obtain a linear dispersion. Figure 1.1 shows the linearized band structure around one of the two Dirac points with the Fermi energy in the conduction band, meaning that the graphene in this case is n-doped, i.e. it has excess negative charge. The vertical arrow in the figure shows the lowest energy interband transition within the graphene.

The interband transitions are responsible for the absorption of energy from radiation by the graphene sheet since the final electron state has a larger energy than before the excitation. By fairly simple calculations it is possible to show that a single layer of graphene is able to absorb 2.3% of the energy of the incoming radiation. Experimentally this was verified in [7] and considering the extremely small lateral dimension of one atom,

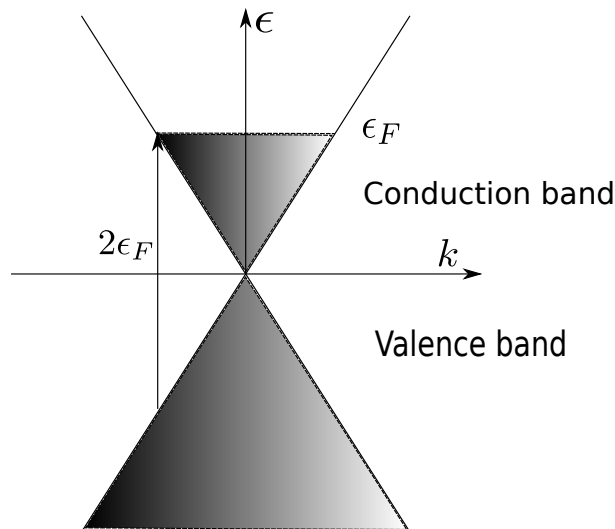


Figure 1.1: Figure showing the linear dispersion of graphene. Here the Fermi energy is in the conduction band and thus the graphene is n-doped, it has excess negative charge. The vertical arrow depicts the lowest energy interband transition an electron can make.

$\approx 1 \text{ \AA}$, this is a large absorption.

Pristine graphene is neutral and has no free charge carriers at zero temperature. Normally however, graphene obtains an excess or deficit charge due to the fabrication process, this is usually called doped graphene in reference to its similarity with semiconductors. It turns out that it is also possible to externally tune this doping level using electrostatic doping by means of an external gate as shown in [2]. This tunability of graphene is in contrast to most conventional materials where the doping levels and thereby frequencies of interest are "God-given", or at the very least fixed for a certain sample. This external tunability opens up the possibility to create tunable devices of various kinds, for instance tunable optical filters and modulators but also allows for tunable transport properties when considering more conventional electronic devices.

1.2 Plasmonics

The field of plasmonics can trace its ancestry all the way back to the beginning of the 20th century. However, examples of the use of what is now known as plasmonic effects can actually be traced back much further than

that. Well known examples are for instance the staining of church windows during medieval times and actually already the romans used plasmonic effects to color cups. These early uses of plasmonics where however lacking in their understanding of the underlying physical effects.

The unification of electricity and magnetism was made by Maxwell in 1865 [8], paving the road for investigation of electromagnetism in a wide range of settings. In 1902, Wood investigated the reflection properties of metallic gratings on a surface and observed unexplained features in their spectra [9], this is usually taken to be the first observation of plasmons in a scientific setting. In 1908, Mie published his theory of light scattering against spherical particles [10] which is still used to this day. However, a more fundamental theory of light scattering against charged matter would have to wait. Langmuir and Tonks experimented with gaseous plasmas in the 1920's and found waves in the plasma [11], these are now known as Langmuir waves. In 1956, Pines realized there was a connection between Langmuir waves and the electron energy losses in the materials he was investigating. He published his work on energy losses in materials due to exciting collective oscillations which he called "plasmons" [12].

Ritchie was around the same time investigating electron energy losses in thin films and discovered that the plasmons could exist on or near the material surface and thus the notion of surface plasmons was born. In 1968, some 60 years after the experiment, Ritchie was able to explain the strange reflection behavior that Woods had found in terms of surface plasmons being excited at the gratings [13].

Somewhat confusingly, within the setting of condensed matter physics, in 1958 Hopfield introduced the term "polariton" to mean a coupled oscillation of light and electrons in a material [14]. Essentially this was the same as what was meant with the word plasmon, at least a surface plasmon that could be interpreted as light being hybridized with the electrons. In 1974, Cunningham and co-workers introduced the term surface-plasmon-polariton (SPP) to describe these oscillatory modes [15]. In the literature both the terms surface plasmon and SPP are often used to mean the same thing, namely oscillatory modes confined to surfaces.

Perhaps the most recent big advancement in plasmonics is the effect plasmons can have on the Raman signal. Raman spectroscopy studies the interaction of light with vibrational modes in a surface and it was discovered by Fleischmann and coworkers that this signal could be enhanced by many orders of magnitude by using surface plasmons [16]. This is nowadays called surface enhanced Raman spectroscopy (SERS) and by using the surface plasmonic field enhancement, the signal may be enhanced by an incredible 10 orders of magnitude [17]. SERS is often used in biosensing applications and is capable of sensing even single molecules under certain conditions [17].

Much of the interest in plasmonics stems from the fact that plasmons have a wavelength smaller than the incident light, leading to localization of energy in the plasmon modes. This is the cause of the large field enhancements which in turn leads to huge enhancement of interaction strengths e.g. the Raman enhancement. Also, small wavelengths are an advantage in the age of miniaturization and one can imagine very small optical devices such as switches, modulators and filters that currently are limited in size by the free space wavelength.

However, the wave localization comes at a price. Large localization usually leads to large losses meaning that the plasmons are highly damped and have short lifetimes. This limits the effectiveness of devices using plasmons and has been a general limiting factor within plasmonics for some time. The conventional material for surface plasmonic purposes is silver as it has relatively low losses compared with other materials. In silver the surface plasmons may propagate up to 1 mm under the right conditions [18]. However, in this regime the SPP wavelength is only a few percent smaller than the free space wavelength [19]. This is where graphene and other two dimensional materials might have a role to play. It turns out that due to the extreme two dimensional nature of these materials, the losses are low compared with silver, even though the wave localization in graphene is larger than in silver and in theory can be of order 100.

There is also an increasing activity in stacking different two dimensional materials to create new tailored materials. Perhaps it will be possible to engineer a stacked material that has even larger wave localization and lower losses than graphene. These stacked materials can also play a role in applications where these materials can be combined to suit specific devices.

1.3 Graphene plasmonics

Graphene plasmonics is a rather new field of research that merges the exciting properties of graphene with that of surface plasmon modes. The first theoretical investigations of plasmons in graphene were performed in [20, 21] where they obtained the same $\omega \propto \sqrt{k}$ as normal 2DEG plasmons¹ but a scaling in density as $\omega \propto n^{1/4}$ instead of $\omega \propto \sqrt{n}$ as the 2DEG plasmon. It was realized that using this density dependence the plasmon frequency in graphene (and 2DEG's) can be tuned by changing the electron density. This can be achieved by for instance using a back gate to which a voltage is applied, thus forcing charges onto or off the graphene sheet. The tunability of the plasmon energy of graphene is one of the advantages of using graphene as a plasmonic material instead of using more conventional materials such as silver. Other main advantages are, as discussed in the previous section, the low losses and large wave localization in graphene.

Wave localization means that the wavelength at a specific energy is smaller for the plasmon than for free space light. Since the wave number (momentum) is $k = 2\pi/\lambda$ this leads to what is known as momentum mismatch between incident light and the plasmon. This is common for all plasmons that exhibit wave localization, not only graphene plasmons, but the mismatch is larger in graphene than for conventional plasmons due to the larger localization. Normally, this means that incident light does not couple to the plasmons. There are several methods to overcome this mismatch and allow incident light to couple to the plasmons. The methods that exist are based either on the notion of evanescent wave coupling (evanescent waves need not obey the free space dispersion) or patterning. Patterning could be done by introducing a single sharp scatterer with some

¹With "normal 2DEG" we mean massive electrons confined in two dimensions, obeying the standard parabolic dispersion $\epsilon_p = \frac{\hbar^2 k^2}{2m}$.

length scale $L = 2\pi/k$ or by making periodic structures where the period is $d = 2\pi/k$.

Graphene plasmons were first demonstrated in 2012 [22, 23], 8 years after the isolation of single layer graphene by Geim and Novoselov. In these papers the plasmons were launched by an SNOM²-tip illuminated by a laser and the plasmons reflected from the edges and were picked up by the same tip. The plasmon then radiated light through the tip that could be detected. The reported wave localization factor was ≈ 30 , meaning the plasmon wavelength was $\lambda_p = \lambda_0/30$, and the propagation distances were around 5-6 wavelengths. Another method to launch plasmons in graphene is to illuminate metal antennas, deposited on top of graphene, with a laser [24]. This method makes it possible to launch plasmons in a specific direction, in contrast to the previously mentioned experiments where the plasmons are launched in a radial pattern. Both the SNOM-method and the antenna method are examples of introducing a single scatterer to overcome the momentum mismatch.

It is also possible to pattern the graphene into microribbon arrays and by the patterning overcoming the momentum mismatch. This technique very much resembles the notion of metamaterials where the patterning is done in order to create materials not found in nature. Patterning graphene into microribbon arrays can be called a plasmonic metamaterial. Such patterning has been performed in [25] and they found that at room temperature the plasmons absorbed 13% of the radiation incident on the surface.

The route followed in this thesis is to consider a nanostructured array, called a grating, on top of the graphene. The idea is that the grating will make the perturbation applied by the incoming light periodic in space and thus induce an effective momentum $k = 2\pi/d$ [31]. Figure 1.2 shows a picture of a grating on top of graphene. This will allow us to consider responses with larger momenta than the incident light and thus explore a larger parameter space. This larger parameter space contains the plasmons.

²Scanning Near-field Optical Microscope

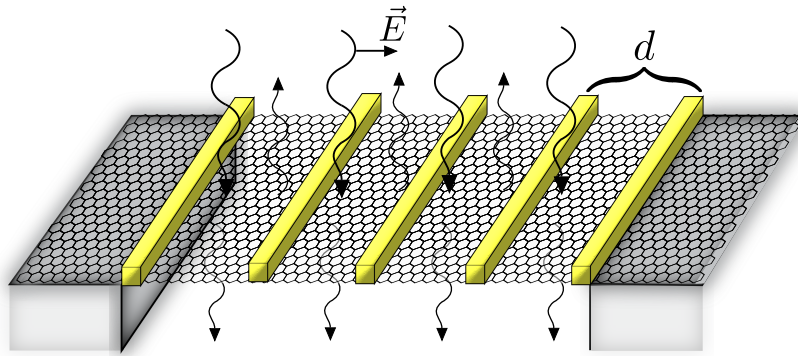


Figure 1.2: A graphene sheet that is suspended with a grating.

Much of the theory developed for graphene plasmons has treated clean graphene and at zero temperature. There is now an increased understanding that impurities, grain boundaries and even patches of bilayer graphene on top of monolayer graphene can have a large influence on the graphene plasmons and their properties. These effects are now starting to be investigated. Impurity scattering effects on graphene plasmons were investigated in [26], in which they included an energy independent relaxation time in a number conserving way using the Mermin result [27]. They found that with a realistic scattering time the plasmons in graphene would still exhibit large localization and low losses. The finite temperature RPA response was calculated in [28] and was also treated in [29] where they also considered finite temperature effects on the plasmon dispersion and the plasmon damping.

The main aim of this thesis is to develop the necessary theory in order to investigate graphene plasmons. We will work with clean graphene at zero temperature and we will in the very end consider the effects of a substrate on the plasmon dispersion. We will compare numerical results of the plasmons dispersion with an analytic result obtained within a widely used approximation (long wavelength approximation), pointing out the range of validity of this approximation.

1.4 Overview of the thesis

In chapter 2 we develop the necessary theory for treating plasmons in graphene starting in section 2.1 with a short treatment of the Maxwell equations and related properties. In section 2.2 we then consider classical light scattering at an interface, both in the standard case of an interface between two dielectrics and the case of a conducting sheet sandwiched between two dielectrics. Next, in section 2.3 we develop the theory of graphene starting with the tight binding Hamiltonian and its full band structure, then linearizing and obtaining the standard Dirac approximation of graphene around the two inequivalent points in the Brillouin zone. Section 2.4 contains a general treatment of linear response theory with an application to the specific case of electrical conductivity. We then proceed in section 2.5 to treat the Random Phase Approximation of the dielectric function. Section 2.6 treats plasmons and related properties and section 2.7 treats properties of different 2-dimensional electron gases.

Chapter 3 contains the main results obtained in the thesis. Section 3.1 contains reflection, transmission and absorption results for nanostructured graphene both in the suspended case and for graphene deposited on dielectric substrates. In section 3.2 we investigate the plasmon resonances we obtain in the scattering coefficients and discuss plasmon decay and the Q-factor.

Chapter 4 provides a brief summary of the theory and the results and we also discuss some possible future directions of research.

This thesis also contains four appendices in which we have placed derivations that were considered too lengthy to put in the main text but that were still considered relevant to treat in some detail. Appendix A contains a derivation of the RPA dielectric function using the method of self-consistent fields. In appendix B we treat Green's functions for the Poisson equation in the bulk and also when the charge is confined in a two-dimensional sheet. Appendix C contains a calculation of the polarizability function for a single band, parabolic 2DEG. Last, appendix D contains a rather lengthy calculation of the polarizability within the Dirac

approximation of graphene at zero temperature.

Chapter 2

Theory

2.1 Maxwell equations

The basic equations that govern the interaction between light and matter are the Maxwell equations. The Maxwell equations in their original form

$$\nabla \cdot \vec{D} = \rho \quad (2.1)$$

$$\nabla \times \vec{H} - \frac{\partial \vec{D}}{\partial t} = \vec{j} \quad (2.2)$$

$$\nabla \times \vec{E} + \frac{\partial \vec{B}}{\partial t} = 0 \quad (2.3)$$

$$\nabla \cdot \vec{B} = 0, \quad (2.4)$$

contain *four* fields (\vec{E} , \vec{D} , \vec{H} , \vec{B}). These are called electric field, displacement field, magnetic field strength and magnetic induction respectively. In vacuum we have the well known connections $\vec{D} = \epsilon_0 \vec{E}$ and $\vec{B} = \mu_0 \vec{H}$, where ϵ_0 and μ_0 are the vacuum values of the permittivity and permeability respectively, also $\sqrt{\frac{1}{\epsilon_0 \mu_0}} = c$. Also, ρ is the charge density and \vec{j} is the current density.

In a more general situation there might be a medium present that behaves in a different way than vacuum. With "medium" we mean a material with charges that are bound to the medium. Basically any material fits this description but we will mostly be considering metals or semiconductors. The charges in the medium will respond when an external field is applied, this may alter the connections between the fields. In general, [30]

chap. 4.3,

$$\vec{D} = \epsilon_0 \vec{E} + \vec{P} \quad (2.5)$$

and

$$\vec{B} = \mu_0 \vec{H} + \vec{M} \quad (2.6)$$

where \vec{P} and \vec{M} are the *polarization* and *magnetization* respectively. This means that we add the polarization field to the vacuum value of the displacement field and likewise the magnetization to the vacuum value of the magnetic induction. The naming convention for the \vec{B} and \vec{H} fields changes between different sources in the literature, we will refer to both fields as the magnetic field in what follows.

We will mainly be interested in the \vec{D} and \vec{E} fields since they are governing the ability of the medium to conduct electricity. Also, many materials exhibit a very weak magnetization and from now on we assume that the magnetization \vec{M} is zero and thus $\vec{B} = \mu_0 \vec{H}$, i.e. the same as for vacuum. We will also make a very important simplification of the treatment of electric fields surrounding materials. We will only consider the *linear response* of the material, meaning that the system response, i.e. \vec{P} , is proportional to the external field \vec{E} . There are different ways to justify this but the simplest justification is that this behavior is what most systems exhibit in accessible field strengths. At very high electric fields this assumption may break down but we will not consider such cases. Consequently we may now write the polarization $\vec{P} = \epsilon_0 \chi \vec{E}$ i.e.

$$\vec{D} = \epsilon_0 \vec{E} + \vec{P} = \epsilon_0 \vec{E} (1 + \chi), \quad (2.7)$$

where χ is the (electric) *susceptibility* of the medium. We may now define a new electric permittivity (compare to the vacuum electric permittivity) as $\tilde{\epsilon} = \epsilon_0 (1 + \chi)$ and the *dielectric function* (relative permittivity) as

$$\epsilon(q, \omega) = \frac{\tilde{\epsilon}(q, \omega)}{\epsilon_0} = 1 + \chi(q, \omega) \quad (2.8)$$

giving us

$$\vec{D} = \tilde{\epsilon} \vec{E}. \quad (2.9)$$

The vacuum permittivity has been altered by the susceptible medium and thus giving rise to a different displacement field. Looking at equation (2.8) it is obvious that a susceptibility of zero reproduces the vacuum value for the \vec{D} field. Materials with high relative permittivity are usually called dielectrics.

Another measurable quantity of interest is the conductivity which in macroscopic terms is defined through Ohms's law as

$$e\vec{j} = \sigma\vec{E} \quad (2.10)$$

i.e. the conductivity is the proportionality constant which relates the applied electric field to the current it induces. We have here defined \vec{j} as the particle current in anticipation of the linear response treatment in section 2.4. In general σ can be a second order tensor, the fact that we only consider a scalar reflects the fact that we consider an isotropic medium. By looking at the Maxwell equations and the definition of conductivity it is possible to relate the conductivity and permittivity as [31]

$$\epsilon(q, \omega) = 1 + \frac{i\sigma(q, \omega)}{\epsilon_0\omega}. \quad (2.11)$$

Combining this with equation (2.8) we obtain a relationship linking the conductivity and the susceptibility as

$$\sigma(q, \omega) = -i\epsilon_0\omega\chi(q, \omega). \quad (2.12)$$

2.2 Fresnel scattering at an interface

In this section we treat the scattering of radiation upon incidence on an interface between two media with different dielectric constants ϵ_1 and ϵ_2 . Without loss of generality we will consider the incoming radiation to be incident from medium 1, with ϵ_1 , onto medium 2, with ϵ_2 . In the case a sheet current and a sheet charge are present, they exist on the boundary between the two media.

2.2.1 Dielectric interface

For the case of a dielectric interface the following expressions for the angular dependent reflection- and transmission amplitudes can be found in [30] pp. 304:

E-field parallel to plane of incidence (p-polarization)

$$r = \frac{\epsilon_2 \cos(\theta_i) - \cos(\theta_t) \sqrt{\epsilon_1 \epsilon_2}}{\cos(\theta_t) \sqrt{\epsilon_1 \epsilon_2} + \epsilon_2 \cos(\theta_i)} \quad (2.13)$$

$$t = \frac{2 \cos(\theta_i) \sqrt{\epsilon_1 \epsilon_2}}{\cos(\theta_t) \sqrt{\epsilon_1 \epsilon_2} + \epsilon_2 \cos(\theta_i)} \quad (2.14)$$

where ϵ_2 is the dielectric constant of the half space that we are transmitting into.

E-field perpendicular to plane of incidence (s-polarization)

$$r = \frac{\sqrt{\epsilon_1} \cos \theta_i - \sqrt{\epsilon_2} \cos \theta_t}{\sqrt{\epsilon_1} \cos \theta_i + \sqrt{\epsilon_2} \cos \theta_t} \quad (2.15)$$

$$t = \frac{2 \sqrt{\epsilon_1} \cos \theta_i}{\sqrt{\epsilon_1} \cos \theta_i + \sqrt{\epsilon_2} \cos(\theta_t)} \quad (2.16)$$

as above ϵ_2 is the dielectric constant of the half space that we are transmitting into.

It is important to note that equations (2.13)-(2.16) are amplitudes and in order to calculate the energy flow we must take the modulus square of the amplitudes and also include a change of group velocity and change in beam size. This can be obtained by studying the Poynting vector and check the energy density flow, see [32] pp. 120. Considering this the reflected and transmitted energy coefficients are

$$\text{reflected energy, } R = |r|^2 \quad (2.17)$$

$$\text{transmitted energy, } T = \sqrt{\frac{\epsilon_2 \cos \theta_t}{\epsilon_1 \cos \theta_i}} |t|^2 \quad (2.18)$$

$$\text{absorbed energy, } A = 1 - R - T \quad (2.19)$$

where θ_i and θ_t are the incoming angle and the transmitted angle respectively. The definition of the absorbed energy comes from energy conservation. The energy that is neither reflected nor transmitted must be absorbed in the interface. Applying this to the formulas for the transmission- and reflection coefficients above we would always get $A = 0$, i.e. no absorption takes place in ordinary, non-conducting dielectric interfaces.

2.2.2 Dielectric interface with current sheet

We now add a conducting interface to the simple picture above, in our case this will be a graphene sheet but the formulas themselves are not restricted to this case. The key difference between this case and the one above is that the electromagnetic boundary conditions change in the presence of sheet currents and charges. In [30] pp. 18 we find the well-known boundary conditions

$$(\vec{D}_2 - \vec{D}_1) \cdot \vec{n} = \rho_s \quad (2.20)$$

$$(\vec{B}_2 - \vec{B}_1) \cdot \vec{n} = 0 \quad (2.21)$$

$$\vec{n} \times (\vec{E}_2 - \vec{E}_1) = 0 \quad (2.22)$$

$$\vec{n} \times (\vec{H}_2 - \vec{H}_1) = \vec{j}_s \quad (2.23)$$

where ρ_s and \vec{j}_s are the sheet charge and sheet current respectively. They are understood to only exist on the boundary between the two media. In this case the formulas become lengthy so we only consider here the normal incidence, $\theta_i = \theta_r = 0$, and print the expressions below.

Normal incidence

$$\text{reflected energy, } R = \left| \frac{\epsilon_2 + \sigma(k, \omega) - \sqrt{\epsilon_1 \epsilon_2}}{\epsilon_2 + \sigma(k, \omega) + \sqrt{\epsilon_1 \epsilon_2}} \right|^2 \quad (2.24)$$

$$\text{transmitted energy, } T = \frac{4\epsilon_2 \sqrt{\epsilon_1 \epsilon_2}}{|\epsilon_2 + \sigma(k, \omega) + \sqrt{\epsilon_1 \epsilon_2}|^2} \quad (2.25)$$

$$\text{absorbed energy, } A = \frac{4\sqrt{\epsilon_1 \epsilon_2} \operatorname{Re}[\sigma(k, \omega)]}{|\epsilon_2 + \sigma(k, \omega) + \sqrt{\epsilon_1 \epsilon_2}|^2} \quad (2.26)$$

For normal incidence both s- and p-polarization scattering reduce to the same expressions above. In general the conductivity can depend on both the incoming momentum and the frequency of the incoming light which is made explicit in the formulas above.

2.3 Graphene

As mentioned in the introduction, graphene is a monolayer of carbon atoms arranged in what is usually called a "honeycomb lattice". There are two inequivalent atoms in the lattice structure, usually called the A and B atoms which build up the underlying triangular A and B lattices. The band structure of an infinite graphene sheet was first treated by Wallace [4] and the full dispersion (with only nearest-neighbor hopping) is [33]

$$\epsilon(k) = \pm t \sqrt{3 + 2 \cos(\sqrt{3}k_y a) + 4 \cos(\sqrt{3}k_y a/2) \cos(3k_x a/2)} \quad (2.27)$$

where $a \approx 1.42 \text{ \AA}$ is the carbon-carbon distance and $t \approx 2.7 \text{ eV}$ is the nearest neighbor hopping term. This dispersion is plotted in figure 2.1 where we clearly see the points where the two bands touch, these points are called the Dirac points. Linearizing the dispersion around these points we obtain the dispersion

$$\epsilon(k) = \pm \frac{3ta}{2} |k| = \pm v_F |k| \quad (2.28)$$

where k now is measured from the Dirac point we are linearizing around and we have defined the Fermi velocity $v_F = 3ta/2 \approx 10^6 \text{ m/s}$.

Perhaps the most striking property that arises is that the low energy electrons behave as *massless* Dirac particles. The linear dispersion relation resembles the photon dispersion but with the slope, i.e. propagation speed, of v_F instead of c for the photons. The speed v_F is approximately $v_F/c \approx 1/300$. The linearized dispersion relation is usually considered to hold for energies below 1 eV, above this energy we would start seeing effects that are not captured by the linearized equations.

Above we simply linearized the dispersion relation to obtain the linear dispersion, it is also possible to linearize the Hamiltonian and solve for

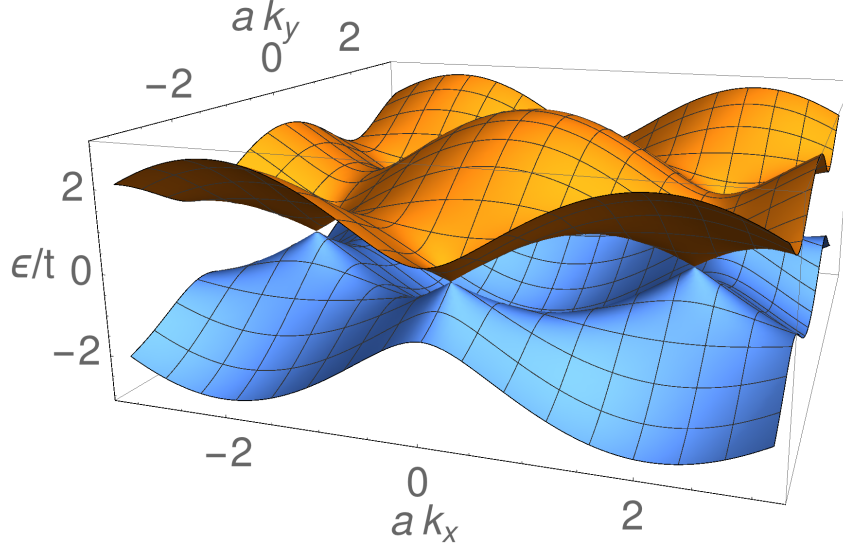


Figure 2.1: Plot of the tight-binding dispersion in equation (2.27).

the eigenenergies and eigenvectors. Below, we closely follow [34] chap. 1. There are only two inequivalent points in the full dispersion to linearize around; we call these \vec{K} and \vec{K}' . The linearized Hamiltonians that one obtains from the linearization procedure are

$$\hat{H}_{\vec{K}}(\vec{k}) = v_F \begin{pmatrix} 0 & k_x - ik_y \\ k_x + ik_y & 0 \end{pmatrix} = -iv_F \vec{\sigma} \cdot \nabla = v_F \vec{\sigma} \cdot \vec{k} \quad (2.29)$$

$$\hat{H}_{\vec{K}'}(\vec{k}) = v_F \begin{pmatrix} 0 & k_x + ik_y \\ k_x - ik_y & 0 \end{pmatrix} = -iv_F (\vec{\sigma} \cdot \nabla)^T = v_F (\vec{\sigma} \cdot \vec{k})^T \quad (2.30)$$

where $\vec{\sigma} = (\sigma_x, \sigma_y)$ i.e. a vector of Pauli matrices. Now, the Hamiltonian $\hat{H}_{\vec{K}}$ acts on spinors for the \vec{K} valley and $\hat{H}_{\vec{K}'}$ on the spinors for the \vec{K}' valley, i.e.

$$\hat{H}_{\vec{K}} \begin{pmatrix} \psi_{KA}(\vec{k}) \\ \psi_{KB}(\vec{k}) \end{pmatrix} = \epsilon(k) \begin{pmatrix} \psi_{KA}(\vec{k}) \\ \psi_{KB}(\vec{k}) \end{pmatrix} \quad (2.31)$$

$$\hat{H}_{\vec{K}'} \begin{pmatrix} \psi_{K'A}(\vec{k}) \\ \psi_{K'B}(\vec{k}) \end{pmatrix} = \epsilon(k) \begin{pmatrix} \psi_{K'A}(\vec{k}) \\ \psi_{K'B}(\vec{k}) \end{pmatrix} \quad (2.32)$$

where the ψ subscripts denote the valley and A or B sub-lattice that the wave function belongs to. It may sometimes be convenient to put all this together in one matrix equation construct and this can be done by putting

the Hamiltonians in a block diagonal form

$$\begin{pmatrix} \hat{H}_{\vec{K}} & 0 \\ 0 & \hat{H}_{\vec{K}'} \end{pmatrix} \Psi(\vec{k}) = \epsilon(k) \Psi(\vec{k}) \quad (2.33)$$

where

$$\Psi(\vec{k}) = \begin{pmatrix} \psi_{K,A}(\vec{k}) \\ \psi_{K,B}(\vec{k}) \\ \psi_{K',A}(\vec{k}) \\ \psi_{K',B}(\vec{k}) \end{pmatrix}. \quad (2.34)$$

In the interest of high degree of symmetry in the equations this is sometimes recast in a different form where one rearranges the K' spinor so that it has the same Hamiltonian as the K spinor, we write it as

$$\begin{pmatrix} \hat{H}_{\vec{K}} & 0 \\ 0 & \hat{H}_{\vec{K}} \end{pmatrix} \Psi_R(\vec{k}) = v_F \left(\tau_0 \otimes \vec{\sigma} \cdot \vec{k} \right) \Psi_R(\vec{k}) = \epsilon(k) \Psi_R(\vec{k}) \quad (2.35)$$

where

$$\Psi_R(\vec{k}) = \begin{pmatrix} \psi_{K,A}(\vec{k}) \\ \psi_{K,B}(\vec{k}) \\ \psi_{K',B}(\vec{k}) \\ -\psi_{K',A}(\vec{k}) \end{pmatrix} \quad (2.36)$$

denotes the rearranged 4-component vector and τ_0 is a unit matrix in valley indices.

Using the forms in equations (2.31) and (2.32) and using the linear dispersion from equation (2.28) we may determine the momentum space eigenspinors to be [33]

$$\psi_K(k) = \begin{pmatrix} \psi_{KA} \\ \psi_{KB} \end{pmatrix} = \frac{1}{\sqrt{2}} \begin{pmatrix} e^{-i\theta_k/2} \\ \pm e^{i\theta_k/2} \end{pmatrix} \quad (2.37)$$

$$\psi_{K'}(k) = \begin{pmatrix} \psi_{K'A} \\ \psi_{K'B} \end{pmatrix} = \frac{1}{\sqrt{2}} \begin{pmatrix} e^{i\theta_k/2} \\ \pm e^{-i\theta_k/2} \end{pmatrix} \quad (2.38)$$

where $\theta_k = \arctan(k_x/k_y)$ and \pm means conduction band (+) and valence band (−) and correspond to the sign in equation (2.28).

2.4 Linear response theory

Linear response theory is a widely used concept within condensed matter physics. Simply put, linear response theory considers systems that are initially in their ground state, which we know how to calculate, and we then perturb the system away from that ground state. If the perturbation that we apply is small, then the deviation from the ground state is also in some sense small. The goal is then to calculate this response in an appropriate form. The linear response of a system is completely determined by its ground state properties, this might seem surprising but is in fact quite natural. In analogy with the Taylor expansion of a function where we write

$$f(x) = f(0) + xf'(0) + \dots \quad (2.39)$$

we may consider the external perturbation as x in the above formula and $f'(0)$ would then correspond to the linear response of the system that is determined by the ground state. This analogy with Taylor expansions also shows us that there are several (in fact infinitely many) higher order terms in the total response. Normally such higher order terms are negligible for small to moderate perturbations but must in some cases be considered to correctly describe the system in question. Since we are only interested in the linear response we will neglect higher order terms. These terms also have the nasty property that they depend on the strength of the applied perturbation itself and are thus not ground state properties and of less fundamental interest. Experimentally it is rather straightforward to know whether the system responds in a linear fashion or not. The linear response is always oscillating at the same frequency as the applied perturbation, whereas the higher order terms respond at several higher harmonic frequencies.

2.4.1 Formal development

We will now treat some general theory of linear response functions, this follows closely the treatment in [35].

Suppose that we have a system described by the time independent

Hamiltonian H_0 , suppose also that we are interested in perturbing the system with some small external field $F(t)$ that is turned on at some time t_0 . Furthermore, suppose we know that the field $F(t)$ couples to an operator $\hat{B}(t)$, the total Hamiltonian of the system is then

$$\hat{H}(t) = \hat{H}_0 + F(t)\hat{B} \quad (2.40)$$

and we are now interested in computing the change that is produced on the average of another operator \hat{A} .

For times $t < t_0$ our assumption was that the system Hamiltonian was \hat{H}_0 . The system then obeys the Schrödinger equation

$$i\hbar\partial_t|\psi(t)\rangle = \hat{H}_0|\psi(t)\rangle \quad (2.41)$$

which has a complete set of orthogonal solutions $|\psi_n(t)\rangle$ with associated eigenenergies ϵ_n . We also know that at finite temperatures the occupation probabilities for the different states are $P_n = \frac{1}{Z}e^{-\beta\epsilon_n}$, where $\beta = \frac{1}{k_B T}$ and $Z = \sum_n e^{-\beta\epsilon_n}$ is the partition function which normalizes the probabilities. For this case we may also compute the expectation value of the operator \hat{A} as

$$\langle\hat{A}\rangle_0 = \sum_n P_n \langle\psi_n|\hat{A}|\psi_n\rangle_0. \quad (2.42)$$

We now turn our attention to the perturbed Hamiltonian, equation (2.40), and our goal is now to compute the deviation of the average of \hat{A} from its unperturbed equilibrium value given by equation (2.42). The system still obeys the Schrödinger equation

$$i\hbar\partial_t|\psi(t)\rangle = \hat{H}|\psi(t)\rangle, \quad (2.43)$$

now with the initial condition $|\psi_n(t_0) = |\psi_n\rangle$. The solution to the new Schrödinger equation can be expressed in terms of the unperturbed solutions as

$$|\psi_n(t)\rangle = \hat{U}(t, t_0)|\psi_n\rangle \quad (2.44)$$

where $\hat{U}(t, t_0)$ is the time evolution operator. This operator evolves the state from time t_0 to t . Inserting equation (2.44) into the Schrödinger equation, equation (2.43), we obtain an operator equation for the time evolution operator as

$$i\hbar\partial_t\hat{U}(t, t_0) = \hat{H}\hat{U}(t, t_0) \quad (2.45)$$

with the initial condition $\hat{U}(t_0, t_0) = \hat{1}$. In the absence of any perturbation we assume the Hamiltonian to be time independent and in that case we may integrate equation (2.45) once and obtain the solution for the time evolution operator as

$$\hat{U}(t, t_0) = e^{-\frac{i}{\hbar}\hat{H}_0(t-t_0)} \quad (2.46)$$

which means that the solution to equation (2.41) is

$$|\psi(t)\rangle = e^{-\frac{i}{\hbar}\hat{H}_0(t-t_0)}|\psi(t_0)\rangle \quad (2.47)$$

i.e. the time evolution is simply rotating an unmeasurable phase of the wave functions. Now, in order to add the effect of the time dependent part to the time evolution operator we write

$$\hat{U}(t, t_0) = e^{-\frac{i}{\hbar}\hat{H}_0(t-t_0)}\hat{U}_F(t, t_0) \quad (2.48)$$

where $\hat{U}_F(t, t_0)$ contains the effects of the perturbation. Inserting this definition into equation (2.43) and remembering that $\hat{U}_0(t, t_0)$ obeys equation (2.45) we may obtain an equation of motion for $\hat{U}_F(t, t_0)$ as

$$i\hbar\partial_t\hat{U}_F(t, t_0) = F(t)\hat{B}(t-t_0)\hat{U}_F(t, t_0) \quad (2.49)$$

where

$$\hat{B}(t-t_0) = \hat{U}_0^{-1}(t, t_0)\hat{B}\hat{U}_0(t, t_0) = e^{\frac{i}{\hbar}\hat{H}_0(t-t_0)}\hat{B}e^{-\frac{i}{\hbar}\hat{H}_0(t-t_0)} \quad (2.50)$$

is the operator \hat{B} in the Heisenberg picture. Equation (2.49) is subject to the initial condition $\hat{U}_F(t_0, t_0) = \hat{1}$ and using this we can recast it into an integral equation on the form

$$\hat{U}_F(t, t_0) = \hat{1} - \frac{i}{\hbar} \int_{t_0}^t dt' F(t')\hat{B}(t'-t_0)\hat{U}_F(t', t_0) \quad (2.51)$$

which in general is hard to solve. We can solve it by iteration, i.e. inserting the total expression for $\hat{U}_F(t, t_0)$ into the right hand side of the expression for the same and obtain

$$\hat{U}_F(t, t_0) = \hat{1} - \frac{i}{\hbar} \int_{t_0}^t dt' F(t')\hat{B}(t'-t_0) \left[\hat{1} - \frac{i}{\hbar} \int_{t_0}^{t'} dt'' F(t'')\hat{B}(t''-t_0)\hat{U}_F(t'', t_0) \right]. \quad (2.52)$$

Doing this in an iterative manner we obtain what is known as a Dyson series for the operator $\hat{U}_F(t, t_0)$

$$\begin{aligned}
\hat{U}_F(t, t_0) &= \hat{1} - \frac{i}{\hbar} \int_{t_0}^t dt' F(t') \hat{B}(t' - t_0) + \\
&+ \left(-\frac{i}{\hbar}\right)^2 \int_{t_0}^t dt' \int_{t_0}^{t'} dt'' F(t') \hat{B}(t' - t_0) F(t'') \hat{B}(t'' - t_0) + \dots \\
&+ \left(-\frac{i}{\hbar}\right)^n \int_{t_0}^t dt' \int_{t_0}^{t'} dt'' \dots \int_{t_0}^{t^{n-1}} dt^n \times \\
&\times F(t') \hat{B}(t' - t_0) F(t'') \hat{B}(t'' - t_0) \dots F(t^n) \hat{B}(t^n - t_0) + \\
&\dots
\end{aligned} \tag{2.53}$$

which allows us to obtain the solution to any order in the perturbation $F(t)$. To first order it is enough to keep only the first two terms and then using equation (2.48) we obtain the total time evolution operator to linear order in the perturbation as

$$\hat{U}(t, t_0) = e^{-\frac{i}{\hbar} \hat{H}_0(t-t_0)} \left(\hat{1} - \frac{i}{\hbar} \int_{t_0}^t \hat{B}(t' - t_0) F(t') dt' \right). \tag{2.54}$$

We will also need its hermitian conjugate which is

$$\hat{U}^\dagger(t, t_0) = \left(\hat{1} + \frac{i}{\hbar} \int_{t_0}^t \hat{B}(t' - t_0) F(t') dt' \right) e^{\frac{i}{\hbar} \hat{H}_0(t-t_0)} \tag{2.55}$$

where we have used that $(\hat{B}F)^\dagger = \hat{B}F$ since this quantity appears in the Hamiltonian which needs to be hermitian.

We are now in a position to calculate the expectation value of operators when the perturbation is applied. The starting point is the usual expression for the expectation value

$$\langle \hat{A}(t) \rangle = \sum_n P_n \langle \psi_n(t) | \hat{A} | \psi_n(t) \rangle = \sum_n P_n \langle \psi_n | \hat{U}^\dagger(t, t_0) \hat{A} \hat{U}(t, t_0) | \psi_n \rangle \tag{2.56}$$

and inserting the expressions for time evolution operator from equations

(2.54) and (2.55) we obtain

$$\begin{aligned}
\langle \hat{A}(t) \rangle &= \sum_n P_n \langle \psi_n | \left(\hat{1} + \frac{i}{\hbar} \int_{t_0}^t \hat{B}(t' - t_0) F(t') dt' \right) e^{\frac{i}{\hbar} \hat{H}_0(t-t_0)} \hat{A} \times \\
&\quad \times e^{-\frac{i}{\hbar} \hat{H}_0(t-t_0)} \left(\hat{1} - \frac{i}{\hbar} \int_{t_0}^t \hat{B}(t' - t_0) F(t') dt' \right) | \psi_n \rangle = \\
&= \sum_n P_n \langle \psi_n | e^{\frac{i}{\hbar} \hat{H}_0(t-t_0)} \hat{A} e^{-\frac{i}{\hbar} \hat{H}_0(t-t_0)} | \psi_n \rangle + \\
&\quad + \sum_n P_n \langle \psi_n | \left(\frac{i}{\hbar} \int_{t_0}^t \hat{B}(t' - t_0) F(t') dt' \hat{A}(t - t_0) - \right. \\
&\quad \quad \left. - \frac{i}{\hbar} \hat{A}(t - t_0) \int_{t_0}^t \hat{B}(t' - t_0) F(t') dt' \right) | \psi_n \rangle - \\
&\quad - \left(\frac{i}{\hbar} \right)^2 \int_{t_0}^t \hat{B}(t' - t_0) F(t') dt' \hat{A}(t - t_0) \int_{t_0}^t \hat{B}(t' - t_0) F(t') dt' \quad (2.57)
\end{aligned}$$

where the first term in the last expression is the average of \hat{A} in the absence of the perturbation, and the last term is quadratic in the perturbation and is dropped since we are considering the linear response. Introducing the notation $\sum_n P_n \langle \psi_n | \dots | \psi_n \rangle = \langle \dots \rangle_0$, we are left with

$$\begin{aligned}
\langle \hat{A}(t) \rangle - \langle \hat{A} \rangle_0 &= \frac{i}{\hbar} \int_{t_0}^t dt' F(t') \langle \left(\hat{B}(t' - t_0) \hat{A}(t - t_0) - \right. \\
&\quad \quad \left. - \hat{A}(t - t_0) \hat{B}(t' - t_0) \right) \rangle_0 = \\
&= \frac{i}{\hbar} \int_{t_0}^t dt' F(t') \langle \left(\hat{B}(t' - t_0) \hat{A}(t - t_0) - \hat{A}(t - t_0) \hat{B}(t' - t_0) \right) \rangle_0 = \\
&= -\frac{i}{\hbar} \int_{t_0}^t \langle [\hat{A}(t - t_0), \hat{B}(t' - t_0)] \rangle_0 F(t') dt' \quad (2.58)
\end{aligned}$$

Next, we realize that since the average, $\langle \dots \rangle_0$, is taken with respect to the ground state which is time independent we may shift both times in the commutator above and obtain

$$\langle \hat{A}(t) \rangle - \langle \hat{A} \rangle_0 = -\frac{i}{\hbar} \int_{t_0}^t \langle [\hat{A}(t), \hat{B}(t')] \rangle_0 F(t') dt' \quad (2.59)$$

where we have assumed $t \geq t_0$. Equation (2.59) is an important result as it allows us to calculate the deviation of the operator \hat{A} from its equilibrium

value due to the applied perturbation. We define the function

$$\chi_{A,B}(t, t') = -\frac{i}{\hbar} \langle [\hat{A}(t), \hat{B}(t')] \rangle_0 \quad (2.60)$$

which is known as a susceptibility or a response function.

We may now rewrite the above result into standard notation. Using our knowledge that the unperturbed Hamiltonian is time independent we can perform a change of variables, $\tau = t - t'$, and rewrite equation (2.60) into

$$\chi_{A,B}(\tau) = -\frac{i}{\hbar} \theta(\tau) \langle [\hat{A}(\tau), \hat{B}] \rangle_0. \quad (2.61)$$

and with this definition equation (2.59) becomes

$$\langle \hat{A}(t) \rangle - \langle \hat{A} \rangle_0 = \int_0^{t-t_0} \chi_{A,B}(\tau) F(t - \tau) d\tau. \quad (2.62)$$

Let us now consider the t_0 in equation (2.59) which represents the time when the perturbation is turned on. We are interested in treating this time as very far in the past and thus we send $t_0 \rightarrow -\infty$. The final expression for the deviation of the operator \hat{A} is then

$$\langle \hat{A}(t) \rangle - \langle \hat{A} \rangle_0 = \int_0^{\infty} \chi_{A,B}(\tau) F(t - \tau) d\tau. \quad (2.63)$$

We will often be interested in the response to a periodic perturbation. In this case the perturbation can be written as

$$F(t) = F_{\omega} e^{-i\omega t} + F_{\omega}^* e^{i\omega t} \quad (2.64)$$

or possibly a sum of such terms. There is however a problem with such a perturbation and that is that it does not vanish as $t \rightarrow -\infty$ as required by the machinery developed above. In order to fix this we need to add the term $e^{\eta t}$ to the perturbation, this is equivalent to adding a small imaginary part $i\eta$ to the frequency of the perturbation so that it becomes

$$F(t) = F_{\omega} e^{-i(\omega+i\eta)t} + F_{\omega}^* e^{i(\omega-i\eta)t}. \quad (2.65)$$

As long as η is positive this perturbation will always tend to zero at $t \rightarrow -\infty$. η is known as a convergence factor and is related to an adiabatic switching on of the perturbation. Physically this means that the turning on of the perturbation happens at a time scale $1/\eta$ much longer

than the period of the perturbation and the memory of the system of the turning on is erased. In order to ensure that the η is small enough we will send it to zero $\eta \rightarrow 0^+$ in the end of the calculation.

Inserting equation (2.65) into (2.63) we get

$$\langle \hat{A}(t) \rangle - \langle \hat{A} \rangle_0 = -\frac{i}{\hbar} \lim_{\eta \rightarrow 0^+} \int_0^\infty d\tau \langle [\hat{A}(\tau), \hat{B}] \rangle_0 e^{i(\omega+i\eta)\tau} F_\omega e^{-i\omega t} + c.c \quad (2.66)$$

and defining

$$\chi_{AB}(\omega) = -\frac{i}{\hbar} \lim_{\eta \rightarrow 0^+} \int_0^\infty d\tau \langle [\hat{A}(\tau), \hat{B}] \rangle_0 e^{i(\omega+i\eta)\tau} \quad (2.67)$$

we write

$$\langle \hat{A}(t) \rangle - \langle \hat{A} \rangle_0 = \chi_{AB}(\omega) F_\omega e^{-i\omega t} + c.c \quad (2.68)$$

and performing a Fourier transform of both sides we get

$$\langle \hat{A}(\omega) \rangle = \chi_{AB}(\omega) (F_\omega + F_\omega^*) \quad (2.69)$$

where we have used that $\chi_{AB}(-\omega) = \chi_{AB}^*(\omega)$. Equation (2.69) represents the final answer for periodic perturbations and it implies that the deviation of \hat{A} from its equilibrium value oscillates at the same frequency as the applied perturbation and that the magnitude of the deviation is determined by the strength of the perturbation. That this dependency is linear is an effect of us throwing away all higher order terms with the motivation that if the perturbation F is small then the linear response will dominate.

2.4.2 External electric field: conductivity and dielectric function

To make things more explicit we now consider an example of linear response theory. We will consider the perturbation to be an harmonic electric field at a single frequency and in this case we may compute the objects discussed in section 2.1 such as the conductivity and dielectric function.

We stated earlier that the system has a known Hamiltonian in the absence of the perturbation, we call it \hat{H}_0 . We now couple this Hamiltonian to an electric field, i.e. the perturbation field. We will here consider only

longitudinal fields, i.e. fields that can be written as potentials but linear response theory can be applied to the more general case of transverse fields as well. In the case of longitudinal fields the Hamiltonian of the perturbed system is

$$\hat{H} = \hat{H}_0 + e \int d\vec{r} V(\vec{r}) \hat{n}(\vec{r}) \quad (2.70)$$

where $\hat{n}(\vec{r}) = \sum_i \delta(\vec{r} - \hat{r}_i)$ is the electron density operator. The potential $V(\vec{r})$, which can always be found for longitudinal fields, couples to the electron density and thus changes the energy in response to the perturbation.

The task now is to compute some macroscopic property, we will chose the electrical current \vec{j} , and then relate our microscopic expression i.e. the expression obtained from our linear response treatment, to the macroscopic properties in section 2.1. The longitudinal current in response to a longitudinal vector potential is [35]

$$\vec{j}_L = \frac{e}{c} \chi_L(q, \omega) \vec{A}(q, \omega) \quad (2.71)$$

where \vec{A} is the longitudinal vector potential and χ_L means current-current susceptibility. We also know from Ohm's law that

$$e\vec{j} = \sigma E, \quad (2.72)$$

where the extra e comes from the fact that we have defined \vec{j} as the current density instead of the electrical current density. Now, using $\vec{E} = \frac{1}{c} \partial_t \vec{A} = i\frac{\omega}{c} \vec{A}$ we can identify

$$\sigma(q, \omega) = -\frac{ie^2}{\omega} \chi_L(q, \omega). \quad (2.73)$$

We may in the longitudinal case, using the continuity equation, relate χ_L to the density-density response. The continuity equation in its original form expresses charge conservation as

$$\partial_t n + \nabla \cdot \vec{j} = 0 \quad (2.74)$$

where n is the electron density and \vec{j} is the current density. Performing a Fourier transform we obtain the continuity equation in Fourier space as

$$\omega n = qj \quad (2.75)$$

where we have used the fact that we deal with longitudinal fields, $\vec{q} \parallel \vec{j}$, so that $\vec{q} \cdot \vec{j} = qj$. Remembering that the current-current susceptibility is written as the expectation value of a commutator in the form $\langle [\hat{j}, \hat{j}] \rangle_0$, see equation (2.67), we can use equation 2.75 and relate

$$\langle [\hat{j}, \hat{j}] \rangle_0 = \frac{\omega^2}{q^2} \langle [\hat{n}, \hat{n}] \rangle_0 \quad (2.76)$$

meaning that we can relate the susceptibilities as

$$\chi_L = \frac{\omega^2}{q^2} \chi_{nn}. \quad (2.77)$$

This expression lets us rewrite the conductivity in equation 2.73 in terms of the density-density susceptibility as

$$\sigma(q, \omega) = -\frac{ie^2\omega}{q^2} \chi_{nn}(q, \omega). \quad (2.78)$$

Of course, equations 2.73 and 2.78 are equivalent but we will find it convenient to work with the density-density response rather than the current-current response. The density-density susceptibility is sometimes called the polarizability and is then denoted Π . We will use this notation in some of what follows below.

Note that what we have called conductivity above will in the case of 2-dimensional electron gases become sheet conductivities. This means that equation (2.11), relating conductivity and dielectric function, does not hold, it only holds for 3-dimensional gases. In order to determine the two dimensional dielectric function we turn to the Random Phase Approximation in the next section.

2.5 Random phase approximation

For a derivation of the RPA dielectric function we refer to Appendix A. In the present section we will only state the final results and consider the effects of dimensionality of sheets.

Since we are interested in the graphene response to perturbations it is important to remember that graphene is 2-dimensional whereas the sur-

rounding space is 3-dimensional. This point might seem trivial but is actually important to remember and as stated in the end of the previous section this forbids us to use equation (2.11) to relate conductivity and dielectric function. It is also important to realize that the perturbing potential is not entirely confined to the graphene but may have an extension into the surrounding space. The potential will be assumed to have the harmonic form $e^{i\vec{x}\cdot\vec{q}-\beta|z|}$ where \vec{x} and \vec{q} are in the graphene plane, z is the direction perpendicular to the plane and $\beta = \sqrt{q^2 - \omega^2/c^2}$. This describes a wave propagating in the graphene plane and is exponentially decaying in the z -direction.

The RPA result for the dielectric function in a graphene sheet is, see equation (A.18),

$$\epsilon(q, \omega) = 1 + \frac{2\pi e^2 \beta}{q^2 \epsilon_r} \Pi(q, \omega) \quad (2.79)$$

where ϵ_r is the relative permittivity of the surrounding medium and the polarizability $\Pi(q, \omega)$ is given by equation (A.20). In the case of different media on either side of the graphene we choose ϵ_r as the average of the two, i.e. $\epsilon_r = \frac{\epsilon_1 + \epsilon_2}{2}$.

Notice that if $q \gg \omega/c$ then $\beta \approx q$ and the result for the dielectric function becomes

$$\epsilon(q, \omega) = 1 + \frac{2\pi e^2}{q \epsilon_r} \Pi(q, \omega) \quad (2.80)$$

which is usually referred to as the 2-d dielectric function.

Equation (2.79) is the RPA result for the dielectric function of a surface but the simplified version in equation (2.80) is very often used instead. The reason is that very often when considering plasmons in graphene the two different dielectric functions coincide, i.e. $q \gg \omega/c$, and the form in (2.80) is more convenient to work with analytically.

2.6 Plasmons and related quantities

The simplest way to describe plasmons is to say that they are collective charge density oscillations in a medium. As this will produce a net charge

separation it means that there will also be an associated electric field to the density oscillation. Under the right conditions this oscillation becomes self-sustaining and may propagate in the medium.

An important remark is that there are different kinds of plasmons and the nomenclature is not entirely well defined. There are localized plasmons, transverse plasmons and longitudinal plasmons. There is also a distinction between bulk plasmons and surface plasmons. The transverse and longitudinal plasmons are often referred to as plasmon-polaritons where the word "polariton" means that the plasmon is a mixture, or a hybridization, of light and charge. Localized plasmons usually occur around metal objects deposited on metallic surfaces and are often treated within Mie theory. We will not consider such plasmon modes.

Transverse plasmons are propagating with the electric field polarized perpendicular to the propagation direction. In this sense they behave much like photons and it turns out that the transverse plasmons and their behavior play a significant role in the behavior of metals and their reflective properties. The transverse plasmons are sometimes called Transverse Electric (TE) modes. Longitudinal plasmons have an associated electric field that is parallel to the direction of propagation. Such modes are sometimes called Transverse Magnetic (TM) modes since their associated magnetic field is perpendicular to the direction of propagation.

2.6.1 Surface plasmon polaritons in metal-dielectric interfaces

The conventional surface plasmon-polaritons exist at the interface between a metal and a dielectric. Let us consider the case of two half spaces where the half-space $z > 0$ is a dielectric (insulating) material and the half space $z < 0$ is a metal. In order to treat this case we combine equations (2.2) and (2.3) we get the equation

$$\nabla \times \nabla \times \vec{E} = -\mu_0 \frac{\partial^2 \vec{D}}{\partial t^2} \quad (2.81)$$

which can be rewritten into ($c=1$)

$$\nabla^2 \vec{E} - \epsilon \frac{\partial^2 \vec{E}}{\partial t^2} = 0 \quad (2.82)$$

where we have assumed that $\epsilon(x)$ does not vary too much over one wavelength in distance. Rather than spending much time on analyzing the possible solutions to equation (2.82) and its analogue for the magnetic field around the metal-dielectric interface we will simply state the result of such an analysis and refer to [31] for further details.

The analysis considers modes that are assumed to be propagating at the interface along the x -direction with wave vector k and we furthermore consider the mode to be exponentially decaying in the z -direction into both the metal and the dielectric. Such a configuration seems natural for a mode confined at the interface. Two important results of such an analysis are worth pointing out. First, it turns out that confined surface modes can only exist at interfaces between materials with opposite signs of the real part of their dielectric functions. This is why we in our treatment initially assumed a metal-dielectric interface. Metals exhibit negative real part of the dielectric functions whereas dielectrics have a real positive dielectric constant. Second, the interface modes can only exist with electric field parallel to the propagation direction and magnetic field perpendicular to it. Such modes are referred to as TM (transverse magnetic) or longitudinal modes (the electric field is longitudinal).

The final expression for the dispersion of the longitudinal modes at the interface is

$$k = \omega \sqrt{\frac{\epsilon_1(\omega)\epsilon_2(\omega)}{\epsilon_1(\omega) + \epsilon_2(\omega)}}. \quad (2.83)$$

As stated earlier we have the requirement of opposite signs of the real parts of the dielectric functions in order to have confined modes. Looking at equation (2.83) we see that this implies that in order for the mode to be propagating, i.e. k is real, we need $\text{Re } \epsilon_1(\omega) + \text{Re } \epsilon_2(\omega) < 0$. The dispersion of the interface modes will be considered further in section 2.7.

2.6.2 Surface plasmon polaritons in two-dimensional sheets

Plasmons in two-dimensional sheets, e.g. graphene, are electron density oscillations in the graphene sheet rather than being interface modes. In contrast to the interface modes considered in the previous section there is

no constraint on the properties of the surrounding space. However, usually the graphene sheet is deposited on top of a dielectric substrate and the other side is subjected to air or the graphene could be "sandwiched" between two dielectric substrates.

Following [26] we consider the longitudinal mode in the graphene, surrounded by half spaces with dielectric constants with ϵ_1 and ϵ_2 respectively. Assuming as previously that we have modes that decay away from the graphene sheet and now also including the conductivity of the graphene when matching boundary conditions of the Maxwell equations we arrive at [26]

$$q = \frac{\epsilon_1 + \epsilon_2}{2} \frac{2i\omega}{\sigma(q, \omega)} \quad (2.84)$$

where q is the in-plane wave vector. Inserting the definition of the conductivity from equation (2.78)

$$\sigma(q, \omega) = -i \frac{\omega e^2}{q^2} \Pi(q, \omega) \quad (2.85)$$

we arrive at the equation

$$\frac{\epsilon_1 + \epsilon_2}{2} + \frac{e^2}{2q} \Pi(q, \omega) = 0. \quad (2.86)$$

This resembles our definition of the dielectric function in equation (2.80), but is lacking a factor 4π in front of the $\Pi(q, \omega)$. We attribute this to different normalization conventions in the Fourier transforms and k -space integrals. So, inserting an extra factor of 4π , this is nothing but the statement that the 2-d dielectric function from equation (2.80) equals zero, i.e.

$$\epsilon(q, \omega) = 0. \quad (2.87)$$

Solving equation (2.87) we obtain the plasmon dispersion $\omega_p(q)$. In section 2.7 we will investigate the plasmon dispersion for some different models of the electron gas.

2.6.3 Wave localization

A common feature for the solutions to equation (2.83) and equation (2.87) is that they will have a shorter wavelength than free space light at the same

frequency. Since the wavenumber $k = \frac{2\pi}{\lambda}$ is inversely proportional to the wavelength, shorter wavelength is equivalent to having larger wavenumber.

Wave localization is the reason for the need of sub-wavelength patterning of the surface where we want to excite plasmons. The sub-wavelength patterning allows for the interaction between the modes with different wavelength that would otherwise be strongly suppressed due to the big momentum mismatch.

The wave localization is conveniently quantified by λ_0/λ_p which measures how many wavelengths of the plasmon mode that can fit in the size of the free space wavelength at the same energy. An interesting property of wave localization is that it usually comes together with an enhancement of the electric field strength. As we discussed in the introduction this can lead to large enhancements of signatures that are otherwise too weak to measure.

2.7 Two-dimensional electron gases

Drude gas

The simplest type of electron gas is the *Drude gas* in which the electrons do not interact amongst themselves but only interact with impurities and/or the lattice that surrounds them and the typical time between two such interactions is τ . τ is called the relaxation time of the gas and its inverse $\gamma = 1/\tau$ is the collision frequency. In the Drude model the electrons are subject to an external electric field that applies a force on the electrons and they are also damped with the frequency γ . The equation of motion for the electrons is

$$m\ddot{\vec{x}} = -m\gamma\dot{\vec{x}} - e\vec{E} \quad (2.88)$$

and assuming a common harmonic time dependence $e^{-i\omega t}$ we get

$$-m\omega^2\vec{x} = im\gamma\omega\vec{x} - e\vec{E} \quad (2.89)$$

which has the solution

$$\vec{x} = \frac{e}{m(\omega^2 + i\gamma\omega)}\vec{E}. \quad (2.90)$$

The macroscopic polarization field is given by $\vec{P} = -ne\vec{x}$ and we have a linear response $\vec{P} = \chi\vec{E}$ so that $\chi = -\frac{ne^2}{m(\omega^2 + i\gamma\omega)}$. We also know that $\epsilon = 1 + \chi$ so that

$$\epsilon(\omega) = \epsilon_0 - \frac{ne^2}{m(\omega^2 + i\gamma\omega)}. \quad (2.91)$$

The plasma frequency of the free electron gas is defined as $\omega_p^2 = \frac{ne^2}{\epsilon_0 m}$, inserting this we get

$$\text{Re } \epsilon(\omega)/\epsilon_0 = 1 - \frac{\omega_p^2}{\omega^2 + \gamma^2} \quad (2.92)$$

$$\text{Im } \epsilon(\omega)/\epsilon_0 = \frac{\omega_p^2 \gamma}{\omega(\omega^2 + \gamma^2)}. \quad (2.93)$$

We now turn to the case of negligible damping and the dielectric constant becomes

$$\epsilon(\omega)/\epsilon_0 = 1 - \frac{\omega_p^2}{\omega^2}. \quad (2.94)$$

Let us recall the discussion about interface plasmons in section 2.6. We will assign the dielectric function in equation (2.94) to the metal in the half space $z < 0$ and for simplicity we will use air as the insulator with which the metal-dielectric interface is created. Inserting this into equation (2.83) we obtain two positive frequency solutions for every wave vector k . In figure 2.2 we plot both frequency branches versus wave vector k and we also add the light line $\omega = k$.

Figure 2.2 shows two modes, since $k = \frac{2\pi}{\lambda}$ the red, high energy mode has a longer wavelength than the free space light at the same frequency. Correspondingly, the blue mode has a shorter wavelength than the free space light for any given frequency. Figure 2.3 shows the wave localization for the confined mode (blue line). We see in the figure that the localization seems to increase as we increase the wavenumber. However, this is an effect of our assumption of no imaginary part (losses) of the dielectric function. Including losses the confinement would at some point exhibit a maximum and then decrease. Also, in figure 2.2 we see that the group velocity $\frac{\partial\omega}{\partial k}$ approaches zero when the confinement is large, meaning that these modes eventually are not propagating at all but are stationary modes

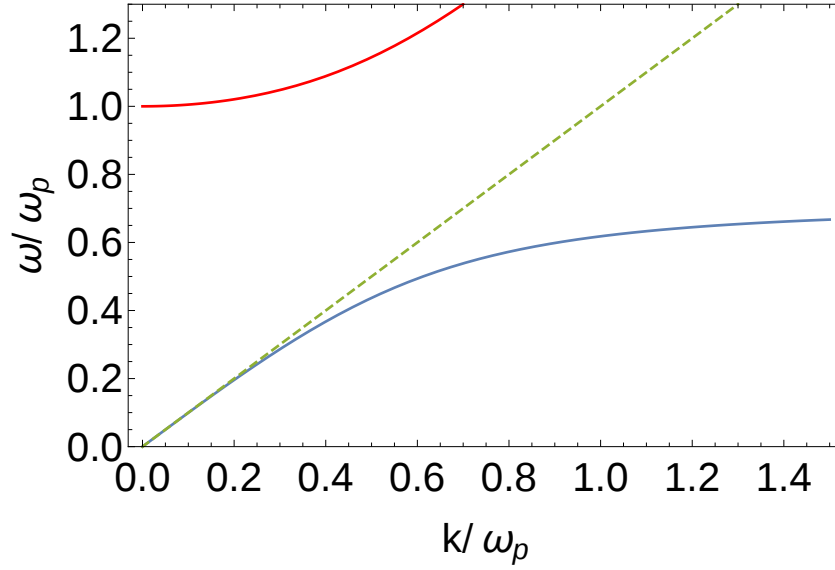


Figure 2.2: The two positive frequency branches for the interface modes between a dielectric and a metal described by the simple Drude dielectric function. Also plotted in the middle green line is the light line $\omega = k$.

at the interface.

Parabolic two-dimensional electron gas

We now turn to a more microscopic picture and consider a 2-dimensional electron gas with parabolic dispersion and with only one band. Even though real systems often will contain multiple bands and thus also have interband transitions, which are of course absent in the single band model, it is nevertheless instructive to investigate the simplest case.

The unperturbed Hamiltonian for massive electrons is

$$\hat{H}_0 = \frac{\hat{p}^2}{2m} \quad (2.95)$$

where m is the effective band mass and need not be the bare electron mass. The 2-dimensional dielectric function for the parabolic band at $T = 0$ was first calculated by Stern [36] in 1967 and the calculation can be found in Appendix C of this thesis. The 2-dimensional dielectric function is sometimes referred to as the 2-dimensional Lindhard function after Jens Lindhard who first computed the 3-dimensional counterpart in 1954 [37].

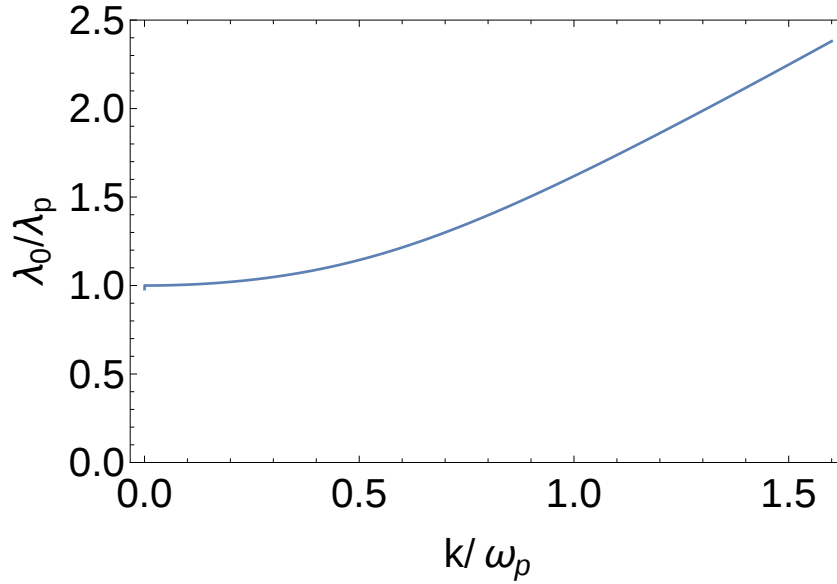


Figure 2.3: The wave localization of the confined mode in figure 2.2.

From [36] we also get that the long wavelength (small k) plasmon dispersion for the 2DEG is

$$\omega_p = \sqrt{\frac{2\pi e^2 n k}{\epsilon_r^* \epsilon_0 m}} \quad (2.96)$$

where $\epsilon_r^* = (\epsilon_1 + \epsilon_2)/2$ is the average of the relative permittivity of the media surrounding the 2DEG, m is the effective band mass and n is the electron density. Notice the $\omega \propto \sqrt{k}$ behavior that is typical for 2-dimensional plasmons and also the dependence on \sqrt{n} .

Dirac two-dimensional gas

The physics of the two dimensional Dirac electron gas was treated in section 2.3 and we here only reprint the Hamiltonian for a single valley and single spin, equation (2.29)

$$\hat{H}_D = \begin{pmatrix} 0 & k_x - ik_y \\ k_x + ik_y & 0 \end{pmatrix}. \quad (2.97)$$

This Hamiltonian describes particles with a linear dispersion relation and has a two band structure that touches at zero energy. The band dispersion is $\epsilon_{\vec{k},s} = s v_F |\vec{k}|$ where $s = \{+, -\}$ is the band index and denotes either the valence band (-) or the conduction band (+). Performing the same

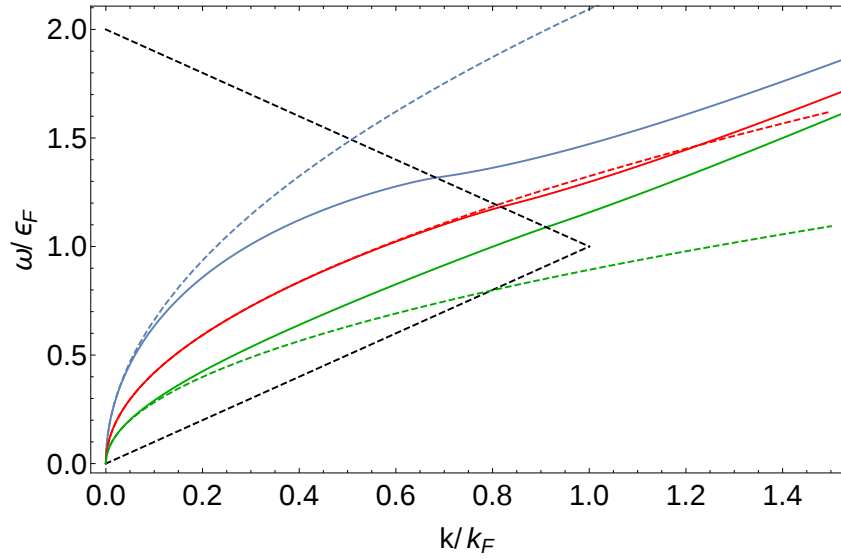


Figure 2.4: The plasmon dispersion in graphene for three different dielectric environments. Solid lines are full numerical solutions and the dashed lines are the long wavelength solutions from equation (2.98). All cases have vacuum on one side of the graphene, the other side is vacuum (blue lines), dielectric with $\epsilon_r = 4$ (red lines) and dielectric with $\epsilon_r = 10$ (green lines). The black dashed lines represent a triangle within which the imaginary part of the polarizability is zero and the plasmons are undamped.

calculation as for the parabolic 2DEG but now with the linear dispersion in the polarizability the answer at $T = 0$ can be found in Appendix D. This calculation was first performed in [20, 21].

Performing an expansion of $\Pi(q, \omega)$ at small k and solving the plasmon condition, equation (2.87), we obtain the long wavelength plasmon dispersion

$$\omega_p = \sqrt{\frac{e^2 \epsilon_F k}{2\pi \epsilon_r^* \epsilon_0}} = \sqrt{\frac{\hbar v_F e^2 \sqrt{n} k}{2\sqrt{\pi} \epsilon_r^* \epsilon_0}}, \quad (2.98)$$

see appendix D. Here $\epsilon_r^* = (\epsilon_1 + \epsilon_2)/2$ is the average of the relative permittivity of the surrounding media. Comparing this with the long-wavelength (small k) answer for the 2DEG plasmons in equation (2.96) we see that they both are proportional to \sqrt{k} but the density dependence is for the Dirac case $\omega_p \propto n^{1/4}$ instead of $\omega_p \propto \sqrt{n}$ as in the 2DEG case.

Figure 2.4 shows the numerical dispersion, full lines, and the long wavelength dispersion from equation (2.98) (dashed lines) for three different dielectric environments (see figure caption). It is clear that the analytic plasmon dispersion is only valid at small k/k_F and for higher values of

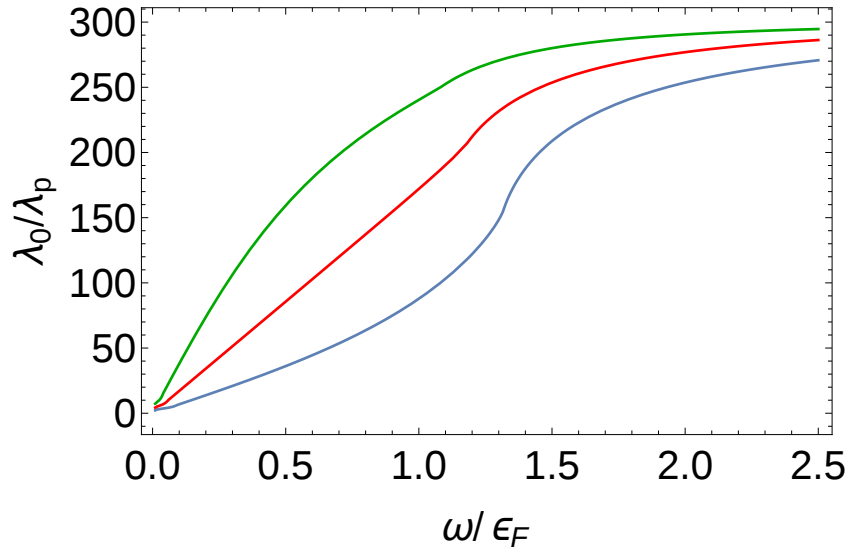


Figure 2.5: The wave localization in graphene obtained from the numerical solutions for the three dielectric environments in figure 2.4. All cases have vacuum on one side of the graphene, the other side is vacuum (blue line), dielectric with $\epsilon_r = 4$ (red line) and dielectric with $\epsilon_r = 10$ (green line).

k/k_F there are clear deviations from the numerical results. Interestingly the deviation depends on the dielectric environment and at some value of ϵ_r^* the analytic expression crosses over from mainly overestimating the energy (blue dashed line) for a certain k/k_F to instead mainly underestimating the energy (green dashed line) of the plasmon.

From the dispersion curves shown in figure 2.4 it is possible to compute the wave localization obtained in graphene. This is shown in figure 2.5. Comparing with the localization for the interface plasmons within the Drude model, see figure 2.3, we see that we can obtain much larger localization using the graphene plasmons. In the interface plasmons the localization is of order 10 whereas in graphene the localization is of order 100, one order of magnitude in difference.

Chapter 3

Scattering Results

In this chapter we consider a graphene sheet with nanostructuring on top, to create an in-plane lattice constant, depicted in figure 3.4. As alluded to previously in the thesis, the nanostructuring is necessary to allow plasmon excitation in the graphene surface. Using the scattering results from section 2.2 together with the graphene conductivity from section 2.6 we may investigate the reflection, transmission and absorption of a graphene surface.

We start out by briefly considering a graphene surface without any nanostructuring, this can be thought of as $k/k_F = 0$. This is because we are considering normal incidence of light so the wave vector of the light is perpendicular to the surface, and k denotes in-plane momentum. Figures 3.1-3.3 show the reflection, transmission and absorption of an ungrated graphene surface. Our results agree with those in [38]. The sheet is reflective for very low energies and then becomes almost perfectly transmissive. At twice the Fermi energy it becomes possible to excite electron-hole pairs that may absorb energy, see figure 1.1. This leads to the non-zero absorption and we get a corresponding lowering of the transmission while the reflection remains low. Notice that we reproduce the experimentally verified value of 2.3% absorption.

We now proceed to investigate light scattering of a nanostructured graphene surface.

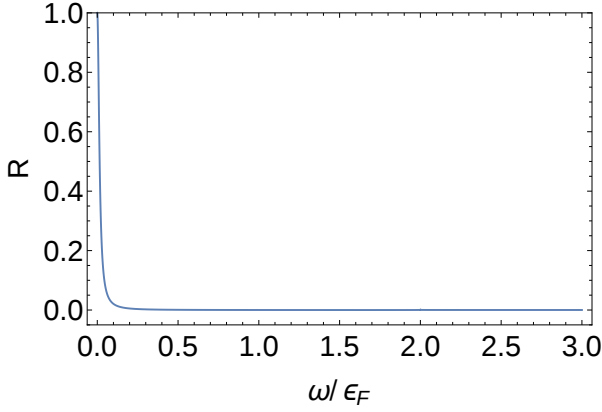


Figure 3.1: Reflection of an ungrated and suspended graphene sheet.

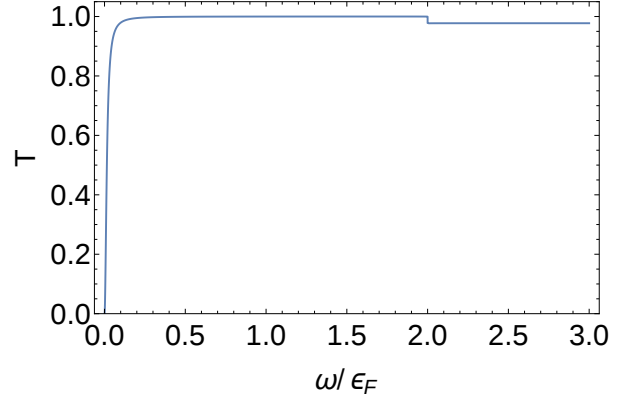


Figure 3.2: Transmission of an ungrated and suspended graphene sheet.

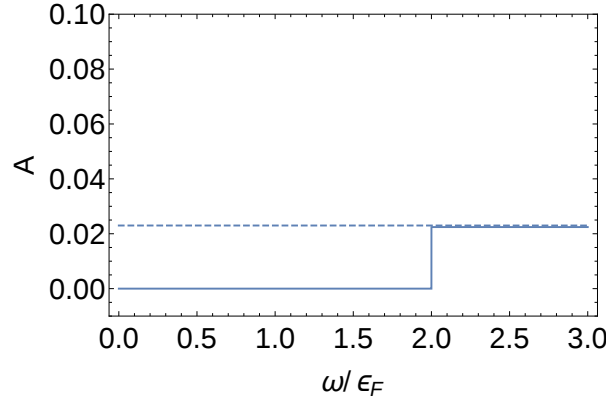


Figure 3.3: Absorption of an ungrated and suspended graphene sheet. The dashed line is 2.3% .

3.1 Light scattering results of a nanostructured graphene surface

An illustration of a graphene sheet with nanostructuring is shown in figure 3.4. Such a nanostructure is called a grating, the distance d in the figure is called the grating distance and should match the wavelength of the plasmons. The grating distance is related to the induced momentum via [31]

$$k = \frac{2\pi}{d}. \quad (3.1)$$

In order to investigate the light scattering properties of a graphene sheet with nanostructuring we make vertical cuts in the dispersion plots, see figures 3.8, 3.12 and 3.16. Physically, one such cut means that we fix the grat-

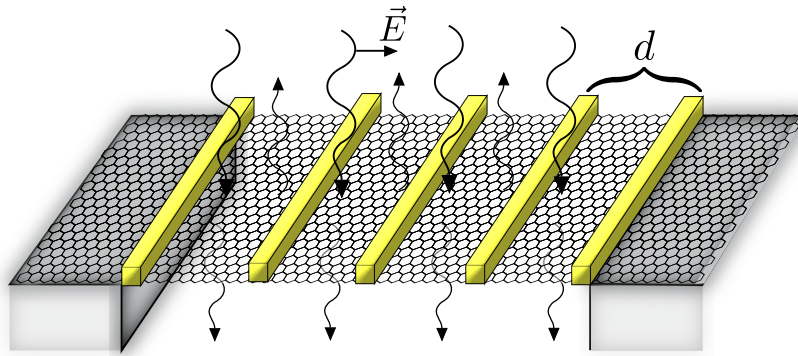


Figure 3.4: A nanostructured graphene sheet that is suspended. This is a reprint of figure 1.2 in the introduction.

ing distance and the Fermi energy ¹ and making several such cuts means that we are considering several physical implementations (Fermi energy and grating distance) for the cases of suspended graphene and graphene on the two different dielectric substrates. We point out that the resonances occur when the energy cut crosses the plasmon dispersion. We are always considering normal incidence of the light.

We will see that at zero temperature, which we are considering, the relevant energy scale for the light scattering behavior at the plasmon resonance is the crossing of the black dashed triangle in the dispersion plots in figures 3.8, 3.12 and 3.16. This triangle signifies the transition between the region without particle-hole damping of the plasmon (inside triangle) and the region with particle-hole damping (outside triangle). Inside the triangle there is an absence of damping from particle-hole excitations because the excitation of such states is forbidden due to energy and momentum conservation.

3.1.1 Suspended graphene

The first case we consider is light scattering from a suspended graphene sheet with vacuum on both sides. Figures 3.5-3.7 show the light scattering results, the differently colored lines correspond to the cut with the same color in figure 3.8. We point out the quite obvious fact that in the absence of the graphene sheet (and grating) the transmission should be unity. This

¹Actually we fix the ratio $k/k_F = \frac{2\pi v_F}{d\epsilon_F}$ so it is $d \cdot \epsilon_F$ that is fixed.

is also what we observe in the results, except when we are close to resonance with the plasmons. When the plasmon resonance lies inside the triangle in figure 3.8 (blue dashed cut and yellow dashed cut) we observe an enhancement of the reflection and outside the triangle the reflection peaks are suppressed and we get some absorption (green dashed cut and red dashed cut). This absorption is quite high in a narrow energy range. When the plasmon resonance is located far from the triangle we see that the transmission on the resonance is getting larger and we seem to regain full transmission even at the plasmon resonance.

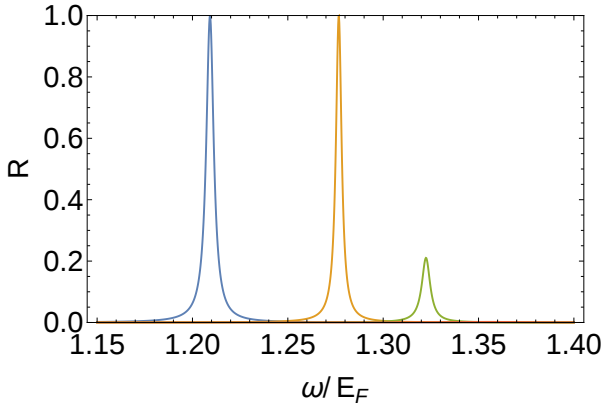


Figure 3.5: Reflection of suspended graphene.

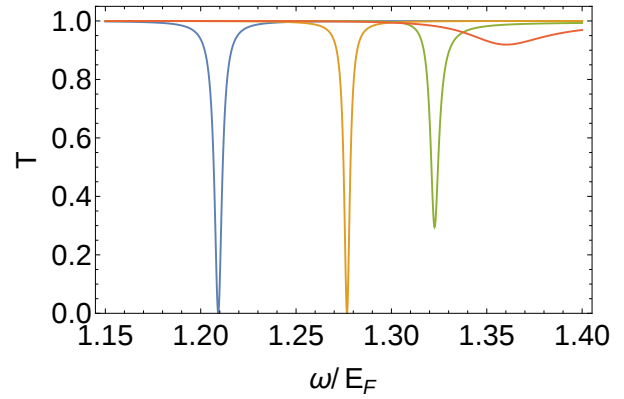


Figure 3.6: Transmission of suspended graphene.

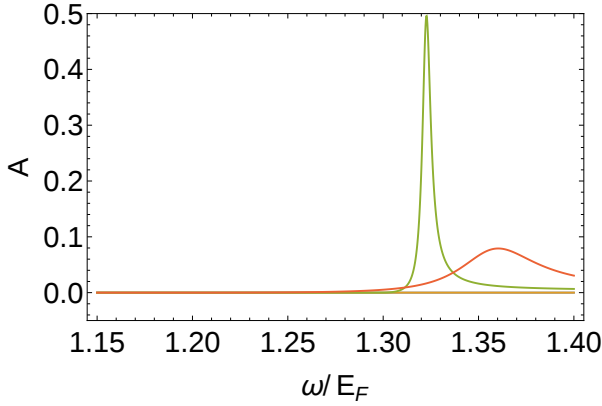


Figure 3.7: Absorption of suspended graphene.

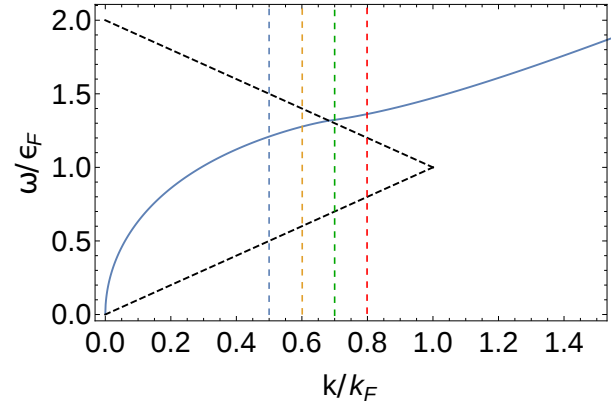


Figure 3.8: Dispersion cuts for suspended graphene.

3.1.2 Graphene on dielectric substrate with $\epsilon_r = 4$

We now consider the graphene to be deposited on top of a dielectric substrate with $\epsilon_r = 4$. In contrast to the suspended case the transmission is not unity in the absence of the graphene. Using our formulas for transmission and reflection in section 2.2 with no graphene we obtain for normal

incidence

$$R = \frac{1}{9} \approx 0.11 \quad (3.2)$$

$$T = \frac{8}{9} \approx 0.89 \quad (3.3)$$

and the absorption in this case must be zero. Figures 3.9-3.11 show the light scattering results for the case of the graphene present. The colored lines correspond to the cuts with the same color in figure 3.12. We see that off resonance we obtain the values in equations (3.2) and (3.3) for the reflection and transmission.

The behavior in figures 3.9-3.11 is much the same as the suspended case on resonance, with peaks in the reflection and dips in the transmission. There are also peaks in the absorption when the plasmon resonances are outside of the triangle (green dashed cut and red dashed cut).

3.1.3 Graphene on dielectric substrate with $\epsilon_r = 10$

For the case of a substrate with $\epsilon_r = 10$ we get that without the graphene we have

$$R \approx 0.27 \quad (3.4)$$

$$T \approx 0.73. \quad (3.5)$$

In figures 3.13-3.15 we show the scattering results with the nanostructured graphene present. The colored lines correspond to the cuts with the same color in figure 3.16. The results behave more or less in the same manner as the previous case for graphene on a dielectric substrate.

3.2 Investigation of scattering resonances

In the previous section we investigated scattering coefficients for energy cuts at some specific values of k/k_F . We clearly saw that the scattering behavior changed between when the plasmon resonance was inside the

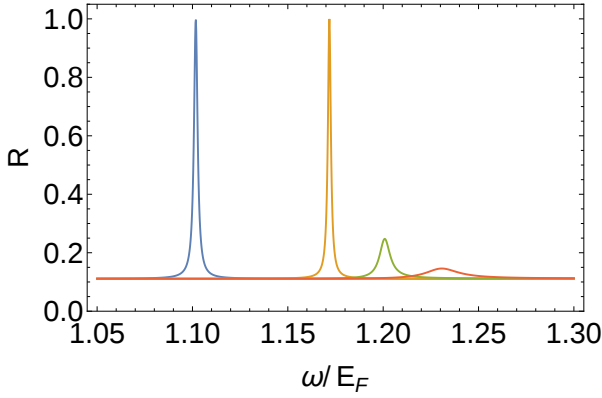


Figure 3.9: Reflection of graphene on a substrate with $\epsilon_r = 4$.

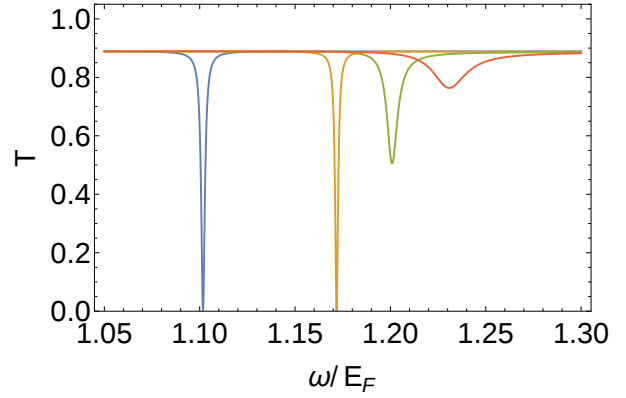


Figure 3.10: Transmission of graphene on a substrate with $\epsilon_r = 4$.

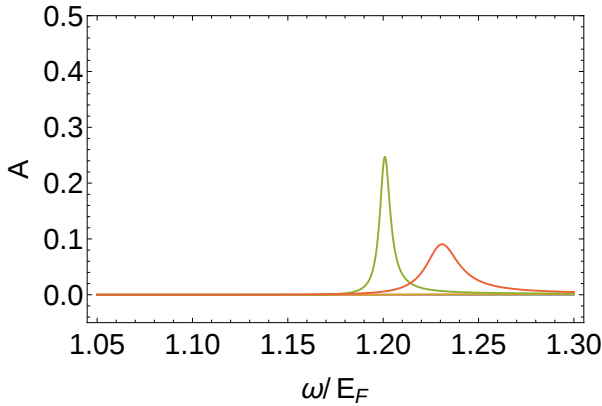


Figure 3.11: Absorption of graphene on a substrate with $\epsilon_r = 4$.

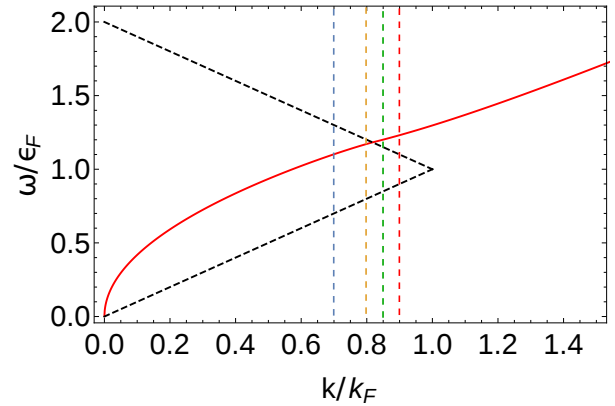
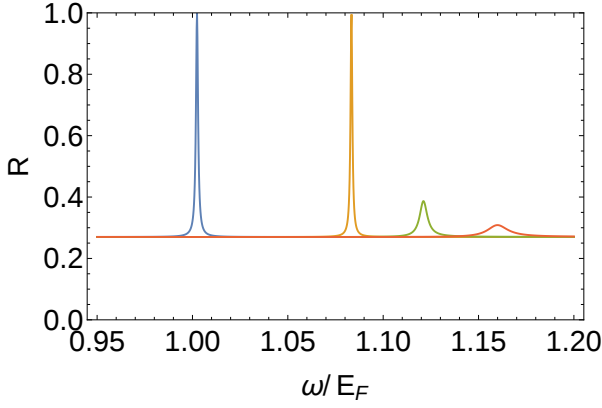
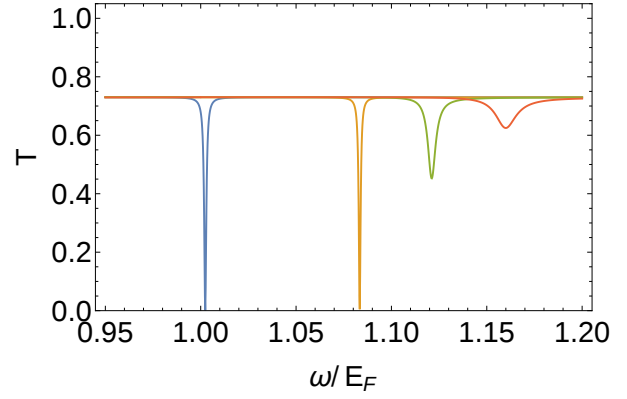
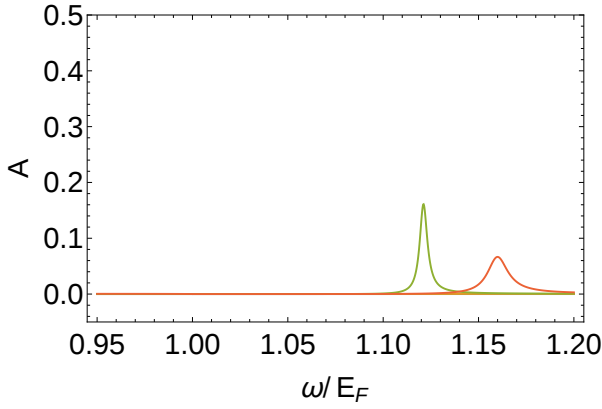
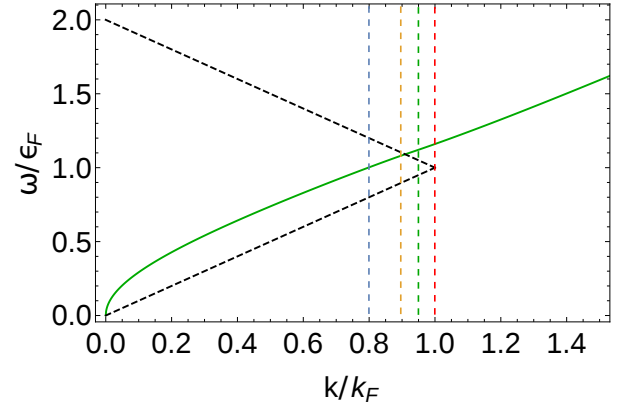


Figure 3.12: Dispersion cuts for graphene on a substrate with $\epsilon_r = 4$.

triangle and when the resonance was outside it. In order to investigate the scattering in more detail we here plot the scattering coefficients along the plasmon dispersion, i.e. we fix the relationship between ω and k so that we are always on the plasmon dispersion curve. This is done in order to look at the maximum plasmon response. We also look at the widths of the resonance peaks along the dispersion.

3.2.1 Scattering coefficients along the plasmon dispersion

Figures 3.17-3.19 show the scattering coefficients along the plasmons dispersions, i.e. the peak/dip heights, for suspended graphene, graphene on a substrate with $\epsilon_r = 4$ and $\epsilon_r = 10$. In these figures we clearly see that the plasmons exhibit three distinctively different behaviors. For low energies the plasmon makes the sheet very reflective on resonance but as the energy of the plasmon increases to just cross out of the triangle we obtain a rather

Figure 3.13: Reflection of graphene on a substrate with $\epsilon_r = 10$.Figure 3.14: Transmission of graphene on a substrate with $\epsilon_r = 10$.Figure 3.15: Absorption of graphene on a substrate with $\epsilon_r = 10$.Figure 3.16: Dispersion cuts for graphene on a substrate with $\epsilon_r = 10$.

large absorption of up to 50%. As we further increase the energy the absorption quickly subsides and we see that on resonance the transmission becomes large. This transmissive behavior is the same behavior as the sheet has when we are far off resonance, this implies that as we increase the energy of the plasmons to lie far above the Fermi energy, the effect of the plasmons becomes small. In fact, we can see in figures 3.17-3.19 that around $\omega/E_F = 1.5$ the reflection, transmission and absorption on resonance tend towards the off-resonant values.

3.2.2 Resonance widths

Figures 3.20-3.22 show the widths of the plasmon resonance peaks as a function of the peak position in frequency (plasmon resonance frequency). We always measure the full width at half maximum (FWHM), we denote it

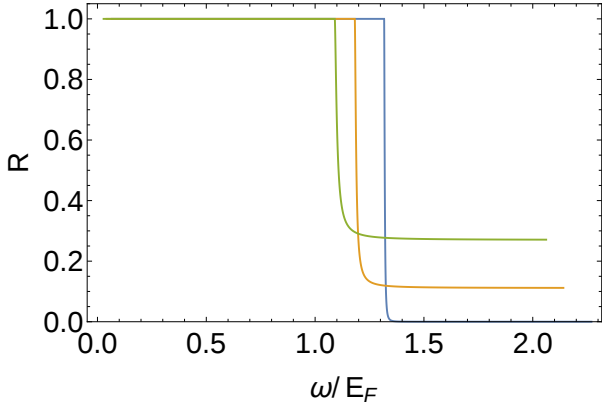


Figure 3.17: Reflection along the plasmon dispersion in graphene. Suspended graphene (blue line), graphene on substrate with $\epsilon_r = 4$ (yellow) and graphene on substrate with $\epsilon_r = 10$ (green).

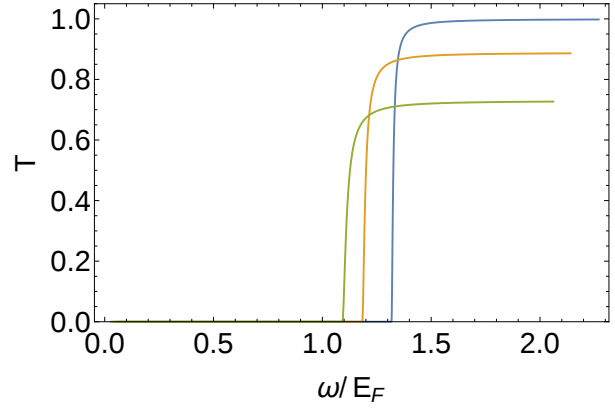


Figure 3.18: Transmission along the plasmon dispersion in graphene. Suspended graphene (blue line), graphene on substrate with $\epsilon_r = 4$ (yellow) and graphene on substrate with $\epsilon_r = 10$ (green).

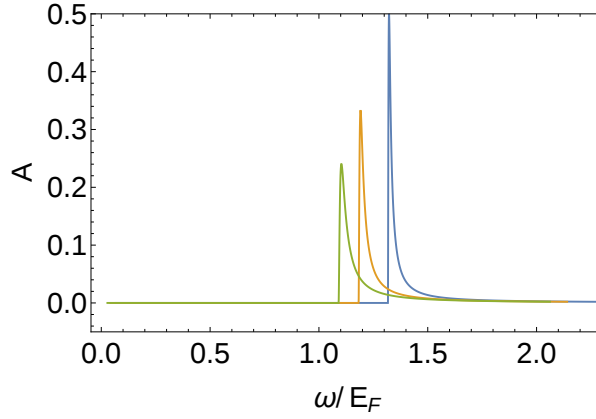


Figure 3.19: Absorption along the plasmon dispersion in graphene. Suspended graphene (blue line), graphene on substrate with $\epsilon_r = 4$ (yellow) and graphene on substrate with $\epsilon_r = 10$ (green).

with γ . In all three figures we observe a sharp transition that represent the transition from the inside of the triangle to the outside. We see that inside the triangle (low energies) the reflection width and transmission width are the same, this comes from the the fact that in this region $R + T = 1$ so a peak in reflection must come together with an equal dip in transmission. Figure 3.22 shows that inside the triangle the absorption width is zero, this is natural since there is no absorption peak at all in this case, this can be seen in figure 3.19 where the absorption is exactly zero for energies inside the triangle.

Inside the triangle the interpretation we make is that the width rep-

resents the coupling between the electromagnetic field and the plasmon resonance. This interaction is created by the presence of the grating that allows for a momentum matching between the incoming radiation and the plasmon. When the plasmon dispersion crosses out from the triangle we obtain a second width, the absorption width. This new decay channel represents plasmon decay into electron hole pairs, as previously stated this can only happen outside the triangle.

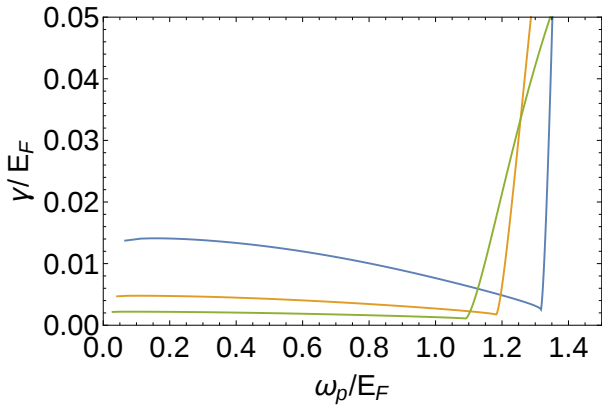


Figure 3.20: Reflection peak width of graphene. Suspended graphene (blue line), graphene on substrate with $\epsilon_r = 4$ (yellow) and graphene on substrate with $\epsilon_r = 10$ (green).

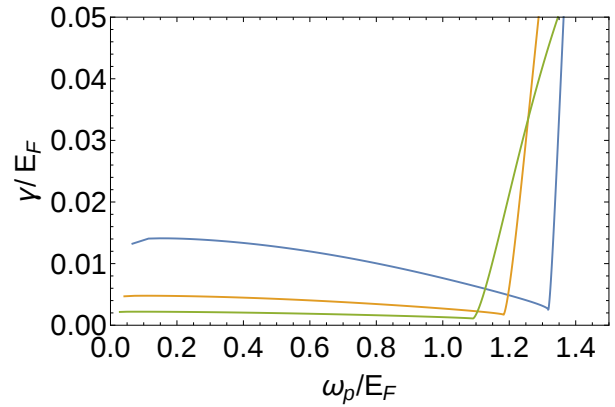


Figure 3.21: Transmission peak width of graphene. Suspended graphene (blue line), graphene on substrate with $\epsilon_r = 4$ (yellow) and graphene on substrate with $\epsilon_r = 10$ (green).

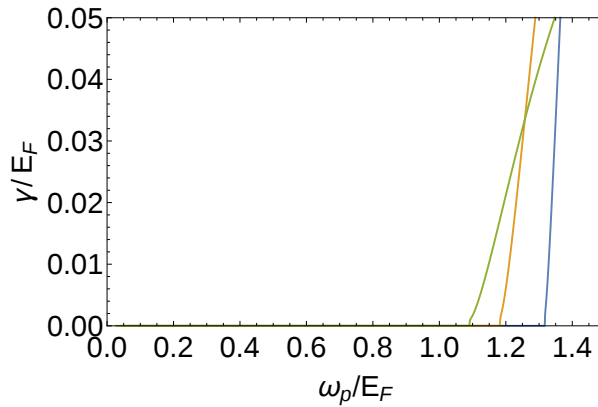


Figure 3.22: Absorption peak width of graphene. Suspended graphene (blue line), graphene on substrate with $\epsilon_r = 4$ (yellow) and graphene on substrate with $\epsilon_r = 10$ (green).

Using the obtained values for the widths of the resonance peaks we may also compute the Q-factor of the resonances. We have chosen to work with the reflection in this case, using instead the transmission we would obtain a very similar result. Figure 3.23 shows the Q-factor as a function of the

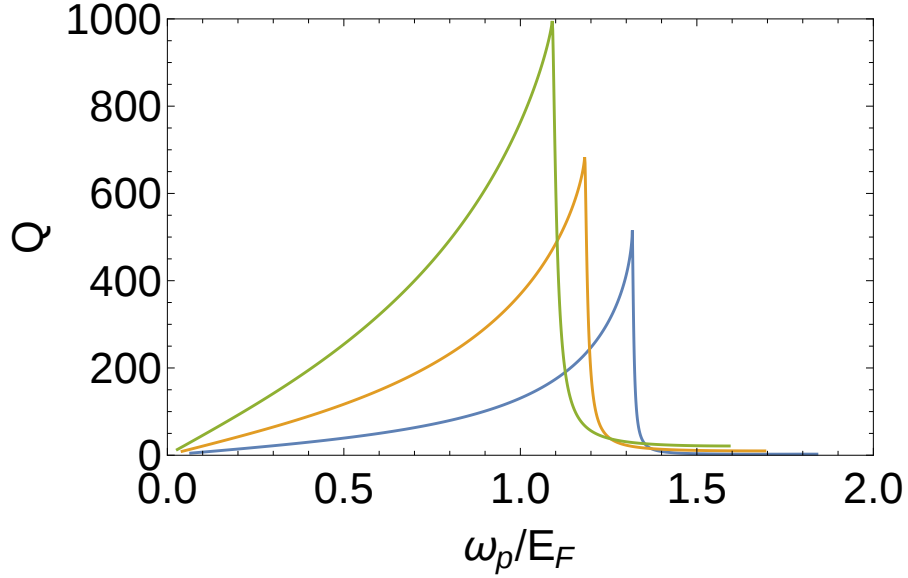


Figure 3.23: The Q-factor of the plasmon resonances obtained in the reflection. Suspended graphene (blue line), graphene on dielectric substrate with $\epsilon_r = 4$ (yellow line) and graphene on dielectric substrate with $\epsilon_r = 10$ (green line).

resonance frequency for the three cases we have considered. The definition of the Q-factor that we have used is

$$Q = \frac{\omega_r}{\Delta\omega} \quad (3.6)$$

where ω_r is the resonance frequency and $\Delta\omega$ is the resonance width. The Q-factor is a measure of the energy loss per oscillation cycle in the system. Small Q-factor means large energy loss per cycle and large Q-factor means small energy loss per cycle. Figure 3.23 shows that the smallest energy loss per oscillation cycle (largest Q-factor) is obtained just before crossing out of the triangle. Outside the triangle the appearance of the new decay channel into electron-hole pairs is the reason for the rapid lowering of the Q-factor in this region. The figure also clearly shows that the substrate with the highest dielectric constant gives the largest Q-factor.

Chapter 4

Summary and Outlook

In summary, this thesis has covered the necessary basic theory for investigating graphene plasmons. Having done so, we have tried to make comparisons with conventional interface plasmons at metal-dielectric interfaces. The graphene plasmons were treated within the Random Phase Approximation and the dispersion relation was investigated both numerically and analytically. We computed and highlighted the large wave localization obtained from the graphene plasmons. This is compared to the more modest localization in the metal-dielectric interface plasmons.

We treated a general theory of linear response and applied it to the electron gas and its conductivity. The conductivity together with the Fresnel scattering theory allowed us to investigate light scattering properties of graphene sheets in different dielectric environments. In chapter 3 we showed the scattering results for a nanostructured graphene sheet in different dielectric environments. We discussed the coupling between the plasmons and the electromagnetic field and also discussed the plasmon resonance Q-factor.

There are numerous possible extensions to the work presented here. Ongoing at the moment is the generalization to finite temperatures, all the results shown in the thesis are obtained at zero temperature. Graphene plasmons are known to exist at room temperature and depending on the doping level of the graphene the energy of the plasmons can be comparable to $k_B T$ for room temperature i.e. ≈ 26 meV. This implies that finite temperature can in some cases play a considerable role, especially for low

doping levels.

Another possible extension is to instead of monolayer plasmons consider bilayer graphene plasmons. The plasmons in bilayer are quite different, less studied in the literature and have more freedom in the sense of model parameters. For example, it is possible to apply an electric field perpendicular to the bilayer surface and open up a gap in the bilayer graphene band diagram. This is in stark contrast to the intrinsic ungapped nature of monolayer graphene considered in this thesis.

Appendices

Appendix A

Derivation of the RPA dielectric function using the method of self-consistent fields

In this note we go through the necessary steps in order to arrive at the RPA result for the dielectric function using the method of self consistent fields. This was first done in [39] which we will follow rather closely in what follows below.

A.1 Electrodynamics

In order to compute the dielectric function or the polarizability within the self consistent field method, or any other method for that matter, we need to know how it is defined. Whenever we are disturbing a system with an electric field it responds to linear order with a polarization field created by the rearranging of charges in the material, the relationship between applied electric field and polarization field is

$$4\pi P(q, \omega) = (\epsilon(q, \omega) - 1) E_0(q, \omega). \quad (\text{A.1})$$

Here E_0 is the externally applied field and P is the polarization field. We know from Maxwells equations that the polarization field is related to the screening charge via $\nabla \cdot P(x, t) = en_s(x, t)$ and we know that $E(x, t) = -\nabla V(x, t)$. Using Fourier analysis we can arrive at $iqP(q, \omega) = en_s(q, \omega)$ and $E_0(q, \omega) = -iqV_0(q, \omega)$ which we insert into equation (A.1) and get

$$\frac{4\pi e}{q} n_s(q, \omega) = (\epsilon(q, \omega) - 1) qV_0(q, \omega). \quad (\text{A.2})$$

This can be rewritten into

$$\epsilon(q, \omega) = 1 + \frac{4\pi e n_s(q, \omega)}{q^2 V_0(q, \omega)} = 1 + \frac{V_s(q, \omega)}{V_0(q, \omega)} = \frac{V_{\text{Tot}}(q, \omega)}{V_0(q, \omega)} \quad (\text{A.3})$$

where in the last step we used that $4\pi e/q^2$ is the Green's function for the Poisson equation so that $V_s(q, \omega) = \frac{4\pi e}{q^2} n_s(q, \omega)$, also $V_{\text{Tot}} = V_0 + V_s$. Equation (A.3) tells us that the dielectric constant is determined by the screening potential of the system divided by the applied potential. The aim of the next section is thus to find the screening potential induced by the external potential.

A.2 Self consistent field method

The basic idea here is to use a density matrix for the system in its ground state ρ_0 and allow it to be perturbed so that the full density matrix is $\rho = \rho_0 + \rho_1$. The fundamental equation that governs the time evolution of the density matrix is the Liouville equation (von Neumann equation)

$$i\hbar\partial_t\rho = [H, \rho]. \quad (\text{A.4})$$

The Hamiltonian in our case is $H = H_0 + eV$ where $i\hbar\partial_t\rho_0 = [H_0, \rho_0]$ i.e. the ground state satisfies the Liouville equation. Now, turning on the perturbation V in the Hamiltonian we must allow the density matrix to deviate from its ground state ρ_0 so we add the perturbed part ρ_1 and insert into equation (A.4) and get

$$i\hbar\partial_t\rho_0 + i\hbar\partial_t\rho_1 = [H_0 + eV, \rho_0 + \rho_1] = [H_0, \rho_0] + [H_0, \rho_1] + [eV, \rho_0] + [eV, \rho_1]. \quad (\text{A.5})$$

Since we are only interested in the linear response of the system we neglect the term $[eV, \rho_1]$ which is the potential correction from the density response, this would be a higher order term. We also know that H_0 and ρ_0 satisfy equation (A.4) so these terms will cancel each other in our expression. Thus we are left with

$$i\hbar\partial_t\rho_1 = [H_0, \rho_1] + [eV, \rho_0], \quad (\text{A.6})$$

we bracket this equation between $\langle k|$ and $|k + q\rangle$ and obtain

$$i\hbar\partial_t\langle k|\rho_1|k + q\rangle = \langle k|[H_0, \rho_1]|k + q\rangle + \langle k|[eV, \rho_0]|k + q\rangle. \quad (\text{A.7})$$

We know the action of the ground state Hamiltonian and density matrix on the state vectors i.e. $H_0|k\rangle = \epsilon_k|k\rangle$ and $\rho_0|k\rangle = f_k|k\rangle$. Expanding the commutators and using these equalities we are left with

$$i\hbar\partial_t\langle k|\rho_1|k+q\rangle = (\epsilon_k - \epsilon_{k+q})\langle k|\rho_1|k+q\rangle + (f_{k+q} - f_k)\langle k|eV|k+q\rangle. \quad (\text{A.8})$$

The idea is now to think of V in this equation as an external perturbation, let us call this external perturbation V_0 and we will assume it has a harmonic time dependence $e^{i\omega t}$. Now, assuming that ρ_1 acquires the same time dependence, which is quite natural (at least in the linear response regime), we obtain

$$\langle k|\rho_1|k+q\rangle = \frac{f_{k+q} - f_k}{\epsilon_{k+q} - \epsilon_k - \hbar\omega} eV_0(q), \quad (\text{A.9})$$

where $V_0(q) = \langle k|V_0|k+q\rangle$. This equation tells us that the response of the system, ρ_1 , is proportional to the external perturbation. Thus, by applying an external perturbation we automatically obtain a system response. We know that this system response will in turn generate its own potential (a screening potential), let us call this new potential V_s . We know that a potential is generated by a density and this is governed by the Poisson equation

$$\nabla^2 V(\vec{x}) = -4\pi en(\vec{x}), \quad (\text{A.10})$$

so we need to convert the density matrix response ρ_1 into a screening electron density n_s that we then can use to obtain the screening potential. The way to obtain the electron density is through the formula

$$\begin{aligned} n_s(\vec{x}) &= \text{Tr}\{\rho_1(\vec{x}, \vec{x})\} = \text{Tr}\{\langle \vec{x}|\rho_1|\vec{x}\rangle\} = \\ &= \int dk \int dk' \langle x|k\rangle \langle k|\rho_1|k'\rangle \langle k'|x\rangle = \int dk \int dk' e^{i(k-k')x} \langle k|\rho_1|k'\rangle. \end{aligned} \quad (\text{A.11})$$

Now, consider the Fourier transform of the electron density i.e.

$$\begin{aligned} n_s(\vec{q}) &= \int dx e^{ixq} n_s(\vec{x}) = \int dx \int dk \int dk' e^{i(k+q-k')x} \langle k|\rho_1|k'\rangle = \\ &= \int dk \int dk' \delta(k+q-k') \langle k|\rho_1|k'\rangle = \int dk \langle k|\rho_1|k+q\rangle. \end{aligned} \quad (\text{A.12})$$

Also, a convenient way of solving the Poisson equation is by using Green's functions

$$V_s(\vec{x}) = \int d^d x' G(x - x') n(\vec{x}') \quad (\text{A.13})$$

where the superscript d is signaling that we need to remember the dimensionality of the problem and $n(x')$ is the electron density (we use n instead of the more conventional ρ to avoid confusion with the density matrix). When Fourier transforming the above equation, due to the properties of the convolution under the transform, we get the simple looking identity

$$V_s(\vec{q}) = G^d(q)n(\vec{q}) \quad (\text{A.14})$$

where the d -superscript now sits on the Green's function. See Appendix B for a treatment of Green's functions. Using the 3-dimensional Green's function and inserting equation (A.12) for the electron density we get

$$V_s(q) = \frac{4\pi e}{q^2} \sum_{k'} \langle k' | \rho_1 | k' + q \rangle. \quad (\text{A.15})$$

So it turns out that the screening potential is proportional to the sum over all k vectors of ρ_1 with q fixed. We now remember that we already have an expression for $\langle k | \rho_1 | k + q \rangle$, namely equation (A.9). We insert (A.9) into the expression for the screening potential, equation (A.15), and obtain

$$V_s(q) = \frac{4\pi e^2}{q^2} \sum_k \frac{f_{k+q} - f_k}{\epsilon_{k+q} - \epsilon_k - \hbar\omega} V_0(q). \quad (\text{A.16})$$

This is then the linear response of the system to the external perturbation V_0 . Now, looking back to equation (A.3) we easily see that

$$\epsilon^{3d}(q, \omega) = 1 + \frac{4\pi e^2}{q^2} \sum_k \frac{f_{k+q} - f_k}{\epsilon_{k+q} - \epsilon_k - \hbar\omega} \quad (\text{A.17})$$

which represents the answer for 3-dimensional quantities. We will be interested in quantities confined to a surface and thus we use the Green's function from equation (B.10) representing the Green's function of a confined potential on the surface and decaying in the direction perpendicular to the surface. With this choice inserted as $G^d(q)$ we get the dielectric function

$$\epsilon^\beta(q, \omega) = 1 + \frac{2\pi e^2 \beta}{q^2} \sum_k \frac{f_{k+q} - f_k}{\epsilon_{k+q} - \epsilon_k - \hbar\omega} \quad (\text{A.18})$$

or if we would have chosen the 2d Green's function we would get the dielectric function

$$\epsilon^{2d}(q, \omega) = 1 + \frac{2\pi e^2}{q} \sum_k \frac{f_{k+q} - f_k}{\epsilon_{k+q} - \epsilon_k - \hbar\omega}. \quad (\text{A.19})$$

We define the polarizability, $\Pi(q, \omega)$, as

$$\Pi(q, \omega) = \sum_k \frac{f_{k+q} - f_k}{\epsilon_{k+q} - \epsilon_k - \hbar\omega} \quad (\text{A.20})$$

and here the expression is the same regardless of dimensionality (even though we need to remember how many dimensions the sum runs through). The polarizability is the function that "dresses" the bare Coulomb interaction, if the polarizability is 1 then the interactions are completely unscreened and if it is 0 it is completely screened.

Appendix B

Green's function for quantities confined to surfaces

B.1 Bulk Green's function for the Poisson equation

The "normal" bulk Green's function for the Poisson equation is easily obtained. We start by writing the equation for the Green's function in a standard manner as

$$\nabla^2 G(\vec{r}) = -4\pi e \delta(\vec{r}). \quad (\text{B.1})$$

Then, inserting that $G(\vec{r})$ and $\delta(\vec{r})$ can be written as their Fourier transforms we obtain

$$\nabla^2 \int d^3k G(k) e^{i\vec{k}\cdot\vec{r}} = -4\pi e \int d^3k e^{i\vec{k}\cdot\vec{r}} \quad (\text{B.2})$$

and letting the derivative act under the integration we get

$$- \int d^3k k^2 G(k) e^{i\vec{k}\cdot\vec{r}} = -4\pi e \int d^3k e^{i\vec{k}\cdot\vec{r}} \quad (\text{B.3})$$

which immediately gives

$$G(k) = \frac{4\pi e}{k^2} \quad (\text{B.4})$$

which could be called the 3d Green's function, bulk Green's function or simply Green's function for the Poisson equation.

B.2 Surface Green's functions for the Poisson equation

Quantities that are confined to a surface have a wave form of the type

$$e^{i\vec{x}\cdot\vec{q}-\beta|z|} \quad (\text{B.5})$$

with $\beta = \sqrt{q^2 - \omega^2/c^2}$ being the decay parameter in the z -direction.

Using the Poisson equation and remembering that the charge distribution in graphene is confined to a single sheet and is essentially a delta function in the z -direction we get the differential equation

$$\nabla^2 V(\vec{x}, z, t) = -4\pi e n(\vec{x}, t)\delta(z) \quad (\text{B.6})$$

where the graphene sheet is the plane $z = 0$, V is the potential and $n(\vec{x}, t)$ is the charge density in the graphene plane. We seek the Green's function to this equation and in order to make sense of this equation we need to integrate the z -direction and we get

$$\int_{-\infty}^{\infty} dz \nabla^2 G(\vec{x}) = -4\pi e \int_{-\infty}^{\infty} dz \delta(\vec{x})\delta(z) \quad (\text{B.7})$$

and inserting the Fourier transforms of $G(\vec{x})$ and $\delta(\vec{x})$ we obtain

$$\int_{-\infty}^{\infty} dz (\nabla_{\vec{x}}^2 + \nabla_z^2) \int d^2 q G(\vec{q}) e^{i\vec{q}\cdot\vec{x}-\beta|z|} = -4\pi e \int d^2 q e^{i\vec{q}\cdot\vec{x}} \quad (\text{B.8})$$

where we also performed the trivial integration of the right hand side. The integral over ∇_z^2 is only going to be a boundary term that vanishes at infinity and performing the z integral and applying $\nabla_{\vec{x}}^2$ we get

$$- \int d^2 q G(q) e^{i\vec{q}\cdot\vec{x}} \frac{2q^2}{\beta} = -4\pi e \int d^2 q e^{i\vec{q}\cdot\vec{x}} \quad (\text{B.9})$$

which gives

$$G(q) = \frac{2\pi e \beta}{q^2}. \quad (\text{B.10})$$

Notice that if $q \gg \omega/c$ then $\beta \approx q$ and the Green's function becomes

$$G(q) = \frac{2\pi e}{q} \quad (\text{B.11})$$

which is usually referred to as the 2-d Green's function. This name comes from the fact that the wave is in this case confined to the surface and decays rapidly in the perpendicular direction.

Appendix C

Calculation of the polarizability $\Pi(q, \omega)$ for a 2DEG with parabolic dispersion at zero temperature

This note presents a thorough calculation of the polarizability for a 2-DEG with parabolic dispersion first published by Stern in [36]. The first section contains important formulas and identities used in the calculation and section 2 contains the actual calculation of the polarizability. Section 3 presents the results in their final form.

C.1 Preliminaries

The main object of discussion in this note is the polarizability from which one can derive numerous properties of the system in question.

C.1.1 Formulas and Identities

The expression for the polarizability is [40][41]

$$\Pi(q, \omega) = \frac{1}{\Omega} \sum_{\vec{k}} G_{\vec{k}} G_{\vec{k}+\vec{q}} \quad (\text{C.1})$$

where G is the non-interacting Green's function and Ω is the normalization area. This expression can be rewritten into [36][40][41]

$$\Pi(q, \omega) = \frac{1}{\Omega} \lim_{\eta \rightarrow 0} \sum_{\vec{k}} \frac{f_0(\epsilon_{\vec{k}}) - f_0(\epsilon_{\vec{k}+\vec{q}})}{\epsilon_{\vec{k}+\vec{q}} - \epsilon_{\vec{k}} - \hbar\omega - i\eta}. \quad (\text{C.2})$$

The goal of this note is to calculate this object and simplify as far as possible. We will make use of some identities and theorems from complex calculus and we also make use of certain primitives, these are listed below.

Whenever we have a limiting procedure on an integral and it takes the form

$$\lim_{\eta \rightarrow 0^+} \int dx \frac{f(x)}{x + i\eta}, \quad (\text{C.3})$$

a convenient way to evaluate it is to use the *Sokhotski-Plemelj theorem*:

$$\begin{aligned} \lim_{\eta \rightarrow 0^+} \int dx \frac{f(x)}{x + i\eta} &= \lim_{\eta \rightarrow 0^+} \int dx \frac{f(x)(x - i\eta)}{x^2 + \eta^2} = \\ &= \lim_{\eta \rightarrow 0^+} \int dx \frac{f(x)x}{x^2 + \eta^2} - i \lim_{\eta \rightarrow 0^+} \int dx \frac{f(x)\eta}{x^2 + \eta^2} = \\ &= \mathcal{P} \int dx \frac{f(x)}{x} - i\pi \int dx \delta(x)f(x) = \mathcal{P} \int dx \frac{f(x)}{x} - i\pi f(0). \end{aligned} \quad (\text{C.4})$$

where \mathcal{P} denotes (Cauchy) principal value. This allows us to interpret the original integral as a sum of its real and imaginary parts which are both non-singular. It basically tells us that the singularity can be avoided if we compensate with a corresponding imaginary part evaluated at the singularity. The above holds if the integration covers the singularity ($x = 0$ in this case).

We will encounter integrals of the type

$$\mathcal{P} \int_{-\infty}^{\infty} dt \frac{1}{t^2 + \alpha}, \quad (\text{C.5})$$

where α is a real number. We can evaluate this integral using the method of residues. Since there are no oscillations (exponential functions) we can choose to close in either the upper or lower complex half plane. We will always close the contours in the upper half plane. It is important to note that the \mathcal{P} tells us to ignore poles that are on the line of integration, i.e. the real axis. This tells us that only imaginary poles will give a non zero

contribution, i.e. only when $\alpha > 0$. The residue theorem from complex analysis states that the value of the real line integral is equal to the sum of its poles, i.e.

$$\int_{-\infty}^{\infty} = 2\pi i \sum_{\text{enclosed poles}} . \quad (\text{C.6})$$

The above holds if the integral over the semicircle that closes the contour goes to zero, which in our case it does since the denominator has two powers more than the nominator. Evaluating the residue yields

$$\mathcal{P} \int_{-\infty}^{\infty} dt \frac{1}{t^2 + \alpha} = \begin{cases} 2\pi i \operatorname{Res}_{t=i\sqrt{\alpha}} \left[\frac{1}{(t+i\sqrt{\alpha})(t-i\sqrt{\alpha})} \right] = 2\pi i \frac{1}{2i\sqrt{\alpha}} = \frac{\pi}{\sqrt{\alpha}}, & \alpha > 0 \\ 0, & \alpha \leq 0, \end{cases} \quad (\text{C.7})$$

where the 0 for $\alpha \leq 0$ comes from the fact that we take the principal value.

We are also going to encounter integrals of the type

$$\int dk \frac{k}{\sqrt{A^2 - k^2}} \quad (\text{C.8})$$

which have a simple primitive

$$\int dk \frac{k}{\sqrt{A^2 - k^2}} = -\sqrt{A^2 - k^2}. \quad (\text{C.9})$$

Also we will encounter the similar integral and primitive

$$\int dk \frac{k}{\sqrt{k^2 - A^2}} = \sqrt{k^2 - A^2}. \quad (\text{C.10})$$

We will also need the well known identity

$$\delta(g(x)) = \sum_{x_i} \frac{\delta(x - x_i)}{|g'(x_i)|} \quad (\text{C.11})$$

where x_i are the zeros of $g(x)$.

C.2 Calculation

We now start with the expression for the polarizability within the RPA

$$\Pi(q, \omega) = \frac{1}{\Omega} \lim_{\eta \rightarrow 0} \sum_{\vec{k}} \frac{f_0(\epsilon_{\vec{k}}) - f_0(\epsilon_{\vec{k}+\vec{q}})}{\epsilon_{\vec{k}+\vec{q}} - \epsilon_{\vec{k}} - \hbar\omega - i\eta} \quad (\text{C.12})$$

where Ω is the normalization area. The first thing we want to do is to convert the sum to an integral and then rewrite the expression into something that is easier to manipulate (here we use $\vec{k}' = \vec{k} + \vec{q}$ and $\vec{k}'' = \vec{k} - \vec{q}$)

$$\begin{aligned} & \frac{1}{\Omega} \lim_{\eta \rightarrow 0} \sum_{\vec{k}} \frac{f_0(\epsilon_{\vec{k}}) - f_0(\epsilon_{\vec{k}'})}{\epsilon_{\vec{k}'} - \epsilon_{\vec{k}} - \hbar\omega - i\eta} = \left\{ \vec{k}' = \vec{k} + \vec{q}, d\vec{k}' = d\vec{k} \right\} = \\ & = \lim_{\eta \rightarrow 0} \left(\int \frac{d\vec{k}}{(2\pi)^2} \frac{f_0(\epsilon_{\vec{k}})}{\epsilon_{\vec{k}'} - \epsilon_{\vec{k}} - \hbar\omega - I\eta} - \int \frac{d\vec{k}'}{(2\pi)^2} \frac{f_0(\epsilon_{\vec{k}'})}{\epsilon_{\vec{k}'} - \epsilon_{\vec{k}'-\vec{q}} - \hbar\omega - i\eta} \right) = \\ & = \left\{ \text{relabel } \vec{k}' \text{ to } \vec{k} \text{ in the second integral} \right\} = \\ & = \lim_{\eta \rightarrow 0} \int \frac{d\vec{k}}{(2\pi)^2} f_0(\epsilon_{\vec{k}}) \left(\frac{1}{\epsilon_{\vec{k}'} - \epsilon_{\vec{k}} - \hbar\omega - i\eta} - \frac{1}{\epsilon_{\vec{k}} - \epsilon_{\vec{k}'} - \hbar\omega - I\eta} \right). \end{aligned} \quad (\text{C.13})$$

We now apply the Sokhotski-Plemelj theorem from equation (C.4), this allows us to convert the limit of the integral into its real- and imaginary parts;

$$\begin{aligned} \Pi(q, \omega) = & \frac{1}{(2\pi)^2} \left(\mathcal{P} \int d\vec{k} f_0(\epsilon_{\vec{k}}) \left(\frac{1}{\epsilon_{\vec{k}'} - \epsilon_{\vec{k}} - \hbar\omega} - \frac{1}{\epsilon_{\vec{k}} - \epsilon_{\vec{k}'} - \hbar\omega} \right) \right. \\ & \left. - i\pi \int d\vec{k} f_0(\epsilon_{\vec{k}}) (\delta(\epsilon_{\vec{k}'} - \epsilon_{\vec{k}} - \hbar\omega) - \delta(\epsilon_{\vec{k}} - \epsilon_{\vec{k}'} - \hbar\omega)) \right) \end{aligned} \quad (\text{C.14})$$

Notice that the above expression is very general; we have made no assumptions of dimensionality or dispersion. It is the general simplified expression of the RPA polarization in (C.2). If we wanted to we could include real self energies in the expression above, since they could be considered as a shift of the ϵ 's, but if the self energies have a finite imaginary part one would need to redo the simplification above.

Imaginary part

We start out by calculating the imaginary part of the polarization. This looks very simple, it is simply a double integral over two delta functions. The important thing to recognize is that the delta functions are one dimensional whereas the integral is two dimensional. This means that when performing one of the integrals we may get some constraints on the other. We now make explicit that we are considering a parabolic dispersion $\epsilon_{\vec{k}} = \frac{\hbar^2}{2m}k^2$, where $k = |\vec{k}|$, and we start out by writing the imaginary part in polar coordinates. Notice that $\epsilon_{\vec{k}+\vec{q}} = \frac{\hbar^2}{2m}|\vec{k} + \vec{q}|^2 = \frac{\hbar^2}{2m}(k^2 + q^2 + 2kq \cos \theta)$ and $\epsilon_{\vec{k}-\vec{q}} = \frac{\hbar^2}{2m}|\vec{k} - \vec{q}|^2 = \frac{\hbar^2}{2m}(k^2 + q^2 - 2kq \cos \theta)$. Also note that at $T = 0$, $f_0(\epsilon_k)$ becomes a step function. We get

$$\begin{aligned}
& -i \frac{1}{4\pi} \int d\vec{k} f_0(\epsilon_{\vec{k}}) (\delta(\epsilon_{\vec{k}'} - \epsilon_{\vec{k}} - \hbar\omega) - \delta(\epsilon_{\vec{k}} - \epsilon_{\vec{k}'} - \hbar\omega)) = \\
& = -i \frac{1}{4\pi} \int_0^\infty dk \int_0^{2\pi} d\theta k f_0(\epsilon_k) \left[\delta\left(\frac{\hbar^2}{2m}(q^2 - 2kq \cos \theta) + \hbar\omega\right) - \right. \\
& \quad \left. - \delta\left(\frac{\hbar^2}{2m}(q^2 + 2kq \cos \theta) - \hbar\omega\right) \right] = \\
& = -i \frac{1}{4\pi} \int_0^{k_F} dk \int_0^{2\pi} d\theta k \left[\delta\left(\frac{\hbar^2}{2m}(q^2 - 2kq \cos \theta + \tilde{\omega})\right) - \right. \\
& \quad \left. - \delta\left(\frac{\hbar^2}{2m}(q^2 + 2kq \cos \theta - \tilde{\omega})\right) \right], \tag{C.15}
\end{aligned}$$

where we have used the step function in f_0 to truncate the integral and we have introduced $\tilde{\omega} = \frac{2m}{\hbar}\omega$. We now exchange the order of integration and use equation (C.11) to rewrite our expression into

$$-i \frac{m}{2\pi\hbar^2} \int_0^{2\pi} d\theta \int_0^{k_F} dk \frac{k}{2q|\cos \theta|} (\delta(k - k_1) - \delta(k - k_2)), \tag{C.16}$$

where $k_1 = \frac{q^2 + \tilde{\omega}}{2q \cos \theta}$, $k_2 = \frac{\tilde{\omega} - q^2}{2q \cos \theta}$ are the zeros of their respective delta function. Now, doing the k -integral is simple and we obtain

$$-i \frac{m}{4\pi\hbar^2 q} \left(\int_{k_1 < k_F} d\theta \frac{k_1}{\cos \theta} - \int_{k_2 < k_F} d\theta' \frac{k_2}{\cos \theta'} \right). \tag{C.17}$$

Notice that this puts a constraint on the θ -integrals. This expression is only valid if the k -integration that we did covers k_1, k_2 respectively. Since we know the constraint on the integrals in k_1 , and k_2 space and we have an explicit relationship between the k_i 's and the θ 's from above it is natural to convert the angle integral into integrals over k_1, k_2 . From the explicit expressions for k_1 and k_2 above we get $dk_1 = \frac{q^2 + \tilde{\omega}}{2q} \frac{\sin \theta}{\cos^2 \theta} d\theta$, $dk_2 = \frac{\tilde{\omega} - q^2}{2q} \frac{\sin \theta'}{\cos^2 \theta'} d\theta'$, $\cos \theta = \frac{\tilde{\omega} + q^2}{2qk_1}$ which gives $\sin \theta = \sqrt{1 - \left(\frac{\tilde{\omega} + q^2}{2qk_1}\right)^2}$ and $\cos \theta' = \frac{\tilde{\omega} - q^2}{2qk_2}$ which gives $\sin \theta' = \sqrt{1 - \left(\frac{\tilde{\omega} - q^2}{2qk_2}\right)^2}$. We also see that as functions of the angles $k_1 > \frac{\tilde{\omega} + q^2}{2q}$ and $k_2 > \frac{\tilde{\omega} - q^2}{2q}$, but still the largest k we can have is k_F . We also need to remember that there are two angles for which the substitution $k_i = A / \cos \theta$ that lie in our region of integration, so we add a factor of 2 in front of our expression to compensate. We can now rewrite the angle integrals above as integrals in the k_i variables as

$$\begin{aligned}
 & -i \frac{m}{2\pi \hbar^2 q} \left(\frac{2q}{q^2 + \tilde{\omega}} \int_{\frac{\tilde{\omega} + q^2}{2q}}^{k_F} dk_1 k_1 \frac{\cos \theta}{\sin \theta} - \frac{2q}{\tilde{\omega} - q^2} \int_{\frac{\tilde{\omega} - q^2}{2q}}^{k_F} dk_2 k_2 \frac{\cos \theta'}{\sin \theta'} \right) = \\
 & = -i \frac{m}{2\pi \hbar^2 q} \left(\frac{2q}{q^2 + \tilde{\omega}} \int_{\frac{\tilde{\omega} + q^2}{2q}}^{k_F} dk_1 k_1 \frac{\frac{\tilde{\omega} + q^2}{2qk_1}}{\sqrt{1 - \left(\frac{\tilde{\omega} + q^2}{2qk_1}\right)^2}} - \right. \\
 & \quad \left. - \frac{2q}{\tilde{\omega} - q^2} \int_{\frac{\tilde{\omega} - q^2}{2q}}^{k_F} dk_2 k_2 \frac{\frac{\tilde{\omega} - q^2}{2qk_2}}{\sqrt{1 - \left(\frac{\tilde{\omega} - q^2}{2qk_2}\right)^2}} \right) = \\
 & = -i \frac{m}{2\pi \hbar^2 q} \left(\int_{\frac{\tilde{\omega} + q^2}{2q}}^{k_F} dk_1 \frac{2qk_1}{\sqrt{(2qk_1)^2 - (\tilde{\omega} + q^2)^2}} - \int_{\frac{\tilde{\omega} - q^2}{2q}}^{k_F} dk_2 \frac{2qk_2}{\sqrt{(2qk_2)^2 - (\tilde{\omega} - q^2)^2}} \right) \tag{C.18}
 \end{aligned}$$

and by using the primitive from equation (C.10) we obtain

$$\begin{aligned}
& -i \frac{m}{2\pi\hbar^2 q} \left(\left[\frac{1}{2q} \sqrt{(2qk_1)^2 - (\tilde{\omega} + q^2)^2} \right]_{k_1 = \frac{\tilde{\omega} + q^2}{2q}}^{k_1 = k_F} - \right. \\
& \quad \left. - \left[\frac{1}{2q} \sqrt{(2qk_2)^2 - (\tilde{\omega} - q^2)^2} \right]_{k_2 = \frac{\tilde{\omega} - q^2}{2q}}^{k_2 = k_F} \right) = \\
& = -i \frac{mk_F}{2\pi\hbar^2 q} \left(D_+ \sqrt{1 - \left(\frac{\tilde{\omega} + q^2}{2qk_F} \right)^2} - D_- \sqrt{1 - \left(\frac{\tilde{\omega} - q^2}{2qk_F} \right)^2} \right) = \\
& = i \frac{D_0 k_F}{q} \left(-D_+ \sqrt{1 - \left(\frac{\omega}{qv_F} + \frac{q}{2k_F} \right)^2} + D_- \sqrt{1 - \left(\frac{\omega}{qv_F} - \frac{q}{2k_F} \right)^2} \right). \tag{C.19}
\end{aligned}$$

where $v_F = \frac{\hbar k_F}{m}$ and $D_0 = \frac{m}{2\pi\hbar^2}$ is the density of states for a 2DEG. $D_+ = 1$ for $1 > \frac{\omega}{qv_F} + \frac{q}{2k_F}$, $D_+ = 0$ otherwise. Also $D_- = 1$ for $1 > \left| \frac{\omega}{qv_F} - \frac{q}{2k_F} \right|$, $D_- = 0$ otherwise. The conditions on D_{\pm} come from the requirement that the upper limit on the integrands must be larger than the lower limit. This represents the final form of the imaginary part of the polarization.

Real part

We now take the real part of equation (C.14), write it in polar coordinates and insert our parabolic dispersion which gives us

$$\begin{aligned}
& \mathcal{P} \int \frac{d\vec{k}}{(2\pi)^2} f_0(\epsilon_{\vec{k}}) \left(\frac{1}{\epsilon_{\vec{k}'} - \epsilon_{\vec{k}} - \hbar\omega} - \frac{1}{\epsilon_{\vec{k}} - \epsilon_{\vec{k}'} - \hbar\omega} \right) = \\
& = -\frac{m}{\hbar^2 2\pi^2} \mathcal{P} \int_0^\infty dk \int_0^{2\pi} d\theta k f(\epsilon_{\vec{k}}) \left(\frac{1}{\tilde{\omega} - q^2 - 2kq \cos \theta} - \frac{1}{\tilde{\omega} + q^2 - 2kq \cos \theta} \right) = \\
& = -\frac{m}{\hbar^2 2\pi^2} \mathcal{P} \int_0^{k_F} dk \int_0^{2\pi} d\theta k \left(\frac{1}{\tilde{\omega} - q^2 - 2kq \cos \theta} - \frac{1}{\tilde{\omega} + q^2 - 2kq \cos \theta} \right) \tag{C.20}
\end{aligned}$$

where we have used the Fermi-Dirac step function behavior (we work at $T = 0$) to truncate the infinite k -integral. To calculate the angular integral we employ "tan($\theta/2$)-substitution" which transforms an angular integral into an integral over the entire real line. The (relevant) substitutions are

$\cos \theta = \frac{1-t^2}{1+t^2}$ and $d\theta = \frac{2}{1+t^2} dt$ and we get

$$\begin{aligned}
 & -\frac{m}{\hbar^2 2\pi^2} \mathcal{P} \int_0^{k_F} dk \int_{-\infty}^{\infty} dt \frac{2k}{1+t^2} \left(\frac{1}{\tilde{\omega} - q^2 - 2kq \frac{1-t^2}{1+t^2}} - \frac{1}{\tilde{\omega} + q^2 - 2kq \frac{1-t^2}{1+t^2}} \right) = \\
 & = -\frac{m}{\hbar^2 \pi^2} \mathcal{P} \int_0^{k_F} dk \int_{-\infty}^{\infty} dt k \left(\frac{1}{t^2(\tilde{\omega} - q^2 + 2kq) + \tilde{\omega} - q^2 - 2kq} \right. \\
 & \quad \left. - \frac{1}{t^2(\tilde{\omega} + q^2 + 2kq) + \tilde{\omega} + q^2 - 2kq} \right) = \\
 & = -\frac{m}{\hbar^2 q 2\pi^2} \mathcal{P} \int_0^{k_F} dk \int_{-\infty}^{\infty} dt k \left(\frac{1}{t^2(A_- + k) + A_- - k} - \frac{1}{t^2(A_+ + k) + A_+ - k} \right) = \\
 & = -\frac{m}{\hbar^2 q 2\pi^2} \mathcal{P} \int_0^{k_F} dk \int_{-\infty}^{\infty} dt k \left(\frac{1}{(A_- + k) \left(t^2 + \frac{A_- - k}{A_- + k} \right)} - \frac{1}{(A_+ + k) \left(t^2 + \frac{A_+ - k}{A_+ + k} \right)} \right) \\
 & \hspace{15em} \text{(C.21)}
 \end{aligned}$$

where we have introduced $A_+ = \frac{\tilde{\omega} + q^2}{2q}$ and $A_- = \frac{\tilde{\omega} - q^2}{2q}$. We recognize the form of the above integral from equation (C.5) and its value depends on the sign of the terms $\frac{A_- - k}{A_- + k}$ and $\frac{A_+ - k}{A_+ + k}$ in the denominators. Only if at least one of these terms is positive the answer is non zero. We see from their definitions that A_+ is always positive whereas A_- can be both negative and positive depending on the sign of $\tilde{\omega} - q^2$.

We start with the term with A_+ since it is the simplest one. In order for $\frac{A_+ - k}{A_+ + k}$ to be positive we need $k < A_+$ which means that we need to restrict our k -integral to $\int_0^{A_+} dk$ because the pole does not contribute¹ if k is larger. Only if $A_+ > k_F$ may we keep the integration limits as $\int_0^{k_F} dk$. We now introduce $L = \min(A_+, k_F)$ to label the appropriate upper limit on the integration when we use residues and proceed to calculate the A_+ contribution

¹This is because it lies on the real line we are taking the principal value which tells us to disregard poles on the integration contour.

$$\begin{aligned}
& \frac{m}{\hbar^2 q 2\pi^2} \mathcal{P} \int_0^{k_F} dk \int_{-\infty}^{\infty} dt k \frac{1}{(A_+ + k)} \frac{1}{\left(t^2 + \frac{A_+ - k}{A_+ + k}\right)} = \\
& = \frac{m}{\hbar^2 q 2\pi^2} \mathcal{P} \int_0^L dk \int_{-\infty}^{\infty} dt k \frac{1}{(A_+ + k)} \frac{1}{\left(t + i\sqrt{\frac{A_+ - k}{A_+ + k}}\right) \left(t - i\sqrt{\frac{A_+ - k}{A_+ + k}}\right)} = \\
& = \left\{ \text{Close contour in the upper complex half plane} \right\} = \\
& = \frac{m}{\hbar^2 q 2\pi^2} \int_0^L dk k 2\pi i \operatorname{Res}_{t=i\sqrt{\frac{A_+ - k}{A_+ + k}}} \frac{1}{(A_+ + k)} \frac{1}{\left(t + i\sqrt{\frac{A_+ - k}{A_+ + k}}\right) \left(t - i\sqrt{\frac{A_+ - k}{A_+ + k}}\right)} = \\
& = \frac{m}{\hbar^2 q 2\pi^2} \int_0^L dk k \frac{1}{(A_+ + k)} 2\pi i \frac{1}{2i\sqrt{\frac{A_+ - k}{A_+ + k}}} = \frac{2mn}{\hbar^2 q k_F^2} \int_0^L dk \frac{k}{\sqrt{A_+^2 - k^2}} = \\
& = -\frac{m}{\hbar^2 q 2\pi} \left[\sqrt{A_+^2 - k^2} \right]_0^L = \frac{2mn}{\hbar^2 q k_F^2} \left(A_+ - \sqrt{A_+^2 - L^2} \right). \quad (\text{C.22})
\end{aligned}$$

Now, inserting the proper L we see that if $A_+ < k_F$ then $L = A_+$ and the square root vanishes. If instead $k_F < A_+$ then the square root remains. In conclusion the A_+ term gives the contribution

$$\frac{m}{\hbar^2 q 2\pi} \left(A_+ - C_+ \sqrt{A_+^2 - k_F^2} \right) \quad (\text{C.23})$$

where $C_+ = 1$ if $k_F < A_+$ and $C_+ = 0$ otherwise.

We now turn to the A_- contribution in equation (C.21). We now need to keep track on whether $A_- = \frac{\tilde{\omega} - q^2}{2q}$ is positive or negative which happens on either side of $\tilde{\omega} = q^2$. We will now introduce \pm and \mp in our calculations where the upper sign is to be used when $A_- > 0$ and the lower sign when $A_- < 0$. In the same manner as above we will need to restrict the k integral and we will call the appropriate limit L as above and now we define it as $L = \min(\pm A_-, k_F)$.

$$\begin{aligned}
 & -\frac{m}{\hbar^2 q 2\pi^2} \mathcal{P} \int_0^{k_F} dk \int_{-\infty}^{\infty} dt k \frac{1}{(A_- + k)} \frac{1}{\left(t^2 + \frac{A_- - k}{A_- + k}\right)} = \\
 & = -\frac{m}{\hbar^2 q 2\pi^2} \mathcal{P} \int_0^L dk \int_{-\infty}^{\infty} dt k \frac{1}{(A_- + k)} \frac{1}{\left(t + i\sqrt{\frac{A_- - k}{k + A_-}}\right)\left(t - i\sqrt{\frac{A_- - k}{k + A_-}}\right)} = \\
 & = \left\{ \text{same residue calculations as above} \right\} = -\frac{2mne^2}{\hbar^2 q^3 k_F^2} \int_0^L dk \frac{k}{A_- + k} \frac{1}{\sqrt{\frac{A_- - k}{A_- + k}}} = \\
 & = \mp \frac{m}{\hbar^2 q 2\pi} \int_0^L dk \frac{k}{\sqrt{(A_- + k)^2 \frac{A_- - k}{A_- + k}}} \quad (\text{C.24})
 \end{aligned}$$

where the \mp in front comes from the fact that when $A_- < 0$ we have to lift $-\frac{1}{A_- + k}$ inside the square root in order to lift in something that is positive. This sign is squared away inside the square root and is only important outside. We now get

$$\begin{aligned}
 & \mp \frac{m}{\hbar^2 q 2\pi} \int_0^L dk \frac{k}{\sqrt{A_-^2 - k^2}} = \pm \frac{2mn}{\hbar^2 q k_F^2} \left[\sqrt{A_-^2 - k^2} \right]_0^L = \\
 & = \pm \frac{2mn}{\hbar^2 q k_F^2} \left(\sqrt{A_-^2 - L^2} - |A_-| \right) \quad (\text{C.25})
 \end{aligned}$$

and we can see that the \pm in front gets canceled by the modulus on the last term so we get

$$\frac{m}{\hbar^2 q 2\pi} \left(\pm \sqrt{A_-^2 - L^2} - A_- \right). \quad (\text{C.26})$$

We also remember that $L = \min(\pm A_-, k_F)$ so the answer becomes

$$\frac{m}{\hbar^2 q 2\pi} \left(C_- \sqrt{A_-^2 - k_F^2} - A_- \right) \quad (\text{C.27})$$

where $C_- = \text{sign}(\tilde{\omega} - q^2)$ if $k_F < |A_-|$ and $C_- = 0$ otherwise.

Now, summing equations (C.23) and (C.27) together to obtain the total answer we get

$$\frac{m}{\hbar^2 q 2\pi} \left(A_+ - A_- - C_+ \sqrt{A_+^2 - k_F^2} + C_- \sqrt{A_-^2 - k_F^2} \right) \quad (\text{C.28})$$

and inserting the definitions of A_\pm and $\tilde{\omega}$ we obtain

$$\begin{aligned} & \frac{m}{\hbar^2 q 2\pi} \left(\frac{\tilde{\omega} + q^2}{2q} - \frac{\tilde{\omega} - q^2}{2q} - C_+ \sqrt{\left(\frac{\tilde{\omega} + q^2}{2q}\right)^2 - k_F^2} + C_- \sqrt{\left(\frac{\tilde{\omega} - q^2}{2q}\right)^2 - k_F^2} \right) = \\ & = \frac{mk_F}{\hbar^2 q 2\pi} \left(\frac{q}{k_F} - C_+ \sqrt{\left(\frac{m\omega}{\hbar q k_F} + \frac{q}{2k_F}\right)^2 - 1} + C_- \sqrt{\left(\frac{m\omega}{\hbar q k_F} - \frac{q}{2k_F}\right)^2 - 1} \right) = \\ & = \frac{D_0 k_F}{q} \left(\frac{q}{k_F} - C_+ \sqrt{\left(\frac{\omega}{qv_F} + \frac{q}{2k_F}\right)^2 - 1} + C_- \sqrt{\left(\frac{\omega}{qv_F} - \frac{q}{2k_F}\right)^2 - 1} \right) \end{aligned} \quad (\text{C.29})$$

where $v_F = \hbar k_F/m$, $D_0 = \frac{m}{2\pi\hbar^2}$ and $C_+ = 1$ if $1 < \frac{\omega}{qv_F} + \frac{q}{2k_F}$ and $C_+ = 0$ otherwise. Also, $C_- = \text{sign}\left(\frac{\omega}{qv_F} - \frac{q}{2k_F}\right)$ if $1 < \left|\frac{\omega}{qv_F} - \frac{q}{2k_F}\right|$ and $C_- = 0$ otherwise.

C.3 Results and analysis

We now take the final forms of the real and imaginary part of $\Pi(q, \omega)$ from equations (C.19) and (C.29) and list them below. Remember that for a 2DEG (without spin) $k_F = \sqrt{4\pi n}$, and that the density of states at the Fermi surface (everywhere actually since it is constant) $D_0 = \frac{m}{\pi\hbar^2}$. We also replace the C_{\pm} and D_{\pm} with step functions making the expressions easier to read. The final polarization is

$$\begin{aligned} \text{Im } \Pi(q, \omega) = D_0 \frac{k_F}{q} & \left(\theta\left(1 - \left|\frac{\omega}{qv_F} - \frac{q}{2k_F}\right|\right) \sqrt{1 - \left(\frac{\omega}{qv_F} - \frac{q}{2k_F}\right)^2} - \right. \\ & \left. - \theta\left(1 - \frac{\omega}{qv_F} - \frac{q}{2k_F}\right) \sqrt{1 - \left(\frac{\omega}{qv_F} + \frac{q}{2k_F}\right)^2} \right) \end{aligned} \quad (\text{C.30})$$

$$\begin{aligned} \text{Re } \Pi(q, \omega) = D_0 & \left(1 - \theta\left(\frac{\omega}{qv_F} + \frac{q}{2k_F} - 1\right) \frac{k_F}{q} \sqrt{\left(\frac{\omega}{qv_F} + \frac{q}{2k_F}\right)^2 - 1} \right. \\ & \left. + \theta\left(\left|\frac{\omega}{qv_F} - \frac{q}{2k_F}\right| - 1\right) \text{sign}\left(\frac{\omega}{qv_F} - \frac{q}{2k_F}\right) \frac{k_F}{q} \sqrt{\left(\frac{\omega}{qv_F} - \frac{q}{2k_F}\right)^2 - 1} \right). \end{aligned} \quad (\text{C.31})$$

This matches the polarizability result in [36].

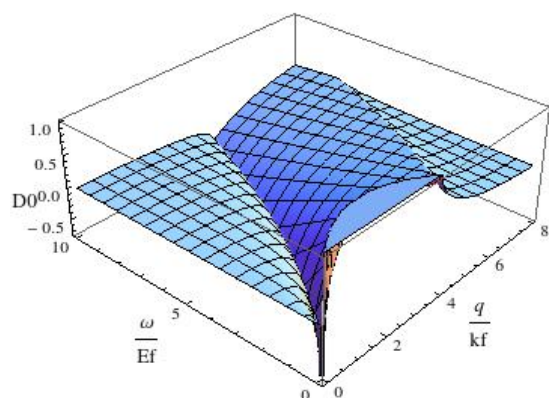


Figure C.1: Real part of the polarizability, the parabolic dispersion is clearly visible as the valley in the middle.

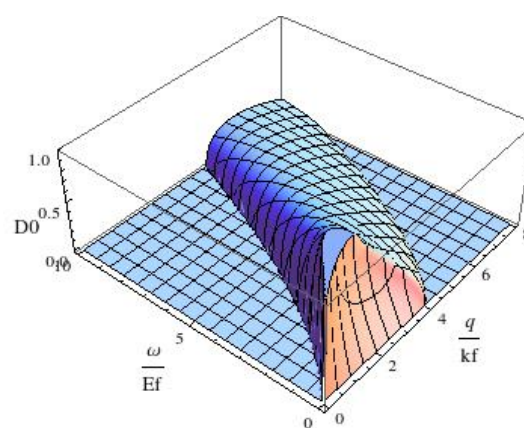


Figure C.2: Imaginary part of the polarizability, notice the flat part to the left of the ridge where it is zero. This is where the plasmon lives and because the imaginary part of the polarization is zero the plasmon should have an infinite lifetime.

Appendix D

Calculation of the polarizability, $\Pi(q, \omega)$ for graphene at zero temperature

This note presents the calculations needed to obtain the expression for the polarizability of graphene calculated in [20] and [21]. The first section contains some preliminary results needed and sections 2 and 3 contain the actual calculations and a summary of the results respectively.

D.1 Preliminaries

An important relation we will use is the so called *Kramers-Kronig* relations, these relate the real part of an analytic function to its imaginary part and vice-versa. It turns out that for the function Π^- defined below, it is easy to compute the imaginary part and then use Kramers-Kronig relations to obtain the real part. The starting point of the Kramers-Kronig relations is the Cauchy residue theorem which states that

$$\oint d\omega' \frac{f(\omega')}{\omega' - \omega} = 0, \quad (\text{D.1})$$

where $f(\omega)$ is analytic within the integration contour. In the case of response functions causality dictates they need to be analytic in the upper half plane, this makes the application of the residue theorem with the contour closed upwards ideal. Choosing the contour to be the real axis (with a small semi circle going above the pole at ω) and closing with an infinitely big semi-circle upwards we obtain

$$\mathcal{P} \int_{-\infty}^{\infty} d\omega' \frac{f(\omega')}{\omega' - \omega} - i\pi f(\omega) + \int_{\frown} d\omega' \frac{f(\omega')}{\omega' - \omega} = 0, \quad (\text{D.2})$$

where $\int_{\frown} d\omega'$ denotes integration over the semicircle that closes the contour. In the case of physical response functions it is usually the case that they approach zero as $\omega \rightarrow \infty$, the physical reason for this is that the system in question cannot respond to changes that occur much, much faster than its "typical time scale". If we assume that $f(\omega) \rightarrow 0$ as $\omega \rightarrow \infty$ then the integral over the semi-circle is zero¹, using this and collecting real and imaginary parts we obtain the final form of the Kramers-Kronig relations

$$\begin{aligned} \text{Re } f(\omega) &= \frac{1}{\pi} \mathcal{P} \int_{-\infty}^{\infty} d\omega' \frac{\text{Im } f(\omega')}{\omega' - \omega} \\ \text{Im } f(\omega) &= -\frac{1}{\pi} \mathcal{P} \int_{-\infty}^{\infty} d\omega' \frac{\text{Re } f(\omega')}{\omega' - \omega}. \end{aligned} \quad (\text{D.3})$$

The expression for the RPA polarizability for graphene is more complicated than for the 2DEG since we now have two different bands that the electrons (holes) can make transitions within and between (we ignore inter-valley transitions). The polarizability is the sum of all inter- and intraband transitions and looks like [20]

$$\Pi(q, \omega) = -\frac{g_s g_v}{\Omega} \lim_{\eta \rightarrow 0^+} \sum_{\vec{k} s s'} \frac{f_{s\vec{k}} - f_{s'\vec{k}'}}{\hbar\omega + \epsilon_{s\vec{k}} - \epsilon_{s'\vec{k}'} + i\eta} F_{ss'}(\vec{k}, \vec{k}') \quad (\text{D.4})$$

where $\vec{k}' = \vec{k} + \vec{q}$, g_s and g_v are the spin- and valley degeneracy respectively, Ω is the normalization area, $s, s' = +, -$ denote band indices, $\epsilon_{\vec{k}s} = s\hbar v_F |\vec{k}|$ is the dispersion, $F_{ss'}(\vec{k}, \vec{k}') = (1 + ss' \cos \theta)/2$, where θ is the angle between \vec{k} and \vec{k}' , is the overlap of states and $f_{s\vec{k}}$ are the Fermi distribution functions for the bands.

D.2 Calculation

Starting with the polarizability

¹This can easily be seen by substituting $\omega' = Re^{i\theta}$ and $d\omega' = iR\theta e^{i\theta}$, the integral over the semi circle then becomes $i \int_0^\pi d\theta \frac{f(Re^{i\theta})\theta Re^{i\theta}}{Re^{i\theta} - \omega}$, where for large R the integrand goes as $f(Re^{i\theta})$. We then see that the condition for the integral to vanish is that f vanishes at infinity in the entire upper half plane.

$$\Pi(q, \omega) = -\frac{g_s g_v}{\Omega} \lim_{\eta \rightarrow 0^+} \sum_{\vec{k} s s'} \frac{f_{s\vec{k}} - f_{s'\vec{k}'}}{\hbar\omega + \epsilon_{s\vec{k}} - \epsilon_{s'\vec{k}'} + i\eta} F_{ss'}(\vec{k}, \vec{k}'), \quad (\text{D.5})$$

where the notation is explained in the previous section. We can perform the s, s' summations in a straightforward way and we note that this will give us terms that contain distribution functions for the $+$ band and for the $-$ band, we group these together in what we call $\Pi^+(q, \omega)$ and $\Pi^-(q, \omega)$ respectively. Consequently we split the original polarizability into two parts so that

$$\Pi(q, \omega) = \Pi^+(q, \omega) + \Pi^-(q, \omega) \quad (\text{D.6})$$

where

$$\begin{aligned} \Pi^+(q, \omega) = & -\frac{g_s g_v}{2\Omega} \lim_{\eta \rightarrow 0^+} \sum_{\vec{k}} \left(\frac{(f_{\vec{k}_+} - f_{\vec{k}'_+})(1 + \cos \theta)}{\hbar\omega + \epsilon_{\vec{k}_+} - \epsilon_{\vec{k}'_+} + i\eta} + \frac{f_{\vec{k}_+}(1 - \cos \theta)}{\hbar\omega + \epsilon_{\vec{k}_+} - \epsilon_{\vec{k}'_-} + i\eta} - \right. \\ & \left. - \frac{f_{\vec{k}'_+}(1 - \cos \theta)}{\hbar\omega + \epsilon_{\vec{k}_-} - \epsilon_{\vec{k}'_+} + i\eta} \right), \end{aligned} \quad (\text{D.7})$$

$$\begin{aligned} \Pi^-(q, \omega) = & -\frac{g_s g_v}{2\Omega} \lim_{\eta \rightarrow 0^+} \sum_{\vec{k}} \left(\frac{(f_{\vec{k}_-} - f_{\vec{k}'_-})(1 + \cos \theta)}{\hbar\omega + \epsilon_{\vec{k}_-} - \epsilon_{\vec{k}'_-} + i\eta} + \frac{f_{\vec{k}_-}(1 - \cos \theta)}{\hbar\omega + \epsilon_{\vec{k}_-} - \epsilon_{\vec{k}'_+} + i\eta} - \right. \\ & \left. - \frac{f_{\vec{k}'_-}(1 - \cos \theta)}{\hbar\omega + \epsilon_{\vec{k}_+} - \epsilon_{\vec{k}'_-} + i\eta} \right). \end{aligned} \quad (\text{D.8})$$

D.2.1 $\Pi^-(q, \omega)$

Now, making explicit that we work at $T = 0$ and we assume that $\epsilon_F \geq 0$ i.e. the valence band is always completely filled, then $\Pi^-(q, \omega)$ takes a particularly simple form, namely

$$\Pi^-(q, \omega) = -\frac{g_s g_v}{2\Omega} \lim_{\eta \rightarrow 0^+} \sum_{\vec{k}} \left(\frac{f_{\vec{k}_-}(1 - \cos \theta)}{\hbar\omega + \epsilon_{\vec{k}_-} - \epsilon_{\vec{k}'_+} + i\eta} - \frac{f_{\vec{k}'_-}(1 - \cos \theta)}{\hbar\omega + \epsilon_{\vec{k}_+} - \epsilon_{\vec{k}'_-} + i\eta} \right) \quad (\text{D.9})$$

since the the first term in the original expression cancels. By using the Sokhotski-Plemelj theorem this can be further manipulated into

$$\begin{aligned}
\Pi^-(q, \omega) &= -\frac{g_s g_v}{2} \lim_{\eta \rightarrow 0^+} \int \frac{d^2 k}{(2\pi)^2} \left[(1 - \cos \theta) \left(\frac{1}{\hbar\omega + \epsilon_{\vec{k}_-} - \epsilon_{\vec{k}'_+} + i\eta} - \frac{1}{\hbar\omega + \epsilon_{\vec{k}_+} - \epsilon_{\vec{k}'_-} + i\eta} \right) \right] = \\
&= -\frac{g_s g_v}{2} \mathcal{P} \int \frac{d^2 k}{(2\pi)^2} \left[(1 - \cos \theta) \left(\frac{1}{\hbar\omega + \epsilon_{\vec{k}_-} - \epsilon_{\vec{k}'_+}} - \frac{1}{\hbar\omega + \epsilon_{\vec{k}_+} - \epsilon_{\vec{k}'_-}} \right) \right] + \\
&+ i \frac{g_s g_v \pi}{2} \int \frac{d^2 k}{(2\pi)^2} \left[(1 - \cos \theta) (\delta(\hbar\omega + \epsilon_{\vec{k}_-} - \epsilon_{\vec{k}'_+}) - \delta(\hbar\omega + \epsilon_{\vec{k}_+} - \epsilon_{\vec{k}'_-})) \right]
\end{aligned} \tag{D.10}$$

Imaginary part

We start out by computing the imaginary part of the answer, starting with writing out the integral in polar coordinates and obtain

$$\begin{aligned}
\text{Im } \Pi^-(q, \omega) &= \frac{g_s g_v}{8\pi} \int_0^\infty dk \int_0^{2\pi} d\theta_{kq} \left[k (1 - \cos \theta_{kk'}) \times \right. \\
&\quad \left. \times (\delta(\hbar\omega + \epsilon_{\vec{k}_-} - \epsilon_{\vec{k}'_+}) - \delta(\hbar\omega + \epsilon_{\vec{k}_+} - \epsilon_{\vec{k}'_-})) \right]
\end{aligned} \tag{D.11}$$

where the integration variable θ_{kq} is the angle between \vec{k} and \vec{q} and the original θ has been relabeled $\theta_{kk'}$ for clarity. Using the law of cosines twice we can obtain $\cos \theta_{kk'} = \frac{k+q \cos \theta_{kq}}{\sqrt{k^2+q^2+2kq \cos \theta_{kq}}}$, inserting this and the linear dispersion we get

$$\begin{aligned}
\text{Im } \Pi^-(q, \omega) &= \frac{g_s g_v}{8\pi} \int_0^\infty dk \int_0^{2\pi} d\theta_{kq} \left[k \left(1 - \frac{k+q \cos \theta_{kq}}{\sqrt{k^2+q^2+2kq \cos \theta_{kq}}} \right) \times \right. \\
&\quad \times \left(\delta(\hbar\omega - \hbar v_F k - \hbar v_F \sqrt{k^2+q^2+2kq \cos \theta_{kq}}) - \right. \\
&\quad \left. \left. - \delta(\hbar\omega + \hbar v_F k + \hbar v_F \sqrt{k^2+q^2+2kq \cos \theta_{kq}}) \right) \right].
\end{aligned} \tag{D.12}$$

We see that the argument in the second delta function is always positive so it will never contribute to the integral and can be dropped². Finding the zero of the remaining delta function is easy; the equation to solve is

²Strictly this is only true as long as ω is positive. Later we will need ω for also negative values, we will then use physical arguments to make the function odd in ω , keeping the second delta function we can see that it actually is an odd function in ω . For brevity we will drop it anyway in the calculations.

$$\frac{\omega - v_F k}{v_F} = \sqrt{k^2 + q^2 + 2kq \cos \theta_{kq}} \quad (\text{D.13})$$

and the solution is

$$k_1 = \frac{\omega^2 - v_F^2 q^2}{2v_F(\omega + v_F q \cos \theta_{kq})}. \quad (\text{D.14})$$

We see that since the k -integral extends only over the positive real line this implies³

$$\omega > v_F q$$

in order for the integration to cover the zero of the delta function. Naming the entire argument of the delta function $g(k)$ and performing a derivative we get

$$g'(k) = -\hbar v_F \left(1 + \frac{k + q \cos \theta_{kq}}{\sqrt{k^2 + q^2 + 2kq \cos \theta_{kq}}} \right) \quad (\text{D.15})$$

and using equation (D.13) we get

$$g'(k_1) = -\hbar v_F \left(1 + v_F \frac{k_1 + q \cos \theta_{kq}}{\omega - v_F k_1} \right) = -\hbar v_F \frac{\omega + q \cos \theta_{kq}}{\omega - v_F k_1}. \quad (\text{D.16})$$

³This condition comes from that the nominator and denominator should be positive, one could also imagine that $\omega < v_F q$ and both nominator and denominator be negative. However, going back to the argument of the delta function which this is supposed to be a zero of we can see that for $\omega < v_F q$ we can never accomplish this.

Using this in our expression for the polarization we get

$$\begin{aligned}
\text{Im } \Pi^-(q, \omega) &= \frac{g_s g_v}{8\pi} \int_0^\infty dk \int_0^{2\pi} d\theta_{kq} \times \\
&\times \left[k \left(1 - \frac{k + q \cos \theta_{kq}}{\sqrt{k^2 + q^2 + 2kq \cos \theta_{kq}}} \right) \frac{\delta(k - k_1)}{|g'(k_1)|} \right] = \\
&= \frac{g_s g_v}{8\pi} \int_0^{2\pi} d\theta_{kq} \left[k_1 \left(1 - \frac{k_1 + q \cos \theta_{kq}}{\sqrt{k_1^2 + q^2 + 2k_1 q \cos \theta_{kq}}} \right) \frac{1}{|g'(k_1)|} \right] = \\
&= \left\{ \text{using equations (D.13) and (D.16)} \right\} = \\
&= \frac{g_s g_v}{8\pi \hbar v_F} \int_0^{2\pi} d\theta_{kq} \left[k_1 \left(1 - \frac{v_F(k_1 + q \cos \theta_{kq})}{\omega - v_F k_1} \right) \frac{\omega - v_F k_1}{\omega + q \cos \theta_{kq}} \right] = \\
&= \frac{g_s g_v}{8\pi \hbar v_F} \int_0^{2\pi} d\theta_{kq} \left[\frac{k_1}{\omega + q \cos \theta_{kq}} (\omega - 2v_F k_1 - v_F q \cos \theta_{kq}) \right] = \\
&= \left\{ \text{using equation (D.14)} \right\} = \\
&= \frac{g_s g_v}{16\pi \hbar v_F^2} (\omega^2 - v_F^2 q^2) \int_0^{2\pi} d\theta_{kq} \left[\frac{\omega - v_F q \cos \theta_{kq}}{(\omega + v_F q \cos \theta_{kq})^2} - \frac{\omega^2 - v_F^2 q^2}{(\omega + v_F q \cos \theta_{kq})^3} \right].
\end{aligned} \tag{D.17}$$

This integral can be calculated⁴ and the answer is

$$\text{Im } \Pi^-(q, \omega) = \frac{g_s g_v}{16\hbar} \frac{q^2}{\sqrt{\omega^2 - v_F^2 q^2}} \theta(\omega - v_F q). \tag{D.18}$$

Also rewriting the prefactor into $D_0 = \frac{g_s g_v k_F}{2\pi \hbar v_F}$ which is the density of states at the Fermi energy we get

$$\text{Im } \Pi^-(q, \omega) = \frac{D_0 \pi v_F}{8 k_F} \frac{q^2}{\sqrt{\omega^2 - v_F^2 q^2}} \theta(\omega - v_F q). \tag{D.19}$$

Real part

We now proceed to calculate the real part of $\Pi^-(q, \omega)$. Instead of tackling the real part of equation (D.10) head on, we will use the Kramers-

⁴Mathematica does it easily using *Integrate* with the assumption that $\omega > v_F q$ which we know from earlier. The integral can also be looked up in [42] pp. 172, the answer is given in a recursive fashion due to the high power in the denominator. This could in principle also be done by a "tan $\frac{\theta}{2}$ substitution" followed by a residue calculation but this seems tedious.

Kronig relations, equation (D.3), to obtain the real part from the previously computed imaginary part, this seems to be easier. The expression we get is

$$\text{Re } \Pi^-(q, \omega) = \frac{1}{\pi} \mathcal{P} \int_{-\infty}^{\infty} d\omega' \frac{\text{Im } \Pi^-(q, \omega')}{\omega' - \omega}. \quad (\text{D.20})$$

As we mentioned earlier we have only considered $\omega > 0$, which is the physical regime, but we now see that we need its values for $\omega < 0$ in order to get the real part of the function. The simplest thing would be to just extend equation (D.19) to negative values of ω i.e. it would become an even function in ω . However, remember that in equation (D.12) we saw that $\Pi^-(q, \omega)$ was an odd function in ω , this also makes physical sense since $\Pi^-(q, \omega)$ is the Fourier transform of the quantity $\Pi^-(x, t - t')$ that connects the macroscopic bare potential to the macroscopic dressed potential felt by a test charge. This quantity is by necessity real which implies that the real part of its Fourier transform is even and the imaginary part is odd. So, making (D.19) an odd function, by inserting a $\text{sign}(\omega)$, we can write equation (D.20) as

$$\begin{aligned} \text{Re } \Pi^-(q, \omega) &= \frac{1}{\pi} \mathcal{P} \int_{-\infty}^{\infty} d\omega' \frac{\text{Im } \Pi^-(q, \omega')}{\omega' - \omega} = \\ &= \frac{D_0 q^2 v_F}{8 k_F} \mathcal{P} \int_{-\infty}^{\infty} d\omega' \frac{\theta(|\omega'| - v_F q) \text{sign}(\omega')}{(\omega' - \omega) \sqrt{\omega'^2 - v_F^2 q^2}} = \\ &= \frac{D_0 q^2 v_F}{8 k_F} \left(\mathcal{P} \int_{-\infty}^{v_F q} d\omega' \frac{\text{sign}(\omega')}{(\omega' - \omega) \sqrt{\omega'^2 - v_F^2 q^2}} + \right. \\ &\quad \left. + \mathcal{P} \int_{v_F q}^{\infty} d\omega' \frac{\text{sign}(\omega')}{(\omega' - \omega) \sqrt{\omega'^2 - v_F^2 q^2}} \right) = \\ &= \frac{D_0 q^2 \pi v_F}{8 k_F} \mathcal{P} \int_{v_F q}^{\infty} d\omega' \frac{1}{\sqrt{\omega'^2 - v_F^2 q^2}} \left(\frac{1}{\omega' + \omega} + \frac{1}{\omega' - \omega} \right). \end{aligned} \quad (\text{D.21})$$

This integral can be computed to be⁵

$$\text{Re } \Pi^-(q, \omega) = \frac{D_0 \pi v_F}{8 k_F} \frac{q^2}{\sqrt{v_F^2 q^2 - \omega^2}} \theta(v_F q - \omega). \quad (\text{D.22})$$

⁵The last integral can be done in Mathematica or with proper change of variables it can be looked up in [42] pp. 101. This is a little bit tricky and requires some effort but can be done.

Here we must remember that this is an even function in ω so the step function is really $\theta(v_F q - |\omega|)$ but normally we only use this expression for $\omega > 0$ so that this does not matter⁶.

D.2.2 $\Pi^+(q, \omega)$

We start by rewriting equation (D.7) into

$$\begin{aligned} \Pi^+(q, \omega) = & -\frac{g_s g_v}{2\Omega} \lim_{\eta \rightarrow 0^+} \sum_{\vec{k}} \left[f_{\vec{k}+} \left(\frac{1 + \cos \theta_{kk'}}{\hbar\omega + \epsilon_{\vec{k}+} - \epsilon_{\vec{k}'_+} + i\eta} + \frac{1 - \cos \theta_{kk'}}{\hbar\omega + \epsilon_{\vec{k}+} - \epsilon_{\vec{k}'_-} + i\eta} \right) \right. \\ & \left. - f_{\vec{k}'_+} \left(\frac{1 + \cos \theta_{kk'}}{\hbar\omega + \epsilon_{\vec{k}+} - \epsilon_{\vec{k}'_+} + i\eta} + \frac{1 - \cos \theta_{kk'}}{\hbar\omega + \epsilon_{\vec{k}_-} - \epsilon_{\vec{k}'_+} + i\eta} \right) \right] \end{aligned} \quad (\text{D.23})$$

where $\theta_{kk'}$ is the angle previously labeled as θ . By writing the sum as an integral and using that $d^2 k = d^2 k'$ we can change the integration variable on the $f_{\vec{k}'_+}$ term. We then relabel $\vec{k}' \rightarrow \vec{k}$ and $\vec{k} \rightarrow \vec{k}'' = \vec{k} - \vec{q}$, also $\vec{k}' = \vec{k} + \vec{q}$. The integration limits stay the same since the integral is between $\pm\infty$. We end up with an expression involving only $f_{\vec{k}+}$

$$\begin{aligned} \Pi^+(q, \omega) = & -\frac{g_s g_v}{2} \lim_{\eta \rightarrow 0^+} \int \frac{d^2 k}{(2\pi)^2} f_{\vec{k}+} \left(\frac{1 + \cos \theta_{kk'}}{\hbar\omega + \epsilon_{\vec{k}+} - \epsilon_{\vec{k}'_+} + i\eta} + \frac{1 - \cos \theta_{kk'}}{\hbar\omega + \epsilon_{\vec{k}+} - \epsilon_{\vec{k}'_-} + i\eta} \right. \\ & \left. - \frac{1 + \cos \theta_{k''k}}{\hbar\omega + \epsilon_{\vec{k}'_+} - \epsilon_{\vec{k}_+} + i\eta} - \frac{1 - \cos \theta_{k''k}}{\hbar\omega + \epsilon_{\vec{k}'_-} - \epsilon_{\vec{k}_+} + i\eta} \right). \end{aligned} \quad (\text{D.24})$$

Using Sokhotski-Plemelj we can perform the limit and thus separate this into its real- and imaginary parts as

$$\begin{aligned} \text{Re } \Pi^+(q, \omega) = & -\frac{g_s g_v}{8\pi^2} \mathcal{P} \int d^2 k f_{\vec{k}+} \left(\frac{1 + \cos \theta_{kk'}}{\hbar\omega + \epsilon_{\vec{k}+} - \epsilon_{\vec{k}'_+}} + \frac{1 - \cos \theta_{kk'}}{\hbar\omega + \epsilon_{\vec{k}+} - \epsilon_{\vec{k}'_-}} - \right. \\ & \left. - \frac{1 + \cos \theta_{k''k}}{\hbar\omega + \epsilon_{\vec{k}'_+} - \epsilon_{\vec{k}_+}} - \frac{1 - \cos \theta_{k''k}}{\hbar\omega + \epsilon_{\vec{k}'_-} - \epsilon_{\vec{k}_+}} \right) \end{aligned} \quad (\text{D.25})$$

⁶It is nice to note that remembering the even nature of this function we can plug this expression back into the Kramers-Kronig relations and obtain the imaginary part (with the sign(ω)) of the expression that we started out with.

$$\begin{aligned}
\text{Im } \Pi^+(q, \omega) &= \frac{g_s g_v}{8\pi^2} \int d^2k f_{\vec{k}_+} \times \\
&\times \left[(1 + \cos \theta_{kk'}) \delta(\hbar\omega + \epsilon_{\vec{k}_+} - \epsilon_{\vec{k}'_+}) + (1 - \cos \theta_{kk'}) \delta(\hbar\omega + \epsilon_{\vec{k}_+} - \epsilon_{\vec{k}'_-}) - \right. \\
&\left. - (1 + \cos \theta_{k''k}) \delta(\hbar\omega + \epsilon_{\vec{k}''_+} - \epsilon_{\vec{k}_+}) - (1 - \cos \theta_{k''k}) \delta(\hbar\omega + \epsilon_{\vec{k}''_-} - \epsilon_{\vec{k}_+}) \right]
\end{aligned} \tag{D.26}$$

where by using the law of cosines we know

$$\cos \theta_{kk'} = \frac{k + q \cos \theta_{kq}}{k'} \tag{D.27}$$

$$\cos \theta_{k''k} = \frac{k - q \cos \theta_{kq}}{k''} \tag{D.28}$$

and θ_{kq} is the angle between the vectors \vec{k} and \vec{q} .

Imaginary part

We now proceed to the imaginary part of the polarizability, i.e. equation (D.26). We use the Fermi function to truncate the integral, insert the dispersion relations and use polar coordinates and obtain

$$\begin{aligned}
\text{Im } \Pi^+(q, \omega) &= \frac{g_s g_v}{8\pi^2} \int_0^{k_F} dk \int_{-\pi}^{\pi} d\theta_{kq} k \left[(1 + \cos \theta_{kk'}) \delta(\hbar\omega + \hbar v_F k - \hbar v_F k') \right. \\
&+ (1 - \cos \theta_{kk'}) \delta(\hbar\omega + \hbar v_F k + \hbar v_F k') - (1 + \cos \theta_{k''k}) \delta(\hbar\omega - \hbar v_F k + \hbar v_F k'') \\
&\left. - (1 - \cos \theta_{k''k}) \delta(\hbar\omega - \hbar v_F k - \hbar v_F k'') \right]
\end{aligned} \tag{D.29}$$

where

$$k' = |\vec{k} + \vec{q}| = \sqrt{k^2 + q^2 + 2kq \cos \theta_{kq}}$$

and

$$k'' = |\vec{k} - \vec{q}| = \sqrt{k^2 + q^2 - 2kq \cos \theta_{kq}}$$

We see that the argument of the second delta function is always a positive number regardless of k, k' . Thus this will never contribute when we

perform the integral and it can be dropped. We call the arguments of the three remaining delta functions g_i i.e.

$$g_1(k) = \hbar\omega + \hbar v_F k - \hbar v_F k' \quad (\text{D.30})$$

$$g_2(k) = \hbar\omega - \hbar v_F k + \hbar v_F k'' \quad (\text{D.31})$$

$$g_3(k) = \hbar\omega - \hbar v_F k - \hbar v_F k''. \quad (\text{D.32})$$

We now find the zeros of these functions and obtain

$$k_1 = \frac{v_F^2 q^2 - \omega^2}{2v_F(\omega - v_F q \cos \theta_{kq})}, \quad v_F q > \omega, \quad \cos \theta_{kq} < \frac{\omega}{v_F q} \quad (\text{D.33})$$

$$k_2 = \frac{v_F^2 q^2 - \omega^2}{2v_F(v_F q \cos \theta_{kq} - \omega)}, \quad v_F q > \omega, \quad \cos \theta_{kq} > \frac{\omega}{v_F q} \quad (\text{D.34})$$

$$k_3 = \frac{\omega^2 - v_F^2 q^2}{2v_F(\omega - v_F q \cos \theta_{kq})}, \quad \omega > v_F q. \quad (\text{D.35})$$

The conditions for the different k 's come from careful investigation of when the arguments become zero, since there is a square root involved the signs of things are tricky. First one should investigate the condition for the ω , $v_F q$ and then one may extract the condition on θ_{kq} by demanding the resulting solution to be positive (since we are only integrating over positive k these are the only ones that can contribute). We also need the derivatives of the g_i so we compute them and get

$$g_1'(k) = \hbar v_F \left(1 - \frac{k + q \cos \theta_{kq}}{k'} \right) \quad (\text{D.36})$$

$$g_2'(k) = \hbar v_F \left(-1 + \frac{k - q \cos \theta_{kq}}{k''} \right) \quad (\text{D.37})$$

$$g_3'(k) = -\hbar v_F \left(1 + \frac{k - q \cos \theta_{kq}}{k''} \right). \quad (\text{D.38})$$

Furthermore we need $|g_i(k_i)|$ and after some simplifications we get

$$|g_1'(k_1)| = \hbar v_F \frac{\omega - v_F q \cos \theta_{kq}}{\omega + v_F k_1} \quad (\text{D.39})$$

$$|g_2'(k_2)| = \hbar v_F \frac{v_F q \cos \theta_{kq} - \omega}{v_F k_2 - \omega} \quad (\text{D.40})$$

$$|g_3'(k_3)| = \hbar v_F \frac{\omega - v_F q \cos \theta_{kq}}{\omega - v_F k_3}. \quad (\text{D.41})$$

Now we want to perform the k -integral, this will introduce an additional constrain on the θ_{kq} integral since we now must take care not to integrate over θ_{kq} 's that make $k_i > k_F$. We also introduce the dimensionless variables $x = \frac{q}{2k_F}$ and $\nu = \frac{\omega}{v_F q}$ and get the constraints

$$\text{First term: } k_1 < k_F \Rightarrow \cos \theta_{kq} > \nu - x(1 - \nu^2), \quad 1 > x(1 - \nu) \quad (\text{D.42})$$

$$\text{Second term: } k_2 < k_F \Rightarrow \cos \theta_{kq} < \nu + x(1 - \nu^2), \quad 1 > x(1 + \nu) \quad (\text{D.43})$$

$$\text{Third term: } k_3 < k_F \Rightarrow \begin{cases} \cos \theta_{kq} > \nu - x(\nu^2 - 1), \quad 1 > x(\nu - 1), \quad 1 < x(\nu + 1) \\ \text{no constraint on } \theta_{kq}, \quad 1 > x(\nu + 1) \end{cases} \quad (\text{D.44})$$

where the constraints that does not include θ_{kq} come from requiring the constraints to be within $[-1, 1]$ in order for $\cos \theta_{kq}$ to be able to fulfill them. We also note that these new constraints are more severe than the old ones and thus also fulfill the old constraints in equations (D.33) - (D.35). We now perform the k -integral, use the dimensionless variables to rewrite the polarizability and we insert the above constraints on the θ_{kq} -integral and obtain

$$\begin{aligned} \text{Im } \Pi^+(q, \omega) = & \frac{g_s g_v}{4\pi^2} \left[\theta(1 - \nu) \times \right. \\ & \times \left\{ \theta(1 - x(1 - \nu)) \int_{\cos \theta_{kq} = \nu - x(1 - \nu^2)}^{\pi} d\theta_{kq} \frac{k_1(1 + \cos \theta_{k_1 k_1'})}{|g_1'(k_1)|} \right. \\ & \left. - \theta(1 - x(1 + \nu)) \int_0^{\cos \theta_{kq} = \nu + x(1 - \nu^2)} d\theta_{kq} \frac{k_2(1 + \cos \theta_{k_2'' k_2})}{|g_2'(k_2)|} \right\} \\ & - \theta(\nu - 1) \left\{ \theta(1 - x(\nu - 1)) \theta(x(\nu + 1) - 1) \int_{\cos \theta_{kq} = \nu - x(\nu^2 - 1)}^{\pi} d\theta_{kq} \frac{k_3(1 - \cos \theta_{k_3'' k_3})}{|g_3'(k_3)|} \right. \\ & \left. + \theta(1 - x(\nu + 1)) \int_0^{\pi} d\theta_{kq} \frac{k_3(1 - \cos \theta_{k_3'' k_3})}{|g_3'(k_3)|} \right\} \left. \right] \quad (\text{D.45}) \end{aligned}$$

where we integrate over the upper half circle and have compensated with a factor of 2 because of the even nature of the integrals. The notation $\cos \theta_{k_i k_i'}$ means that we are supposed to insert the corresponding k_i in the expression for cosine of the angle, see equations (D.27) and (D.28), doing

this and simplifying we obtain

$$1 + \cos \theta_{k_1 k'_1} = \frac{\omega + v_F q \cos \theta_{kq} + 2v_F k_1}{\omega + v_F k_1} \quad (\text{D.46})$$

$$1 + \cos \theta_{k_2'' k_2} = \frac{-\omega - v_F q \cos \theta_{kq} + 2v_F k_2}{v_F k_2 - \omega} \quad (\text{D.47})$$

$$1 - \cos \theta_{k_3'' k_3} = \frac{\omega + v_F q \cos kq - 2v_F k_3}{\omega - v_F k_3}. \quad (\text{D.48})$$

We now insert the modulus of the g_i 's and our expressions for the angles into equation (D.45) and we get the following expression (when all is converted to the variables x and ν)

$$\begin{aligned} \text{Im } \Pi^+(q, \omega) &= \frac{g_s g_v q}{8\pi \hbar v_F} \left[\theta(1 - \nu) \times \right. \\ &\times \left\{ \theta(1 - x(1 - \nu)) \int_{\cos \theta_{kq} = \nu - x(1 - \nu^2)}^{\pi} d\theta_{kq} \left((1 - \nu^2) \frac{\nu + \cos \theta_{kq}}{(\nu - \cos \theta_{kq})^2} + \frac{(1 - \nu^2)^2}{(\nu - \cos \theta_{kq})^3} \right) \right. \\ &\quad \left. - \theta(1 - x(1 + \nu)) \int_0^{\cos \theta_{kq} = \nu + x(1 - \nu^2)} d\theta_{kq} \times \right. \\ &\quad \left. \times \left(-(1 - \nu^2) \frac{\nu + \cos \theta_{kq}}{(\cos \theta_{kq} - \nu)^2} + \frac{(1 - \nu^2)^2}{(\cos \theta_{kq} - \nu)^3} \right) \right\} \\ &\quad - \theta(\nu - 1) \left\{ \theta(1 - x(\nu - 1)) \theta(x(\nu + 1) - 1) \int_{\cos \theta_{kq} = \nu - x(\nu^2 - 1)}^{\pi} d\theta_{kq} \times \right. \\ &\quad \times \left((\nu^2 - 1) \frac{\nu + \cos \theta_{kq}}{(\nu - \cos \theta_{kq})^2} - \frac{(\nu^2 - 1)^2}{(\nu - \cos \theta_{kq})^3} \right) + \\ &\quad \left. \left. + \theta(1 - x(\nu + 1)) \int_0^{\pi} d\theta_{kq} \left((\nu^2 - 1) \frac{\nu + \cos \theta_{kq}}{(\nu - \cos \theta_{kq})^2} - \frac{(\nu^2 - 1)^2}{(\nu - \cos \theta_{kq})^3} \right) \right\} \right] \quad (\text{D.49}) \end{aligned}$$

These primitives can be looked up in [42] pp. 172 or be done in *Mathematica*. After inserting the proper limits in all the primitives and simplifying

the answer becomes

$$\begin{aligned}
\text{Im } \Pi^+(q, \omega) &= \frac{g_s g_v q}{8\pi \hbar v_F} \left[\frac{\theta(1-\nu)}{\sqrt{1-\nu^2}} \left\{ \theta(1-x(1-\nu)) \times \right. \right. \\
&\times \left(-\text{arctanh} \left(\sqrt{1 - \frac{2x}{1+x(1+\nu)}} \right) + \frac{(1+x\nu)\sqrt{1-(\nu-x(1-\nu^2))^2}}{2x^2\sqrt{1-\nu^2}} \right) + \\
&\quad \left. \left. + \theta(1-x(1+\nu)) \times \right. \right. \\
&\quad \left. \left. \times \left(\text{arccoth} \left(\sqrt{\frac{1+x(1-\nu)}{1-x(1+\nu)}} \right) - \frac{(1-x\nu)\sqrt{1-(\nu+x(1-\nu^2))^2}}{2x^2\sqrt{1-\nu^2}} \right) \right\} \right. \\
&- \frac{\theta(\nu-1)\theta(1-x(\nu-1))}{\sqrt{\nu^2-1}} \left\{ \frac{\pi}{2} + \theta(x(\nu+1)-1) \left(-\text{arccot} \left(\sqrt{\frac{1-x(\nu-1)}{x(\nu+1)-1}} \right) \right. \right. \\
&\quad \left. \left. + \frac{(1-x\nu)\sqrt{1-(\nu-x(\nu^2-1))^2}}{2x^2\sqrt{\nu^2-1}} \right) \right\} \left. \right]. \tag{D.50}
\end{aligned}$$

We now convert back to the variables q and ω and obtain finally

$$\begin{aligned}
\text{Im } \Pi^+(q, \omega) &= \frac{D_0 v_F}{4 k_F} \left[\frac{\theta(v_F q - \omega)}{\sqrt{v_F^2 q^2 - \omega^2}} \left\{ \theta(2k_F v_F - (v_F q - \omega)) \times \right. \right. \\
&\times \left(-q^2 \text{arctanh} \left(\sqrt{1 - \frac{2v_F q}{2k_F v_F + v_F q + \omega}} \right) + f(q, \omega)/2 \right) \\
&\quad \left. \left. + \theta(2k_F v_F - (v_F q + \omega)) \times \right. \right. \\
&\quad \left. \left. \times \left(q^2 \text{arccoth} \left(\sqrt{1 + \frac{2v_F q}{2v_F k_F - (v_F q + \omega)}} \right) - f(q, -\omega)/2 \right) \right\} \right. \\
&- \frac{\theta(\omega - v_F q)\theta(2k_F v_F - (\omega - v_F q))}{\sqrt{\omega^2 - v_F^2 q^2}} \left\{ \frac{\pi q^2}{2} + \theta((\omega + v_F q) - 2k_F v_F) \times \right. \\
&\times \left. \left(-q^2 \text{arccot} \left(\sqrt{\frac{2v_F q}{\omega + v_F q - 2k_F v_F}} - 1 \right) + f(q, -\omega)/2 \right) \right\} \left. \right] \tag{D.51}
\end{aligned}$$

with

$$f(q, \omega) = \frac{(2k_F v_F + \omega)}{v_F^2} \sqrt{|(2k_F v_F + \omega)^2 - v_F^2 q^2|}. \tag{D.52}$$

Real part

The expression for the imaginary part is rather complicated and instead of using the Kramers-Kronig relations we now compute the real part head

on. We insert the dispersion relations into equation (D.25) and use polar coordinates and the real part takes the form

$$\begin{aligned} \text{Re } \Pi^+(q, \omega) = & -\frac{g_s g_v}{8\pi^2 \hbar} \mathcal{P} \int_0^\infty dk \int_{-\pi}^\pi d\theta_{kq} k f_{\vec{k}^+} \left(\frac{1 + \cos \theta_{kk'}}{\omega + v_F k - v_F k'} + \frac{1 - \cos \theta_{kk'}}{\omega + v_F k + v_F k'} \right. \\ & \left. - \frac{1 + \cos \theta_{k''k}}{\omega + v_F k'' - v_F k} - \frac{1 - \cos \theta_{k''k}}{\omega - v_F k'' - v_F k} \right) \end{aligned} \quad (\text{D.53})$$

where $k = |\vec{k}|$, $k' = |\vec{k} + \vec{q}|$ and $k'' = |\vec{k} - \vec{q}|$. We now write the two first terms and the two last terms over the same denominator respectively and get

$$\begin{aligned} \text{Re } \Pi^+(q, \omega) = & -\frac{g_s g_v}{4\pi^2 \hbar} \mathcal{P} \int_0^{k_F} dk \int_{-\pi}^\pi d\theta_{kq} k \times \\ & \times \left(\frac{\omega + 2v_F k + v_F q \cos \theta_{kq}}{(\omega + v_F k)^2 - v_F^2 k'^2} - \frac{\omega - 2v_F k + v_F q \cos \theta_{kq}}{(\omega - v_F k)^2 - v_F^2 k''^2} \right) \end{aligned} \quad (\text{D.54})$$

where we have used the Fermi function to truncate the k integral. We now perform a "tan $\frac{\theta}{2}$ -substitution", i.e. $\int_{-\pi}^\pi d\theta_{kq} \rightarrow \int_{-\infty}^\infty dt \frac{2}{1+t^2}$ and $\cos \theta_{kq} \rightarrow \frac{1-t^2}{1+t^2}$. Inserting this and simplifying we obtain

$$\begin{aligned} \text{Re } \Pi^+(q, \omega) = & -\frac{g_s g_v}{2\pi^2 \hbar} \int_0^{k_F} dk \mathcal{P} \int_{-\infty}^\infty dt \frac{k}{1+t^2} \times \\ & \times \left(\frac{t^2(\omega + 2v_F k - v_F q) + (\omega + 2v_F k + v_F q)}{t^2(\omega^2 - v_F^2 q^2 + 2v_F k(\omega + v_F q)) + (\omega^2 - v_F^2 + 2v_F k(\omega - v_F q))} - \right. \\ & \left. - \frac{t^2(\omega - 2v_F k - v_F q) + (\omega - 2v_F k + v_F q)}{t^2(\omega^2 - v_F^2 q^2 - 2v_F k(\omega + v_F q)) + (\omega^2 - v_F^2 - 2v_F k(\omega - v_F q))} \right). \end{aligned} \quad (\text{D.55})$$

In this form it is obvious that it is convenient to evaluate the t -integral using the method of residues, i.e. $\int_{-\infty}^\infty dt = 2\pi I \sum_{\text{enclosed residues}}$. Whenever the poles lie on the real axis we are instructed by the principal value, \mathcal{P} , to ignore the pole. Thus we need only include terms in the upper half plane⁷ and we proceed to find the poles of our integrand.

⁷We could equally well choose to enclose the lower half plane, this would mean to sum the poles in the negative half plane.

For the first term we need to solve

$$t^2(\omega^2 - v_F^2 q^2 + 2v_F k(\omega + v_F q)) + (\omega^2 - v_F^2 q^2 + 2v_F k(\omega - v_F q)) = 0 \quad (\text{D.56})$$

which has the solutions

$$t_1 = \pm i \sqrt{\frac{\omega^2 - v_F^2 q^2 + 2v_F k(\omega - v_F q)}{\omega^2 - v_F^2 q^2 + 2v_F k(\omega + v_F q)}}. \quad (\text{D.57})$$

Similarly the second term has the poles

$$t_2 = \pm i \sqrt{\frac{\omega^2 - v_F^2 q^2 - 2v_F k(\omega - v_F q)}{\omega^2 - v_F^2 q^2 - 2v_F k(\omega + v_F q)}}. \quad (\text{D.58})$$

Because of the common prefactor, both terms also have poles at

$$t = \pm i. \quad (\text{D.59})$$

It is now a matter of studying when these poles are in the upper half plane and when they are on the real line and should be excluded. In order to be included the expressions under the square root should be positive, this requirement may restrict the outer k -integral to not go all the way to its upper limit k_F . We start by factorizing the first term

$$\frac{\omega^2 - v_F^2 q^2 + 2v_F k(\omega - v_F q)}{\omega^2 - v_F^2 q^2 + 2v_F k(\omega + v_F q)} = \frac{(\omega - v_F q)(\omega + v_F q + 2v_F k)}{(\omega + v_F q)(\omega - v_F q + 2v_F k)}. \quad (\text{D.60})$$

We see that for $\omega > v_F q$ this expression is always > 0 and should always be included. For the case $\omega < v_F q$ we see that the nominator is always negative which means that the denominator must also be negative to contribute. This is true if $2v_F k < v_F q - \omega$, this means that if $2v_F k_F < v_F q - \omega$ then the integral remains limited by k_F but if $2v_F k_F > v_F q - \omega$ then the k -integral is restricted to $k_{\max} = \frac{v_F q - \omega}{2v_F}$.

We now turn our attention to the second term and the expression under the square root that must be positive is

$$\frac{\omega^2 - v_F^2 q^2 - 2v_F k(\omega - v_F q)}{\omega^2 - v_F^2 q^2 - 2v_F k(\omega + v_F q)} = \frac{(\omega - v_F q)(\omega + v_F q - 2v_F k)}{(\omega + v_F q)(\omega - v_F q + 2v_F k)}. \quad (\text{D.61})$$

If $\omega > v_F q$ then both the nominator and the denominator may become negative. In order for the term to be positive we either need both positive

or both negative. Both are positive if $2v_F k < \omega - v_F q$ (because this automatically means that $2v_F k < \omega + v_F q$). This means that if $k_F < \frac{\omega - v_F q}{2v_F}$ we may integrate to k_F but if $k_F > \frac{\omega - v_F q}{2v_F}$ we must restrict ourselves to $k_{\max} = \frac{\omega - v_F q}{2v_F}$. Both terms are negative if $2v_F k > \omega + v_F q$, this means that for $2v_F k_F > \omega + v_F q$ our integration ranges from $k_{\min} = \frac{\omega + v_F q}{2v_F} v_F$ to k_F .

If $\omega < v_F q$ we see that the denominator is always negative so the numerator also needs to be negative i.e. $2v_F k > \omega + v_F q$. This means that only if $2v_F k_F > \omega + v_F q$ we get a contribution and the integration goes from $k_{\min} = \frac{\omega + v_F q}{2v_F}$ to k_F .

So finally we get for the first term

$\omega > v_F q$	always	$\int_0^{k_F} dk$
$\omega < v_F q$	$k_F < \frac{v_F q - \omega}{2v_F}$	$\int_0^{k_F} dk$
	$k_F > \frac{v_F q - \omega}{2v_F}$	$\int_0^{\frac{v_F q - \omega}{2v_F}} dk$

and for the second term

$\omega > v_F q$	$k_F < \frac{\omega - v_F q}{2v_F}$	$\int_0^{k_F} dk$
	$k_F > \frac{\omega - v_F q}{2v_F}$	$\int_0^{\frac{\omega - v_F q}{2v_F}} dk$
	$k_F > \frac{\omega + v_F q}{2v_F}$	$\int_{\frac{\omega + v_F q}{2v_F}}^{k_F} dk$
$\omega < v_F q$	$k_F < \frac{v_F q + \omega}{2v_F}$	0
	$k_F > \frac{v_F q + \omega}{2v_F}$	$\int_{\frac{v_F q + \omega}{2v_F}}^{k_F} dk$

The residues are now evaluated at $t = i$ and $t = t_1$ for the first term in equation (D.55) and at $t = i$ and $t = t_2$ for the second term in equation (D.55). Starting by evaluating the residue of both terms at $t = i$, taking the difference (because of the minus sign between the terms) and integrating

over k , gives a contribution

$$-\frac{\pi k_F}{v_F}. \quad (\text{D.62})$$

Now, evaluating the residue of the first term at $t = t_1$ and integrating to get the primitive we get two different functions depending on the relationship between ω and q ,

$$F_{1a}(k) = \frac{\pi}{8v_F^2 \sqrt{\omega^2 - v_F^2 q^2}} \left((2kv_F + \omega) \sqrt{(2kv_F + \omega)^2 - v_F^2 q^2} - v_F^2 q^2 \log \left(2kv_F + \omega + \sqrt{(2kv_F + \omega)^2 - v_F^2 q^2} \right) \right) \quad (\text{D.63})$$

$$F_{1b}(k) = \frac{\pi}{8v_F^2 \sqrt{v_F^2 q^2 - \omega^2}} \left((2kv_F + \omega) \sqrt{v_F^2 q^2 - (2kv_F + \omega)^2} + v_F^2 q^2 \arctan \left(\frac{2kv_F + \omega}{\sqrt{v_F^2 q^2 - (2kv_F + \omega)^2}} \right) \right) \quad (\text{D.64})$$

where $F_{1a}(k)$ is valid for $\omega > v_F q$ and $F_{1b}(k)$ is valid for $\omega < v_F q$. Proceeding to the second term and finding the primitive in the two regimes gives us⁸

$$F_{2a}(k) = \text{sign}(2kv_F - (\omega + v_F q)) \frac{\pi}{8v_F^2 \sqrt{\omega^2 - v_F^2 q^2}} \times \left((2kv_F - \omega) \sqrt{(2kv_F - \omega)^2 - v_F^2 q^2} - v_F^2 q^2 \log \left(2kv_F - \omega + \sqrt{(2kv_F - \omega)^2 - v_F^2 q^2} \right) \right) \quad (\text{D.65})$$

$$F_{2b}(k) = -\frac{\pi}{8v_F^2 \sqrt{v_F^2 q^2 - \omega^2}} \left((2kv_F - \omega) \sqrt{v_F^2 q^2 - (2kv_F - \omega)^2} + v_F^2 q^2 \arctan \left(\frac{2kv_F - \omega}{\sqrt{v_F^2 q^2 - (2kv_F - \omega)^2}} \right) \right) \quad (\text{D.66})$$

where $F_{2a}(k)$ is valid for $\omega > v_F q$ and $F_{2b}(k)$ is valid for $\omega < v_F q$. Now, using all the residues we can evaluate the integrals in equation (D.55) and

⁸The notation with the sign function is not ideal, we will later enter a value of k that will make the argument 0, the sign function is defined as 0 in this case. This is not what we are after, we want to have the sign determined by the rest of the integration range, we keep this in mind for later.

the unsimplified result is

$$\begin{aligned}
\text{Re } \Pi^+(q, \omega) = & -\frac{g_s g_v}{2\pi^2 \hbar} \left[-\frac{\pi k_F}{v_F} + \theta(\omega - v_F q) \times \right. \\
& \times \left\{ F_{1a}(k_F) - F_{1a}(0) - \theta(\omega - v_F q - 2k_F v_F) (F_{2a}(k_F) - F_{2a}(0)) - \right. \\
& -\theta(2k_F v_F - (\omega - v_F q)) \left(F_{2a}\left(\frac{\omega - v_F q}{2v_F}\right) - F_{2a}(0) \right) - \theta(2k_F v_F - (\omega + v_F q)) \times \\
& \quad \left. \times \left(F_{2a}(k_F) - F_{2a}\left(\frac{\omega + v_F q}{2v_F}\right) \right) \right\} \\
& +\theta(v_F q - \omega) \left\{ \theta(v_F q - \omega - 2k_F v_F) (F_{1b}(k_F) - F_{1b}(0)) + \right. \\
& +\theta(2k_F v_F - (v_F q - \omega)) \left(F_{1b}\left(\frac{v_F q - \omega}{2v_F}\right) - F_{1b}(0) \right) - \\
& \quad -\theta(v_F q + \omega - 2k_F v_F) (F_{2b}(k_F) - F_{2b}(0)) - \\
& \quad \left. \left. -\theta(2k_F v_F - (v_F q + \omega)) \left(F_{2b}\left(\frac{v_F q + \omega}{2v_F}\right) - F_{2b}(0) \right) \right\} \right] \quad (\text{D.67})
\end{aligned}$$

which can be simplified to

$$\begin{aligned}
\text{Re } \Pi^+(q, \omega) = & -\frac{g_s g_v}{2\pi^2 \hbar} \left[-\frac{\pi k_F}{v_F} + \theta(\omega - v_F q) \left\{ F_{1a}(k_F) - F_{1a}(0) + F_{2a}(0) \right. \right. \\
& -\theta(\omega - v_F q - 2k_F v_F) F_{2a}(k_F) - \theta(2k_F v_F - (\omega - v_F q)) F_{2a}\left(\frac{\omega - v_F q}{2v_F}\right) \\
& \quad \left. \left. -\theta(2k_F v_F - (\omega + v_F q)) \left(F_{2a}(k_F) - F_{2a}\left(\frac{\omega + v_F q}{2v_F}\right) \right) \right\} \right. \\
& +\theta(v_F q - \omega) \left\{ \theta(v_F q - \omega - 2k_F v_F) F_{1b}(k_F) + \theta(2k_F v_F - (v_F q - \omega)) F_{1b}\left(\frac{v_F q - \omega}{2v_F}\right) \right. \\
& \quad \left. \left. -\theta(v_F q + \omega - 2k_F v_F) F_{2b}(k_F) - \theta(2k_F v_F - (v_F q + \omega)) F_{2b}\left(\frac{v_F q + \omega}{2v_F}\right) \right\} \right]. \quad (\text{D.68})
\end{aligned}$$

Also this expression is a bit cumbersome to work with, by inserting the arguments for k in the F -functions (remembering our convention with the sign-function in F_{2a}) and picking up all minus signs inside our logarithms and cancel the resulting imaginary parts we can obtain an answer that is

simpler. We define the functions ($f(q, \omega)$ is defined as before)

$$f(q, \omega) = \frac{(2k_F v_F + \omega)}{v_F^2} \sqrt{|(2k_F v_F + \omega)^2 - v_F^2 q^2|} \quad (\text{D.69})$$

$$g(q, \omega) = q^2 \log\left(\left|\frac{2k_F v_F + \omega + \sqrt{|(2k_F v_F + \omega)^2 - v_F^2 q^2|}}{v_F q}\right|\right) \quad (\text{D.70})$$

$$h(q, \omega) = q^2 \arctan\left(\frac{2k_F v_F + \omega}{\sqrt{|(2k_F v_F + \omega)^2 - v_F^2 q^2|}}\right) \quad (\text{D.71})$$

and the real part can then finally be written as

$$\begin{aligned} \text{Re } \Pi^+(q, \omega) = & -\frac{D_0 v_F}{8 k_F} \left(-\frac{8k_F}{v_F} + \frac{\theta(\omega - v_F q)}{\sqrt{\omega^2 - v_F^2 q^2}} \left\{ f(q, \omega) - g(q, \omega) \right. \right. \\ & \left. \left. + (\theta(\omega - v_F q - 2k_F v_F) - \theta(2k_F v_F - \omega - v_F q)) (f(q, -\omega) - g(q, -\omega)) \right\} \right. \\ & \left. + \frac{\theta(v_F q - \omega)}{\sqrt{v_F^2 q^2 - \omega^2}} \left\{ \frac{\pi q^2}{2} (\theta(2k_F v_F - v_F q - \omega) + \theta(2k_F v_F - v_F q + \omega)) \right. \right. \\ & \quad \left. \left. + \theta(v_F q - \omega - 2k_F v_F) (f(q, \omega) + h(q, \omega)) + \right. \right. \\ & \quad \left. \left. + \theta(v_F q + \omega - 2k_F v_F) (f(q, -\omega) + h(q, -\omega)) \right\} \right) \quad (\text{D.72}) \end{aligned}$$

D.3 Summary of results

In summary, the graphene polarizability can be written as

$$\Pi(q, \omega) = \Pi^+(q, \omega) + \Pi^-(q, \omega) \quad (\text{D.73})$$

where the contribution from the valence band is

$$\Pi^-(q, \omega) = \frac{D_0 \pi v_F}{8 k_F} \left(\frac{q^2}{\sqrt{v_F^2 q^2 - \omega^2}} \theta(v_F q - \omega) + i \frac{q^2}{\sqrt{\omega^2 - v_F^2 q^2}} \theta(\omega - v_F q) \right) \quad (\text{D.74})$$

and $D_0 = \frac{g_s g_v k_F}{2\pi \hbar v_F}$. The contribution from the conduction band is

$$\begin{aligned} \text{Re } \Pi^+(q, \omega) = & D_0 \left(1 - \frac{v_F}{8k_F} \frac{\theta(\omega - v_F q)}{\sqrt{\omega^2 - v_F^2 q^2}} \left\{ f(q, \omega) - g(q, \omega) + \right. \right. \\ & + \left. \left(\theta(\omega - v_F q - 2k_F v_F) - \theta(2k_F v_F - \omega - v_F q) \right) \times \right. \\ & \left. \left. \times \left(f(q, -\omega) - g(q, -\omega) \right) \right\} \right. \\ & - \frac{v_F}{8k_F} \frac{\theta(v_F q - \omega)}{\sqrt{v_F^2 q^2 - \omega^2}} \times \\ & \times \left\{ \frac{\pi q^2}{2} \left(\theta(2k_F v_F - v_F q - \omega) + \theta(2k_F v_F - v_F q + \omega) \right) \right. \\ & + \theta(v_F q - \omega - 2k_F v_F) \left(f(q, \omega) + h(q, \omega) \right) + \\ & \left. \left. + \theta(v_F q + \omega - 2k_F v_F) \left(f(q, -\omega) + h(q, -\omega) \right) \right\} \right) \quad (\text{D.75}) \end{aligned}$$

$$\begin{aligned}
\text{Im } \Pi^+(q, \omega) = & \frac{D_0 v_F}{4 k_F} \left[\frac{\theta(v_F q - \omega)}{\sqrt{v_F^2 q^2 - \omega^2}} \left\{ \theta(2k_F v_F - (v_F q - \omega)) \times \right. \right. \\
& \times \left(-q^2 \text{arctanh} \left(\sqrt{1 - \frac{2v_F q}{2k_F v_F + v_F q + \omega}} \right) + f(q, \omega)/2 \right) \\
& + \theta(2k_F v_F - (v_F q + \omega)) \times \\
& \times \left(q^2 \text{arccoth} \left(\sqrt{1 + \frac{2v_F q}{2v_F k_F - (v_F q + \omega)}} \right) - f(q, -\omega)/2 \right) \left. \right\} - \\
& - \frac{\theta(\omega - v_F q) \theta(2k_F v_F - (\omega - v_F q))}{\sqrt{\omega^2 - v_F^2 q^2}} \left\{ \frac{\pi q^2}{2} + \right. \\
& + \theta((\omega + v_F q) - 2k_F v_F) \times \\
& \times \left. \left(-q^2 \text{arccot} \left(\sqrt{\frac{2v_F q}{\omega + v_F q - 2k_F v_F} - 1} \right) + f(q, -\omega)/2 \right) \right\} \Big] \tag{D.76}
\end{aligned}$$

where

$$f(q, \omega) = \frac{(2k_F v_F + \omega)}{v_F^2} \sqrt{|(2k_F v_F + \omega)^2 - v_F^2 q^2|} \tag{D.77}$$

$$g(q, \omega) = q^2 \log \left(\left| \frac{2k_F v_F + \omega + \sqrt{|(2k_F v_F + \omega)^2 - v_F^2 q^2|}}{v_F q} \right| \right) \tag{D.78}$$

$$h(q, \omega) = q^2 \arctan \left(\frac{2k_F v_F + \omega}{\sqrt{|(2k_F v_F + \omega)^2 - v_F^2 q^2|}} \right). \tag{D.79}$$

D.4 Long wavelength expansion of the polarizability

The above form of the polarizability is rather cumbersome; but in order to get the plasmon dispersion we only need the long wavelength behavior of the real part. Thus we make a series expansion around $q = 0$ (in Mathematica) and we obtain

$$\Pi(q \rightarrow 0, \omega) = -D_0 \frac{v_F q^2}{2\omega k_F} \left(\frac{v_F k_F}{\omega} + \frac{1}{2} \log \left(\frac{2k_F v_F - \omega}{2k_F v_F + \omega} \right) \right) \tag{D.80}$$

valid for $\omega < 2v_F k_F$ and $\omega > v_F q$ which is the relevant conditions for plasmons. This can be seen in the plot of the imaginary part of Π , the fact that it is 0 in this region means that the plasmon is undamped here and may thus propagate. Putting the above expression for the long wavelength behavior of Π , neglecting the logarithmic correction term, into the plasmon condition $\epsilon(q, \omega) = 0$ yields the plasmon dispersion

$$\omega_p(q) = \sqrt{\frac{g\alpha_g\epsilon_F v_F q}{4}} \quad (\text{D.81})$$

where α_g is the fine structure constant of graphene $\alpha_g = \frac{e^2}{\epsilon_r^* v_F}$ and $\epsilon_r^* = (\epsilon_1 + \epsilon_2)/2$ is the average relative permittivity of the two media surrounding the graphene. Here we clearly see the typical two-dimensional \sqrt{q} behavior and the relativistic $n^{1/4}$ behavior (since $n \propto \epsilon_F^2$).

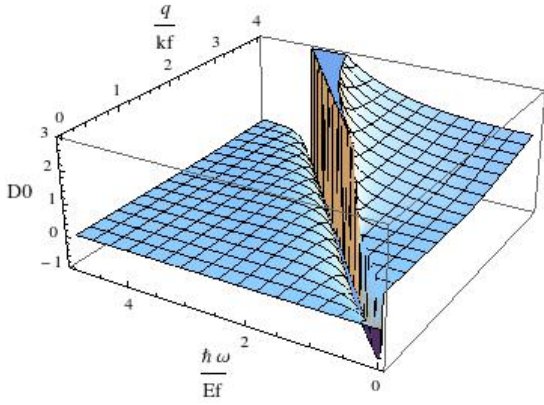


Figure D.1: Real part of the polarizability, the linear dispersion is clearly visible as the valley in the middle. From this function it is possible to find the dispersion of the (longitudinal) plasmons using the criterion $\epsilon(q, \omega) = 0$. The fact that the polarizability goes to zero for large frequency is signaling that the electron plasma is not effective at screening EM-radiation at high frequencies, the plasma behaves more like the vacuum.

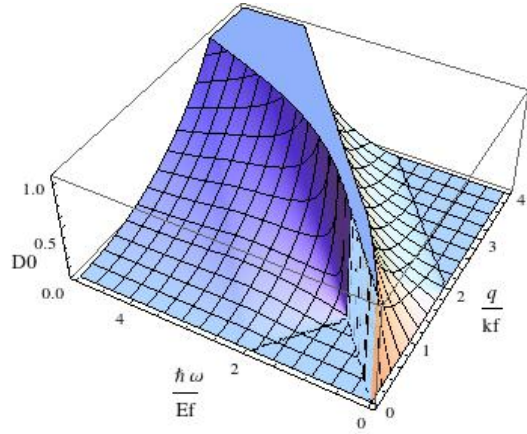


Figure D.2: Imaginary part of the polarizability, notice the flat part on the left side of the ridge where it is zero. This is where the plasmon lives and because the imaginary part of the polarization is zero the plasmon should have an infinite lifetime. In the parts where the function is non-zero the plasmons would be Landau damped and very quickly give off its energy to the single particle continuum, thus acquiring a very short lifetime.

Bibliography

- [1] J.W. Kysar C. Lee, X. Wei and J. Hone. Measurement of the elastic properties and intrinsic strength of monolayer graphene. *Science*, 321, 2008.
- [2] K. S. Novoselov, A. K. Geim, S. V. Morozov, D. Jiang, Y. Zhang, S. V. Dubonos, I. V. Grigorieva, and A. A. Firsov. Electric field effect in atomically thin carbon films. *Science*, 306(5696):666–669, 2004.
- [3] Alexander A. Balandin, Suchismita Ghosh, Wenzhong Bao, Irene Calizo, Desalegne Teweldebrhan, Feng Miao, and Chun Ning Lau. Superior thermal conductivity of single-layer graphene. *Nano Letters*, 8(3):902–907, 2008.
- [4] P. R. Wallace. The band theory of graphite. *Phys. Rev.*, 71:622–634, May 1947.
- [5] Kenneth W. K. Shung. Dielectric function and plasmon structure of stage-1 intercalated graphite. *Phys. Rev. B*, 34:979–993, Jul 1986.
- [6] J. González, F. Guinea, and M.A.H. Vozmediano. Non-fermi liquid behavior of electrons in the half-filled honeycomb lattice (a renormalization group approach). *Nuclear Physics B*, 424(3):595 – 618, 1994.
- [7] R. R. Nair, P. Blake, A. N. Grigorenko, K. S. Novoselov, T. J. Booth, T. Stauber, N. M. R. Peres, and A. K. Geim. Fine structure constant defines visual transparency of graphene. *Science*, 320(5881):1308, 2008.
- [8] J. Clerk Maxwell. A dynamical theory of the electromagnetic field. *Philosophical Transactions of the Royal Society of London*, 155:459–512, 1865.

- [9] R.W. Wood. On a remarkable case of uneven distribution of light in a diffraction grating spectrum. *The London, Edinburgh, and Dublin Philosophical Magazine and Journal of Science*, 4(21):396–402, 1902.
- [10] Gustav Mie. Beiträge zur optik trüber medien, speziell kolloidaler metallösungen. *Annalen der Physik*, 330(3):377–445, 1908.
- [11] Lewi Tonks and Irving Langmuir. Oscillations in ionized gases. *Phys. Rev.*, 33:195–210, Feb 1929.
- [12] David Pines. Collective energy losses in solids. *Rev. Mod. Phys.*, 28:184–198, Jul 1956.
- [13] R. H. Ritchie, E. T. Arakawa, J. J. Cowan, and R. N. Hamm. Surface-plasmon resonance effect in grating diffraction. *Phys. Rev. Lett.*, 21:1530–1533, Nov 1968.
- [14] J. J. Hopfield. Theory of the contribution of excitons to the complex dielectric constant of crystals. *Phys. Rev.*, 112:1555–1567, Dec 1958.
- [15] S. L. Cunningham, A. A. Maradudin, and R. F. Wallis. Effect of a charge layer on the surface-plasmon-polariton dispersion curve. *Phys. Rev. B*, 10:3342–3355, Oct 1974.
- [16] M. Fleischmann, P.J. Hendra, and A.J. McQuillan. Raman spectra of pyridine adsorbed at a silver electrode. *Chemical Physics Letters*, 26(2):163 – 166, 1974.
- [17] Evan J. Blackie, Eric C. Le Ru, and Pablo G. Etchegoin. Single-molecule surface-enhanced raman spectroscopy of nonresonant molecules. *Journal of the American Chemical Society*, 131(40):14466–14472, 2009.
- [18] William L. Barnes, Alain Dereux, and Thomas W. Ebbesen. Surface plasmon subwavelength optics. *Nature*, 424(6950):824–830, 2003.
- [19] William L Barnes. Surface plasmon-polariton length scales: a route to sub-wavelength optics. *Journal of Optics A: Pure and Applied Optics*, 8(4):S87, 2006.
- [20] E.H. Hwang and S. Das Sarma. Dielectric function, screening, and plasmons in two-dimensional graphene. *Phys. Rev. B*, 75, 2007.

- [21] F. Sols B. Wunsch, T. Stauber and F. Guinea. Dynamical polarization of graphene at finite foping. *New Journal of Physics*, 8, 2006.
- [22] Jianing Chen et al. Optical nano-imaging of gate-tunable graphene plasmons. *Nature*, 487(7405):77–81, 2012.
- [23] Z. Fei et al. Gate-tuning of graphene plasmons revealed by infrared nano-imaging. *Nature*, 487(7405):82–85, 2012.
- [24] P. Alonso-González et al. Controlling graphene plasmons with resonant metal antennas and spatial conductivity patterns. *Science*, 344(6190):1369–1373, 2014.
- [25] Long Ju et al. Graphene plasmonics for tunable terahertz metamaterials. *Nature Nanotechnology*, 6(10):630–634, 2011.
- [26] Marinko Jablan, Hrvoje Buljan, and Marin Soljačić. Plasmonics in graphene at infrared frequencies. *Phys. Rev. B*, 80:245435, Dec 2009.
- [27] N. D. Mermin. Lindhard dielectric function in the relaxation-time approximation. *Phys. Rev. B*, 1:2362–2363, Mar 1970.
- [28] M R Ramezanali et al. Finite-temperature screening and the specific heat of doped graphene sheets. *Journal of Physics A: Mathematical and Theoretical*, 42(21):214015, 2009.
- [29] S. Das Sarma and Qiuzi Li. Intrinsic plasmons in two-dimensional dirac materials. *Phys. Rev. B*, 87:235418, Jun 2013.
- [30] John Jackson. *Classical Electrodynamics*. John Wiley & Sons Inc., 3rd edition, 1999.
- [31] Stefan Maier. *Plasmonics: Fundamentals and Applications*. Springer, 2007.
- [32] Eugene Hecht. *Optics*. Addison Wesley, 2002.
- [33] A. H. Castro Neto, F. Guinea, N. M. R. Peres, K. S. Novoselov, and A. K. Geim. The electronic properties of graphene. *Rev. Mod. Phys.*, 81:109–162, Jan 2009.
- [34] Mikhail I. Katsnelson. *Graphene: Carbon in two dimensions*. Cambridge University Press, 2012.

-
- [35] Gabriele F. Giuliani and Giovanni Vignale. *Quantum theory of the electron liquid*. Cambridge University Press, 2005.
- [36] Frank Stern. Polarizability of a two-dimensional electron gas. *Phys. Rev. Lett.*, 18, 1967.
- [37] J. Lindhard. On the properties of a gas of charged particles. *Kgl. Danske Videnskab. Selskab Mat.-fys. Medd.*, Vol: 28, No. 8, 1954.
- [38] T. Stauber, N. M. R. Peres, and A. K. Geim. Optical conductivity of graphene in the visible region of the spectrum. *Phys. Rev. B*, 78:085432, Aug 2008.
- [39] H. Ehrenreich and M. H. Cohen. Self-consistent field approach to the many-electron problem. *Phys. Rev.*, 115:786–790, Aug 1959.
- [40] Gerald Mahan. *Many-Particle Physics*. Plenum Press, 2nd edition, 1993.
- [41] A. Altland and B. Simons. *Condensed Matter Field Theory*. Cambridge University Press, 2nd edition, 2010.
- [42] I. S. Gradshteyn and I. M. Ryzhik. *Table of Integrals, Series, and Products*. Academic Press Inc., 4th edition, 1980.